European Commission
Information Society and Media

SEVENTH FRAMEWORK PROGRAMME

Specific Targeted Research Projects

SOLDER

Spectrum OverLay through aggregation
of heterogeneous DispERsed Bands

FP7 Contract Number: 619687

WP3 – Aggregation of Heterogeneous dispersed spectrum bands in HetNet and h-RATs

D3.3
Final report CA in h-RAT, PHY and system results

Contractual Date of Delivery:	30 June 2016
Actual Date of Delivery:	1st July 2016
Responsible Beneficiary:	TCS
Contributing Beneficiaries:	ISI/ATHENA RC, EURECOM, IS-WIRELESS, KCL, SEQ, TCS
Security:	Public
Nature	Report
Version:	2.0

Document Information

Document ID: D3.3.doc
Version Date: 30 June 2016
Total Number of Pages: 79

Abstract This report captures the outcomes of the activities held in WP3, dealing with MAC/PHY and RRM aspects of carrier aggregation. Several aspects of CA are addressed, from "regular" CA as defined by the 3GPP standard to more exotic cases, involving unlicensed spectrum or 5G-like waveforms.

Keywords Carrier aggregation, Link adaptation, Radio resource management, system capacity, spectrum databases, WiFi, LTE, LTE-U, 5G.

Authors

Name	Organisation	Email
Fotis Foukalas	ISI/AthenaRC	Foukalas@isi.gr
Apostolis Galanopoulos	ISI/AthenaRC	agalanop@isi.gr
Apostolis Xenakis	ISI/AthenaRC	axenakis@isi.gr
George Ropokis	ISI/AthenaRC	ropokis@isi.gr
Oliver Holland	KCL	oliver.holland@kcl.ac.uk
Maria Lema	KCL	maria.lema_rosas@kcl.ac.uk
Aravindh Raman	KCL	aravindh.raman@kcl.ac.uk
Mateusz Buczkowski	ISW	m.buczkowski@is-wireless.com
Sylvain Traverso	TCS	sylvain.traverso@thalesgroup.com
Guillaume Vivier	SEQ	gvivier@sequans.com
Florian Kaltenberger	EUR	florian.kaltenberger@eurecom.fr
George Arvanitakis	EUR	george.arvanitakis@eurecom.fr

Document History

Revision	Date	Modification	Editor
1.0	2016-06-28	Document delivered to the coordinator	ISW
2.0	2016-06-30	Document delivered to the Project Officer	ISI

*see BSCW for full history

Executive Summary

This report is the last report from WP3. It captures the final outcomes of all the tasks, covering several enablers for carrier aggregation (CA).

The report is structured in 4 main sections: aggregation of conventional LTE, aggregation of heterogeneous radio access technologies (h-RAT), use of unlicensed spectrum and aggregation of 5G waveforms.

In the context of conventional LTE aggregation, we first investigate the scheduling aspects. We propose a Radio Resource Management (RRM) algorithm, which is able to efficiently assign resources to all users connected to the base station (BS). An important feature of the described solution is its completeness - it covers scheduling from very beginning - including Component Carrier (CC) activation/deactivation and Modulation and Coding Scheme (MCS) selection through priority calculation ending with creating final scheduling decision compliant with an LTE-A standard.

Then, we investigate the aspect of aggregation of TDD and FDD carriers using simulation environment. The key idea is to select the suitable number of UL and DL frames under certain channel conditions. This is achieved using a utility-based cross-layer design (CLD) framework.

Finally, we investigated the case of heterogeneous network (HetNet) deployment involving macro-cells and small-cells. Propose uplink/downlink (UL/DL) decoupling schemes designed for CA scenarios are presented. In terms of KPI (key performance indicator) outlined in D2.3, they show significant potential for throughput enhancement, as well as others such as outage probability reduction.

In the h-RAT aggregation context, we investigate the LTE+WiFi aggregation from a large-scale system level standpoint based on analytical models using stochastic geometry and queuing theory. The main conclusions are that it is important to model interference based on the load of the base stations, and that proper load-balancing between the two networks is needed to guarantee best performance.

Then, we investigate dynamic spectrum reallocation in which one could imagine of allocating a given spectrum band to the legacy RAT. This is compatible to 3GPP concept of joint multi-RAT coordination, where either spectrum refarming or reallocation can be used. In this context, we propose a dynamic spectrum reallocation solution based on particular QoS criteria.

We then address power allocation to minimize power consumption per component carrier in CA systems. Optimal power allocation policies are derived assuming full or quantized feedback. RF impairments are also taken into account at the second part of our contribution.

Unlicensed spectrum could be definitely considered for CA. This is the focus of the third main section of the report. Here, we first provide a quite update on spectrum database-based solutions, which yield significant potential spectrum that might be used for aggregation purposes to realize future demands—we also provide a quick analysis of important changes that have transpired in the TVWS case in the UK through this. Next, moving the onus for spectrum assessment in the unlicensed spectrum case onto the terminal, we investigate two dedicated studies applied to Licensed Assisted Access (LAA), the 3GPP way to combine carrier aggregation and unlicensed spectrum. We consider UL CA and propose an overbooking principle in order to fulfil user requirement despite the constraint brought by the listen before talk (LBT) mechanism. Such mechanism is indeed mandatory as per regulation. The second proposal intends to address another regulatory rule that force any transmitting device to use at least 80% of the bandwidth. We evaluated a scheme based on interlacing chunk of resource blocks that allows multiplexing several users still fulfilling the regulatory constraint.

However such proposal may harm the peak-to-average ratio of the waveform and degrades significantly the performance.

The last topic addressed in this report is therefore new waveforms that could provide much better property in terms of spectrum occupancy, enabling intra band CA at the PHY level, at least when coupled with digital pre-distortion and PAPR reduction techniques. We highlight the most relevant linearization techniques and we present a new parameter selection procedure. Finally, the benefit of the joint use of digital calibration, PAPR reduction and linearization is emphasized by the mean of realistic simulations.

Table of contents

List of Figures

List of Tables

1. Introduction

This report is the last report from WP3. It captures the final outcomes of the partner's investigation on CA enablers.

Originally, we partition our work by radio technologies and by type of spectrum to be aggregated. We follow this approach because of the use cases identified in WP2 and initially addressed in D3.1 and D3.2. However, it appears that such split is less useful since many radio technologies are now adapted to work in various spectrum types (for instance LTE was adapted to work in unlicensed band). Somehow, we confirm what we foresee at the beginning of the project that is the concept of the convergence between cognitive radio and mobile wireless systems especially due to the evolution of CA within the 3GPP in the course of the project implementation. This is a significant conclusion for the project and confirms the technology proposal from the consortium a few years ago.

This report is therefore the last one for the WP3 that is structured as follows. Section 2 deals with the conventional aggregation of LTE-A system and beyond, with contribution in the radio resource management (RRM) domain for any type of deployment, homogeneous or heterogeneous and a contribution on the dynamic adaptation of the TDD frame boundary. Section 3 deals with aggregation of heterogeneous radio access technologies that is a progress beyond 4G and towards 5G, first from the practical case of WiFi + LTE aggregation, and then addressing the problem of spectrum allocation. Section 4 deals with the use of unlicensed spectrum, with a special attention paid to the regulatory rules. Section 5 then provides outlook on predistortion techniques that could be used to control the spectrum of FBMC, one candidate for 5G waveform when used in CA scenario. Such a solution is important for the future PHY layer implementation. Finally, Section 6 concludes this report and also summarizes the algorithms that were selected for the proof-of-concepts developed in parallel in work-package 4. However, part of the algorithmic solutions for the proof-of-concept was developed within the D3.2.

We follow the approach taken for D3.2 to limit the size of the report. We deliberately try to reduce the replication of material that we have already published as part of our SOLDER work, and provide the full publications as appendices for more detailed information. Notably, a good amount of scientific papers were produced by both D3.2 and D3.3 presented in WP5 in details.

2. Aggregation of LTE

2.1 Radio resource management

2.1.1 Overview

Aggregation of LTE carriers is a scenario, which is covered by the 3GPP specifications. Documents starting from Re.10 onwards define how component carriers (CC) can be configured and used in LTE-A system. All required procedures for activating and deactivating additional carriers for the users are defined. What is not defined is how these additional resources should be managed by the base station. This is up to operator's or stack provider's implementation.

In this section, we propose a Radio Resource Management (RRM) algorithm, which is able to efficiently assign resources to all users connected to the base station in carrier aggregation (CA) environment. This algorithm is based on work presented in previous WP3 deliverable [D3.2].

2.1.2 Scheduling algorithms

Basic scheduling algorithm is Round Robin (RR). User Equipments (UEs) get the resources in circular manner in such a way that each user gets the same amount of Physical Resource Blocks (PRBs) over some observation time. In theory, it is less efficient from an operator/network perspective [VAR11]. Opposite scheduling approach is maxCQI – it allocates resources based on measured channel quality. User with best conditions in particular PRB gets the resource. This is the most efficient approach from network perspective – highest possible throughput is achieved [VAR11]. This algorithm might not schedule cell edge users at all if anyone will have better conditions than these users. This means that fairness of this scheduling algorithm is low.

These two schedulers show that increasing one metric can lead to decreased performance in terms of other measurement (in this case it is eNB vs. UE throughput – maxCQI maximize eNB throughput, while neglecting UE throughput; RR assigns equal number of PRB neglecting eNB throughput).

More advanced algorithms tend to find balance between more metrics (e.g. eNB throughput, fairness, packet delay, etc.).

First example of such algorithm is Proportional Fair (PF). It takes into account channel conditions and previous throughput of particular UE [HOL01][YEO09]. This algorithm tends to work as maxCQI, but is also limited by the UE throughput. If particular UE has higher average rate than other UEs its priority is lower. On the other hand, in case of low average rate priority rises. Such approach provides higher eNB throughput than in RR case and do not neglect cell edge users as it is done in maxCQI.

Adding more metrics into consideration can give better results – not always in terms of throughput. If for example some service has packets with very short time to live (TTL), PF algorithm might fail since the packet delay is not taken into account. Therefore, it might be better to sacrifice throughput a little to make sure that packets are delivered in time.

Example of an algorithm that includes packet delay is the Largest Weighted Delay First (LWDF) [STO01] or its modification – M-LWDF [XIA11]. Calculation of the priority is enhanced with the delay of head-of-line (HOL) packet. HOL is the first packet in the queue waiting to be scheduled.

Another enhancement of PF algorithm can be Modified Queue-Based Exponential Rule (M-QBER) – an algorithm where size of the queue is taken into account. Users having higher variance in queue length compared to average value are given more preference [PRA10].

2.1.3 Proposed algorithm

LTE eNB Scheduler, which is a commercial name of the algorithm proposed by the IS-Wireless, takes three main steps while assigning radio resources to users. They are presented in Figure 1.

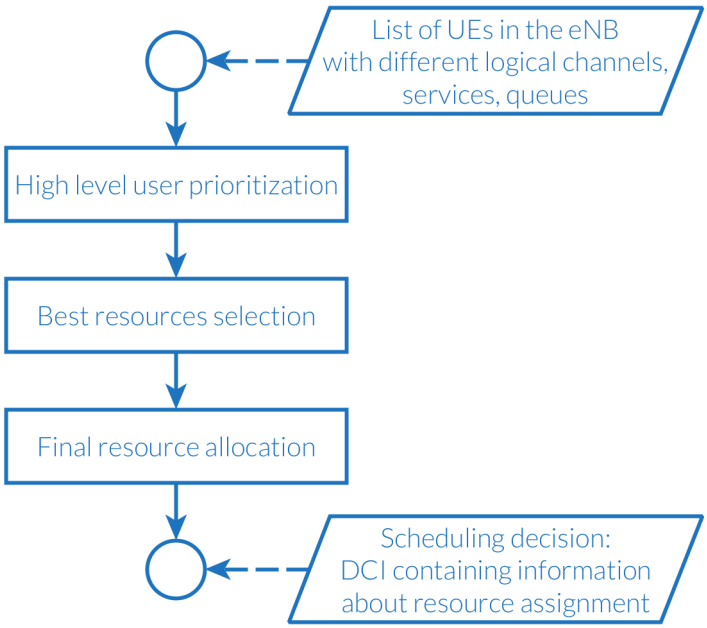

Figure 1. Main steps of scheduling algorithm

At the beginning, the list of users connected to eNB is prioritized. This step allows to sort users according to their data rate requirements and retransmission needs. From all users in each TTI scheduler selects those users whose QoS parameter imposes guaranteed bit rate (GBR). Such users, called GBR users, must get sufficient amount of PRBs, which will allow them to reach their target throughput. GBR users are served with higher priority than regular users – it means that scheduling for non-GBR users is performed on the resources that are not allocated after GBR users scheduling.

During this step the scheduler also decides, if particular UE can benefit from additional CC and whether it is feasible from eNB point of view. First constrain is UE capability – if UE does not support CA, then scheduling algorithm cannot assign additional CC, even if user has lots of data to transmit. If both UE and eNB support CA, scheduler decides about CC assignment in few steps:

1. Scheduler verifies if all UEs, which have more than one carrier active still need these resources – if not, second carrier will be deactivated for that user
2. Scheduler verifies if any of the carriers can serve more users and marks them as “available”
3. Scheduler searches for users that do not use “available” CC and verifies if they need additional resources – if yes, then second carrier will be activated for that user

Exemplary results of the second carrier activation/deactivation are presented in the Figure 2.

Figure 2 presents dependency of the UE buffer size on activation or deactivation of additional CCs. Buffer size in the plot is normalized; meaning that maximum capacity is 1, and minimum is 0. Buffer size corresponds to the needs for throughput – the more data is to send the higher throughput is expected. This is simplified case, used just for demonstration. Single line in the plot means single carrier, while double line means two carriers for this UE.

At this plot one can see that:

- if UE requirements are increasing and rise above defined threshold (UE1) and there are available resources, then additional CC is activated
- if UE requirements are decreasing and fall below defined threshold (UE2) then additional CC is deactivated.
- if UE requirements are low (UE3) it has only one CC
- if UE requirements are maintained at the high level (UE4) its CC assignment does not change

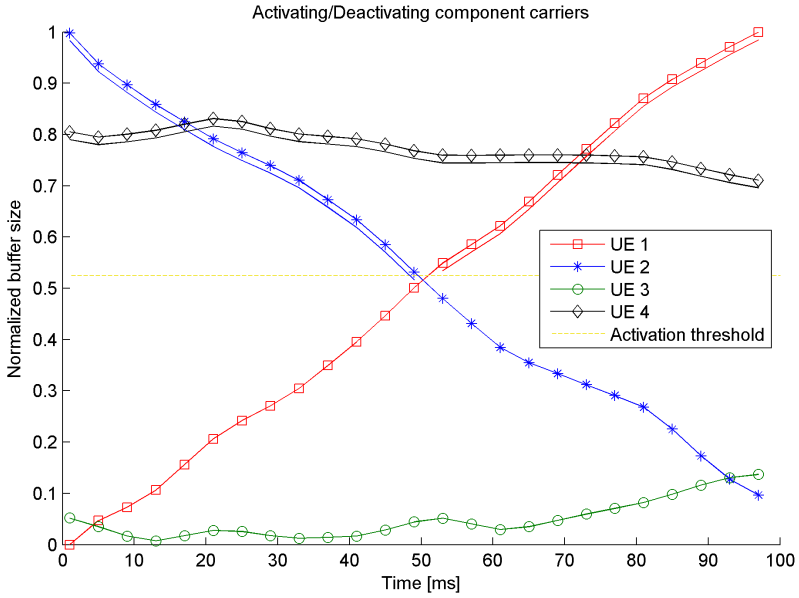

Figure 2. Activation/deactivation of additional component carriers

In the next step, the algorithm selects resources for all users by calculating their priority per each available resource block. Priority depends on multiple features, namely queue length, packet delay, channel conditions and historical throughput. Formula for calculating priority is as follows:

$$P = (1 + w_1 CQI_{prior}) \cdot (1 + w_2 p_w) \cdot (1 + w_3 r_{historical}^{-1}) \cdot (1 + w_4 N_{prior})$$

Where:

P – priority for the user
CQI_{prior} – priority related to the channel quality
p_w – priority related to the packet waiting time
$r_{historical}^{-1}$ – priority related to the user historical throughput
N_{prior} – priority related to the size of the buffer queue
$w_1 - w_4$ – weights related to particular priority components

Introducing weights in user priority calculations allows customizing behavior of the LTE eNB Scheduler. Importance of the particular priority component can be easily increased or decreased. In specific case, where w_n is set to 0, component can be disabled from calculating user priority.

Exemplary possible customizations are:

- Focusing on increasing total eNB throughput by increasing weight w_1, which is related to the current channel conditions (UEs with better channel conditions will be favored)
- Focusing on decreasing latency by increasing weight w_2, which is related to the packet waiting time (UEs with most delayed packets will be favored)
- Focusing on increasing scheduling fairness by increasing weight w_3, which is related to the historical throughput and by decreasing weights w_2 and w_4. This will lead to equalization of the UEs throughput regardless buffer sizes and packet delays.

This step also includes correction of real-life UE imperfections. UE measures channel conditions using reference signals transmitted in the downlink frame. Based on this measurement UE sends feedback with channel quality indication (CQI). Different UEs might report slightly different CQI values for the same channel conditions, which will cause wrong selection of modulation and coding scheme (MCS) at the scheduler. To deal with this LTE eNB Scheduler monitors number of successful and unsuccessful transmissions and based on that compensates differences in CQI reporting.

LTE eNB Scheduler tends to keep defined target BLER. If $\frac{N_{NACK}}{N_{NACK}+N_{ACK}}$ ratio is higher than a target BLER it means that too high CQI is reported and therefor, too high MCS is used. On the other hand, if this ratio is lower than target BLER it means that too low CQI is reported and higher MCS can be used by this UE.

Figure 3 depicts averaged CQI correction value for different types of users over time. It shows that CQI offset, which is added to the reported CQI value reaches stable value on average after 300-400 TTIs, depending on CQI error. The larger the CQI error, the longer it might take to find proper CQI offset. Figure 3 shows also that if proper CQI is reported, no offset is introduced by the LTE eNB Scheduler.

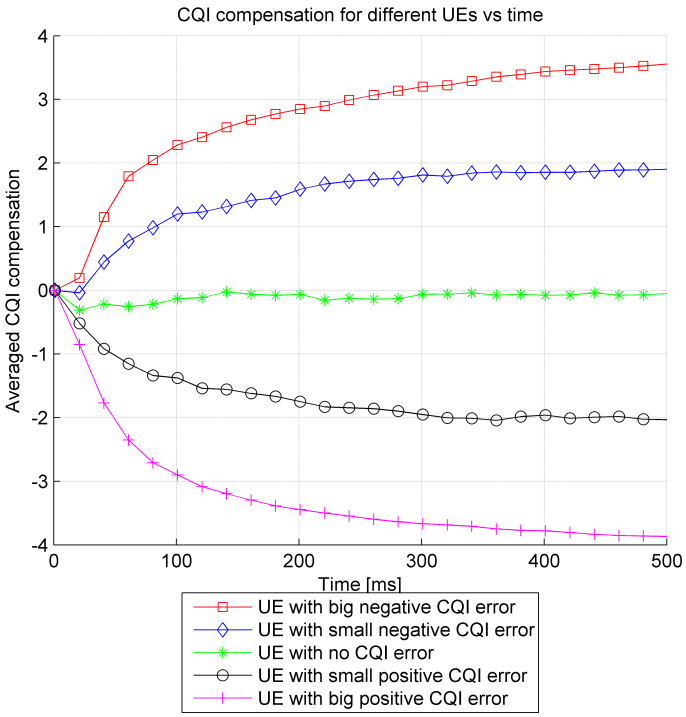

Figure 3. Wrong CQI correction

Scheduling decision provided by the scheduler must be compliant with 3GPP specifications - resource assignment must be in specific format, it must take into account-reserved resources for control/signaling region and capabilities of the user equipment.

In the last step, LTE eNB Scheduler maps calculated priorities to final scheduling decision, which fulfills 3GPP requirements.

One of the restrictions from 3GPP specifications is that not every possible combination of PRBs is valid. In some cases it is impossible to assign PRBs with highest priorities - based on the set of the possible DCI allocation types scheduler must pick best allocation type matching to the best PRBs. Exemplary situation is presented in the Figure 4.

Figure 4 presents exemplary priorities for different PRBs for particular UE. Scheduler, for this case, has two possible formats for selecting 4 PRBs - either first or second part of the resources (b)) or on the other hand even or odd PRBs (c)).

Total priorities for each of the case are depicted on the right. Best option in presented example is selection type A - red color. This approach gives total priority of 25. As we can see in the d) the best possible solution cannot be represented by any of these selection types and gives priority equal 30.

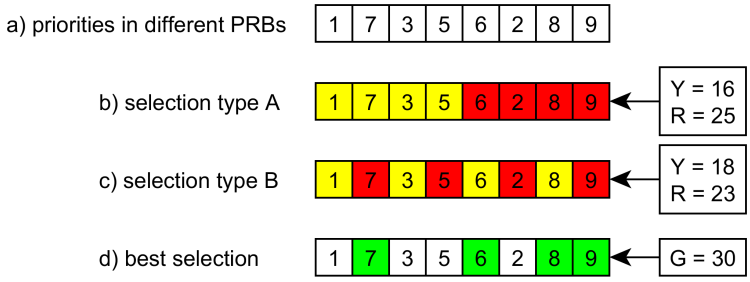

Figure 4. Format selection example

2.1.4 Performance analysis

Scheduling algorithm was verified using LTE MAC Lab tool - system-level simulator capable of simulating HetNets and CA. Scheduling algorithm was developed within this tool, which allows to obtain reliable results and compare performance against benchmark cases - RR and PF. Network layout is presented in the Figure 5. It consists of two types of base stations - macro base stations and small cells. In the base stations CA is enabled - this means that users can use two CCs if scheduler will activate them.

More detailed simulation parameters are gathered in Table 1.

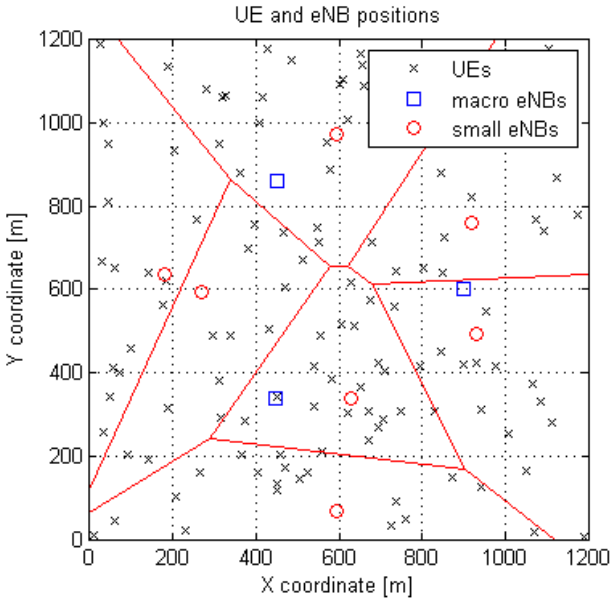

Figure 5. Format selection example

Table 1. Simulation parameters

Parameter	Value
Area size	1.2 km x 1.2 km
Environment	Urban
Number of users	120
Simulation time	50
SINR mapping	MIESM
Number of CC	2
CC Bandwidth	5 MHz

Results provided in this chapter show performance of the scheduler. Algorithm is compared to two well-known algorithms, namely RR and PF. Simulation scenarios are alike – the only difference is scheduling algorithm. Proposed scheduling algorithm is marked as ISW proprietary.

Two main outcomes of the simulations are presented in the paper, namely eNB throughput CDF, peak/edge user throughput and relation between total eNB throughput and number of users connected to that eNB.

Figure 6 shows distribution of throughput for different scheduling algorithms. ISW proprietary scheduling algorithm offers higher throughput for all users compared to RR and PF. PF is calibrated in similar way to proposed algorithm and provides better performance for users with good channel conditions without significant degradation of cell edge users.

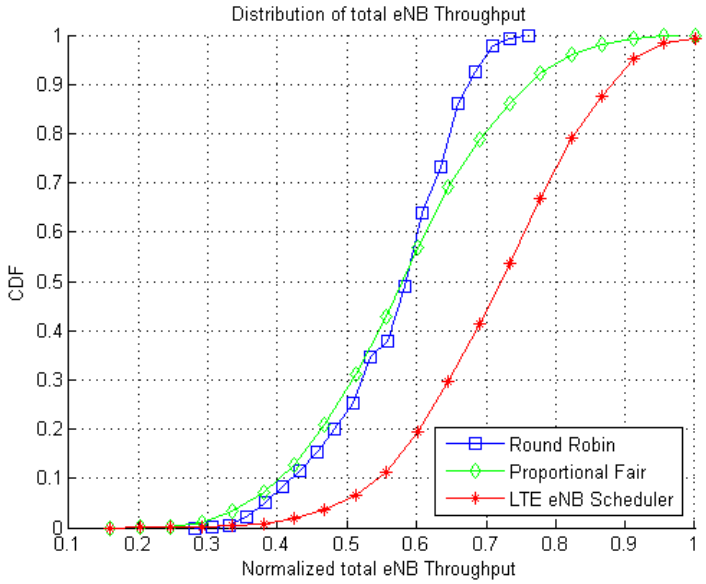

Figure 6. Normalized total eNB throughput

This is also visible in the Figure 7, where peak (90-percentile) throughput and throughput for cell edge users (10-percentile) is presented.

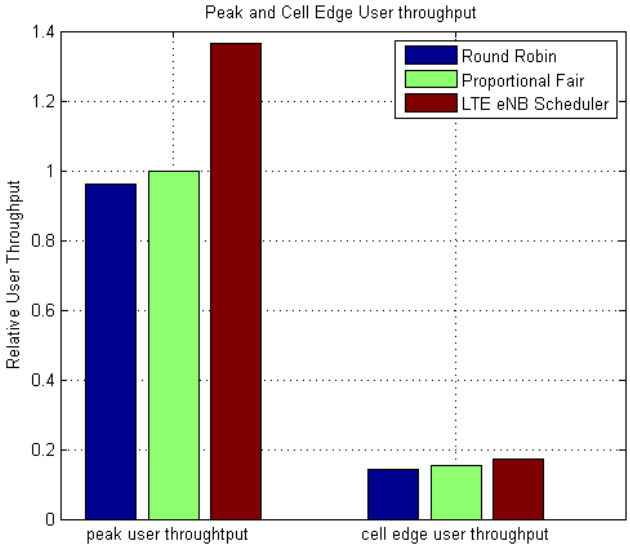

Figure 7. Relative peak and cell edge user throughput

In comparison to RR, PF offers slightly higher peak and edge throughput - this shows that even simple algorithm can utilize the same resources in more efficient way. Using more advanced algorithms, like ISW proprietary in this case, gives even better results. Not only peak user data rate is more than 35% higher, but also cell edge users get a bit higher throughput.

2.1.5 Conclusions

As scheduling is an important aspect of eNB deployment we presented novel scheduling algorithm and its performance in HetNet deployment with CA. An important feature of the

described solution is its completeness - it covers scheduling from very beginning - including CC activation/deactivation and MCS selection through priority calculation ending with creating final scheduling decision compliant with an LTE-A standard. Evaluation presented in this chapter is based on MATLAB model of C language implementation of the complete algorithm, which is developed in WP4.

2.2 TDD UL/DL frame adaptation

We provide the aggregation of the FDD and TDD spectrum bands within the context of 3GPP LTE-A system. To be specific, we provide the framework for TDD frame adaptation within the LTE-A system. To this end, we first provide a cross-layer design (CLD) analysis to obtain the achievable throughput using the TDD mode for transmission in LTE-A system. Under particular QoS requirements and certain channel conditions, the achievable throughput is derived and evaluated. The QoS requirements originate from the upper layers, where the file size, the window size and the latency for efficient transmission are incorporated in the final formulation. Having obtained the formulation, simulation results highlight the impact of the QoS parameters to different TDD frame format, wherein the number of DL and UL subframes vary. The aim of this framework is to provide the options of choosing different TDD frame formats by calculating the DL:UL subframes ratio under certain channel conditions and QoS requirements. We also provide flowchart procedures of how such a solution can be implemented within the 3GPP LTE-A context and this is also implemented to obtain our simulation results. Simulation results are carried out, which reveal the probability of choosing the different TDD frame formats under certain channel conditions and QoS requirements.

We consider an LTE-A system, which consists of a primary serving cell (PCell) and a secondary cell (SCell) in HetNets, as shown in Figure 8. We assume that the PCell is equipped with FDD mode and the SCell with TDD mode. The FDD cell offers the Band-3 at 1800MHz and the TDD cell the Band-38 at 2600MHz providing higher coverage and capacity respectively to a user equipment (UE) that is able to communicate with both cellular networks through dual connectivity or carrier aggregation capability. According to [DUAL2016], the FDD/TDD CA can be facilitated by the dual connectivity concept. In this case, the UE is able to have access to both FDD and TDD bands. Both cells using their signaling from the eNodeB to the UE provide the component carrier allocation. Thus, two component carriers (CCs) are allocated to the CA-enables UE with bandwidth of 20MHz. Figure 8 depicts the UE that is connected to PCell using the FDD mode and the CC-1 and to SCell under TDD mode using CC-2. The system model under consideration is actually the 3GPP's deployment scenario 2 (i.e. inter-frequency scenario) for dual connectivity or CA, wherein macro and small cells on different carrier frequencies are connected via non-ideal backhaul. Dual connectivity provides two data paths (user plane connections), on different carriers with different frequencies for UE . UE communicates with the PCell via FDD DL/UL flows and with SCell via TDD radio frames. As a consequence, UE is assumed CA enabled in DL among FDD and TDD flows per subframe basis.

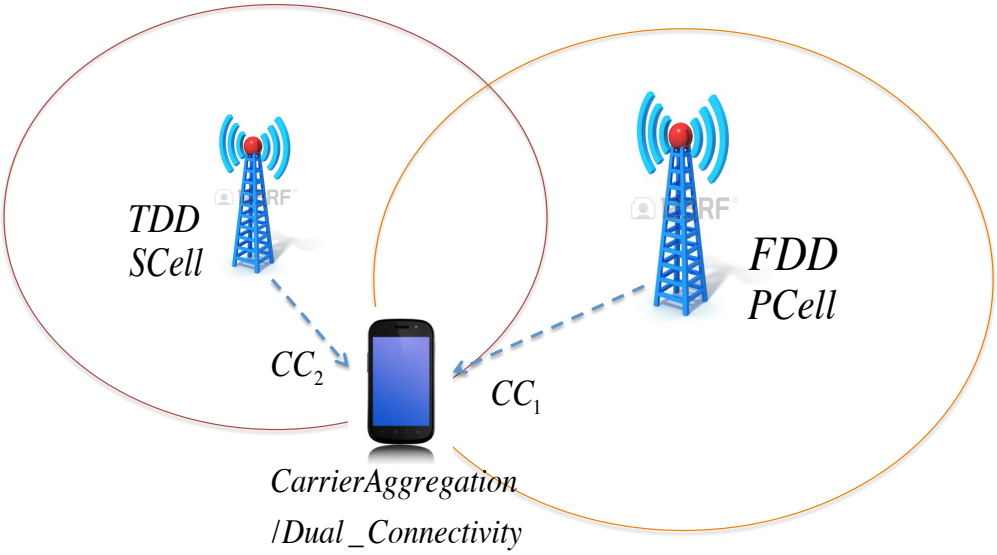

Figure 8. FDD/TDD carrier aggregation/dual connectivity enabled network

There are seven TDD configurations within the 3GPP TDD system [TDD-FDD]. The subframes are divided into standard subframes and special subframes. The special subframes consist of three fields such as guard period (GP), downlink pilot time slots (DwPTS) and uplink pilot time slots (UpPTS). In case of TDD duplex mode, we assume that the SCell and the UE operate under any of the 7 proposed 3GPP TDD configurations, where DL/UL ratios are asymmetric. In particular, the configuration 0 (TDD-0) is considered as UL-heavy since the radio frame consists of more UL subframes. The TDD-5 is considered as DL-heavy since the radio frame consists of more DL subframes. We assume that the UE and SCell communicate via DL-heavy and UL-heavy TDD configurations.

Having the DL/UL ratio as a key design factor, we devise a CLD approach that can incorporate the following parameters: 1) We assume that UE is performing an FTP reliable connection with eNB to download a file size, equal to L_{ftp}. Reliability is guaranteed as soon as there is ACK for each downloaded portion of the file. 2) TCP mechanism is related to TCP window size, which is a transport layer parameter and expresses TCP layer congestion control mechanism. 3) HARQ is a PHY layer mechanism, which quantifies the timing delays between the transmission of some portion of data (in downlink channel) and the backwards transmission of feedback ACK/NACK (in uplink channel).

In Sec.3.1 of Appendix 2.2, there is a detailed description of the cross-layer QoS requirements and how they are mapped into the CLD parameters in the TDD mode. Further, we provide in Sec.3.2 of Appendix 2.2 the TDD mode throughout formulation in order to evaluate the impact of the CLD parameters to the performance of the TDD mode. In this way, we highlight the tradeoffs that the TDD-FDD CA framework explained below must take into account. The actual tradeoffs can be found from the pictures in Sec.3.3 of Appendix 2.2, where a few selected of them are presented here below.

The results are obtained through simulation highlighting the impact of the CLD approach presented above. The LTE network parameters used in the simulations include 20MHz bandwidth, 100 Resource Blocks per subframe, HARQ latencies per TDD configuration and radio frame, and LTE radio frame size of 10 subframes. The simulation environment is CA-enabled and thus, we consider two independent CCs for the FDD and TDD modes respectively.

Figure 9 depicts the throughput versus the TCP window size *W* values for TDD configuration modes TDD-0, TDD-1 and TDD-5. It is obvious that the TDD-0 lead to worst throughput for all window sizes. For values of *W* less that threshold of 10^5 bits, TDD-1 is preferable as compared to TDD-5, although TDD-1 has more UL subframes than TDD-5. This is expected because bad channel conditions, with low SNR and high BER, UE transmits more NACKs than ACKs, therefore, the time required to acknowledge all downloaded data in combination with the shortage of UL subframes for TDD-5, leads to throughput degradation. On the contrary, when $W \geq 10^5$ bits, TDD-5 is clearly the best TDD configuration choice as compared to TDD-1 and TDD-0

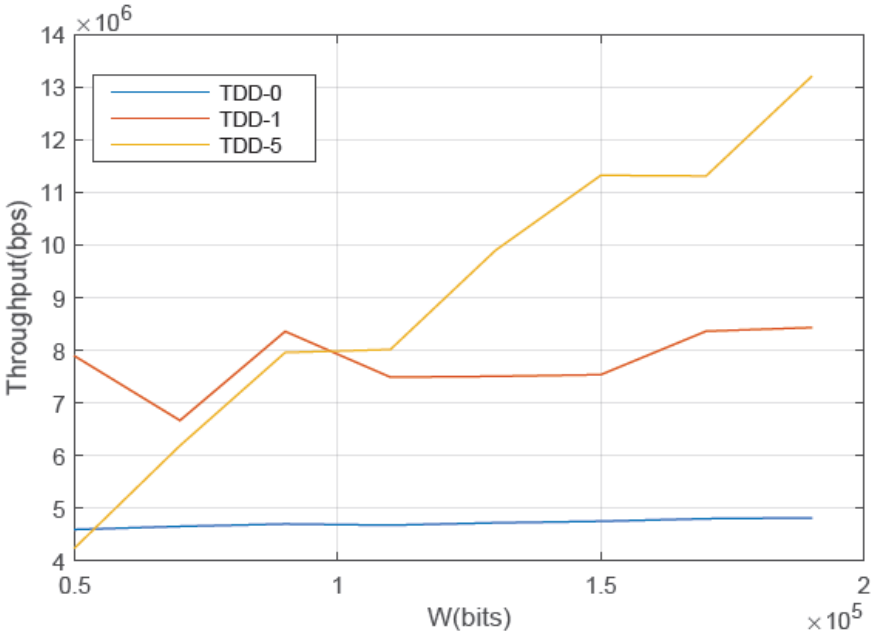

Figure 9. Throughput vs W for SNR = -5 dB and TDD-0, TDD-1 and TDD-5

Error! Reference source not found. depicts achievable TDD throughput vs SNR for a small CP window size W = 20 Kbits, for the TDD-0, TDD-1 and TDD-5 configuration modes. In this case, for all SNR values TDD-5 leads to worst throughput as compared to TDD-0 and TDD-1. For small W values, eNB cannot send new data stream to UE unless it received ACKs for all previously downloaded data portion. Therefore, in this case, UE cannot take advantage of TDD-5 large *DL/UL* ratio, because the shortage of UL subframes in conjunction with HARQ delays increase the total time to download the file. Although DL-heavy TDD configurations with large *DL/UL* ratios are preferable in high SNR cases, window size plays a crucial regulator role. We also observe that for higher SNR values, throughput is increased for all TDD configuration.

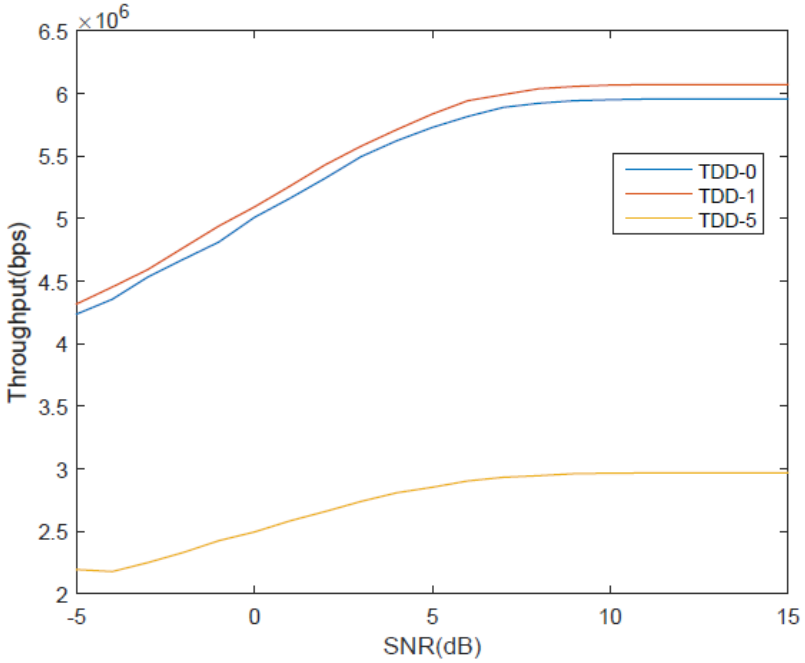

Figure 10. Throughput vs SNR for W = 20kbps, L_{ftp} = 800 Kbits and TDD-0, TDD-1, TDD-5

Figure 11 depicts the impact of packet success rate (PSR) on throughput for TDD-0, TDD-1 and TDD-5 configurations with window size W = 200Kbits. This figure highlights that for small PSR threshold values, i.e. 10^{-3} and small window size, TDD-5 configuration leads to worse throughput as compared to TDD-0 and TDD-1. In this case there is no straightforward decision to be made as which TDD configuration is most preferable for eNB and UE. In cases of frequent channel errors, the number of NACKs is more frequent as compared to ACKs and therefore data re-transmissions have a negative impact on throughput. For larger BER values, TDD-5 clearly is the most preferable choice.

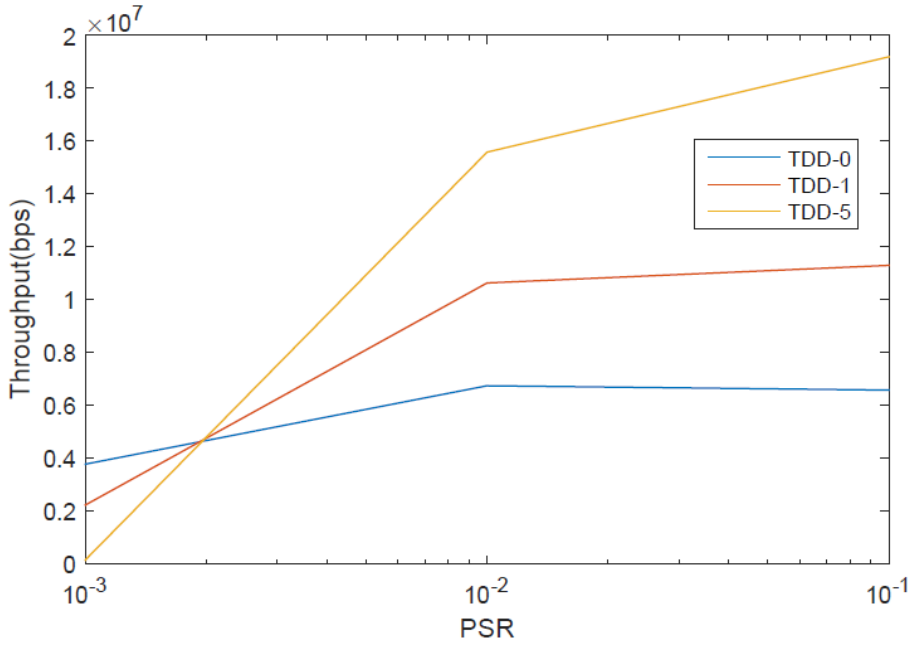

Figure 11. Throughput vs PSR for W = 200Kbits, SNR = 10dB and TDD-0, TDD-1 and TDD-5

2.2.1 TDD Frame Adaptation for FDD/TDD Carrier Aggregation

We define a *Utility Function* $U(i)$, where $i = 0 \ldots \frac{N_{tot}}{10}$ denote the radio frames that are transmitted between the TDD SCell and the UE. The value of $U(i)$ is a net number and it is used to rank each TDD configuration that lead to higher throughput. The utility function $U(i)$ will be evaluated at the end of each radio frame *i,* ${N_{DL}}^{i}$, ${N_{UL}}^{i}$ denotes the number of DL and UL subframes per $i-th$ radio frame, and ${N_{ack}}^{i}$ denotes the number of DL subframes per i_{th} radio frame received without errors. We define the utility $U(i)$ as follows;

$$U(i) = \left[\frac{\{N\}_{ack}^{i} \times \{N\}_{W}}{l_{harq}^{i}} \times \frac{\{N\}_{DL}^{i}}{\{N\}_{UL}^{i}} \right] \quad (1)$$

where $\{N\}_{DL}^{i}$ and $\{N\}_{UL}^{i}$ denotes the number of DL and UL subframes per $i-th$ radio frame, and $\{N\}_{ack}^{i}$ denotes the number of DL subframes per $i-th$ radio frame received without errors.

The SCell evaluates Eq(1) making a decision about the TDD configuration to apply in order to guarantee DL throughput boost, when UE aggregates FDD and TDD flows. This decision is taken at the end of each $i-th$ radio frame. The required time share proportion (i.e. ratio) between DL and UL transmission is calculated and the TDD frame adaptation with the nearest R_{DU} ratio is configured. The number of DL/UL subframes needed for the next *i+1* radio frame, i.e. ${N_{DL}}^{i+1}$ and N_{UL}^{i+1} is determined according to the following equation:

$$\{N\}_{DL}^{i+1} = \left[1 - \frac{U_{i-1}}{U_{i}} \right] \times 10 \quad \text{and} \quad \{N\}_{UL}^{i+1} = 10 - \mathrm{N}_{DL} \quad (2)$$

Using Eq.(2), the eNB is able to calculate the DL/UL ratio. In particular, at the end of i_{th} frame, eNB evaluates $U(i)$ and compares its value with the utility of the previous subframe $i-1$. To this end, it decides to change TDD configuration as long as the $U(i) > U(I-1)$ holds. Therefore, the fraction $1 - \frac{U(i-1)}{U(1)}$ gets value of 1, if the utility function of the current radio frame i increases. This means that a DL-heavy TDD configuration is requested to guarantee the QoS requirements. The required time share portion between DL and UL transmission is estimated, however, the ratio is not identical to those proposed by 3GPP. Hence, we propose a *mapping* to the nearest 3GPP ratio according to the following Table 2:

Table 2. TDD Configuration mapping to 3GPP

N_{DL}/N_{UL}	3GPP TDD configuration
0/10	0
1/9	0
2/8	0
3/7	6
4/6	1
5/5	2 or 3
6/4	2 or 3 or 4
7/3	4
8/2	5
9/1	5
10/0	5

Additionally, we use the notion *probability* of TDD configuration P_{TDD}^{k}, with $k = 0\ldots6$, which is the metric used throughout our simulations, depicting the number of radio frames $\{rf\}_k$ while a certain TDD configuration *k* was chosen, as compared to the total number of radio frames $\{rf\}_{tot}$ used by UE to download the file, and it is defined as follows: $P_{TDD}^{k} = \frac{\{rf\}_k}{\{rf\}_{tot}}$

2.2.2 TDD Frame Adaptation Proposed Implementation

In this section, we provide details about the implementation of TDD frame adaptation solution in the context of 3GPP. According to the previous subsection, eNB decides which TDD configuration to use at the i_{th} radio frame, evaluated at the *i-1* radio frame. Three out of ten spare bits in Master Information Block (MIB can be used to identify which which TDD configuration is being used between eNB and UE in the i_{th}radio frame. To this end, Figure 12 depicts an example flowchart process for MIB-based TDD configuration for eNB. According to Figure 12 for a given period of 1 radio frame, eNB decides which TDD configuration mode to use. A determination may be made whether the identified TDD configuration information from the monitored traffic is different from the previous used TDD configuration used by UEs in communication with the eNB. If the identified TDD configuration is different from previous radio frame, the TDD configuration can be communicated to the UEs using the MIB 3 spare bits to formulate the desired TDD configuration. However, a mapping is being done, according to Table 2,, as to which 3GPP configuration eNB is going to use. If eNB decides that the TDD configuration should not change, based on the information from the utility function, no MIB update happens and eNB/UE continues to use the same TDD configuration from the previous radio frame

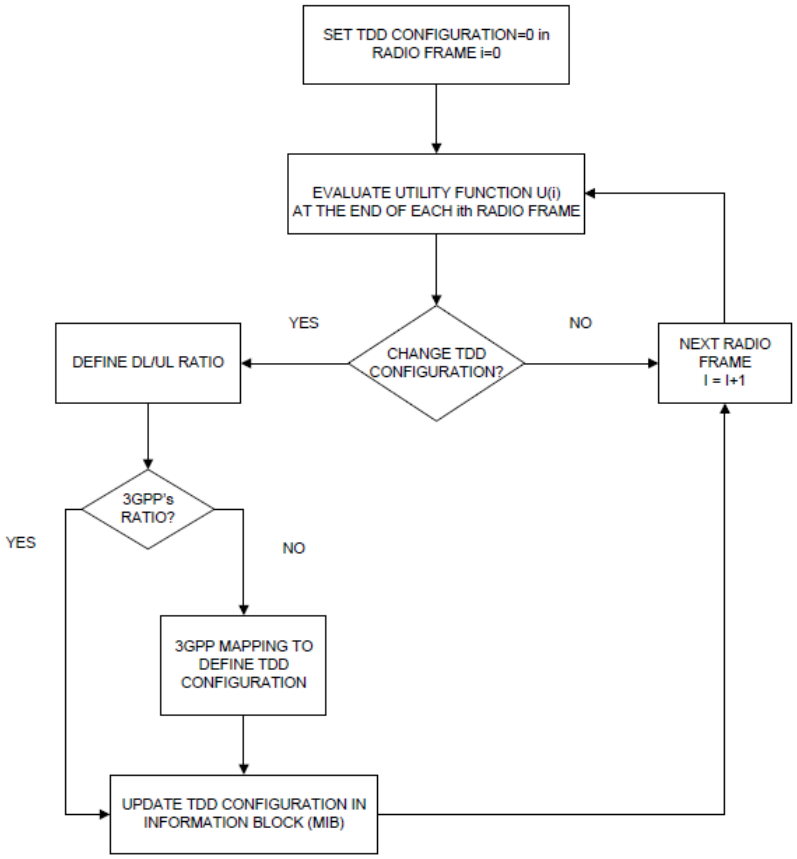

Figure 12. eNodeB TDD frame configuration procedure flowchart

Figure 13 depicts the TDD configuration decision process flowchart for UE. Due to the dual connectivity, UE is connected to PCell and SCell. If it is only connected to PCell, then data reception is done according to FDD duplex mode. Otherwise, if UE is in connection mode with SCell, it received data via TDD duplex mode. For UE that are not idle (i.e. connected UEs), a determination is made whether the UE is in DRX mode. For UEs in DRX, the UE reads TDD configuration using MIB upon waking up. For UEs in idle state, they update TDD configuration based on MIB, whether they become connected. For UE not in DRX mode, they ready TDD configuration directly from MIB. In any case, if TDD configuration for *i+1* radio frame has not changed, UE use the previous TDD configuration from i_{th} frame and starts the process again. Otherwise, it reads updated TDD configuration and applies it to the next *i+1* radio frame.

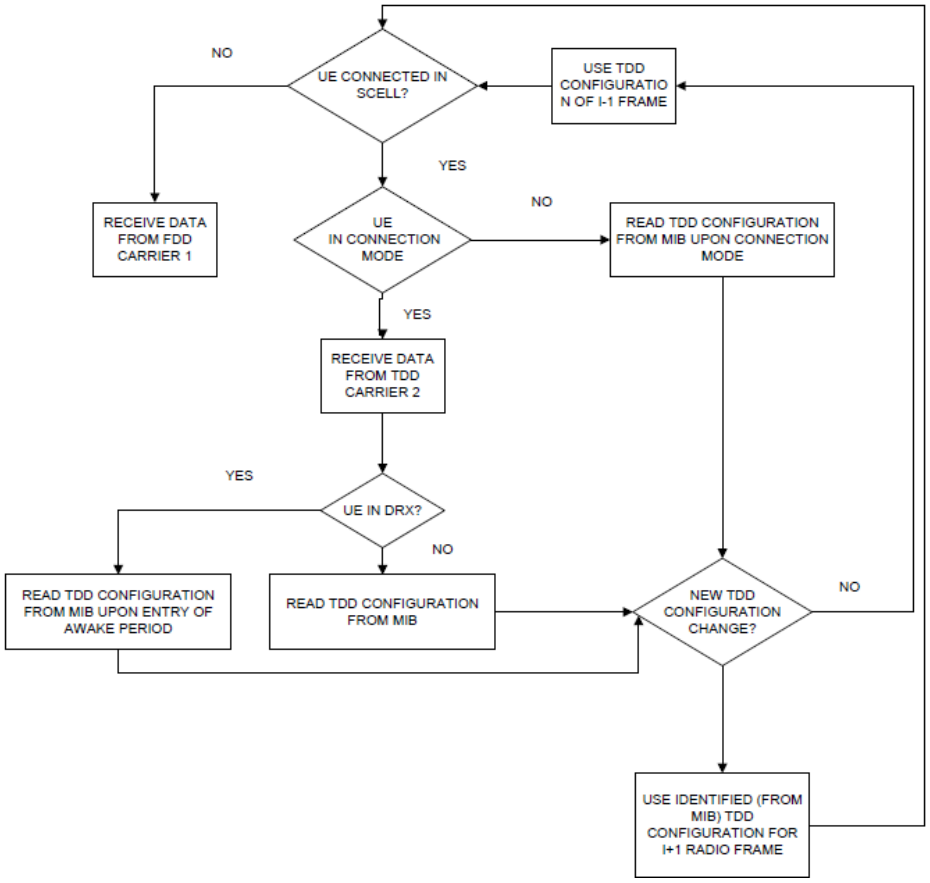

Figure 13.UE TDD frame configuration procedure flowchart

2.2.3 TDD Frame Adaptation Performance Evaluation

Following, we present our simulation results concerning the TDD frame adaptation mechanism presented previously. We compare the probability for TDD-5 (DL-heavy) and TDD-0 (UL-heavy) configurations versus SNR for the following use cases:

- Use-case A: W = 20 kbits, L_{ftp} = 800 kbits
- Use-case B: W = 200 kbits, L_{ftp} = 800 kbits

Figure 14 depicts the results for the use-case A, wherein for the case of small W, TDD-5 is not the best choice since it cannot take advantage of its DL-heavy nature. Therefore the probability of TDD-5 is less than the probability of TDD-0 for all SNR values. For the use-case B, the probability of TDD-5 is higher compared with the probability of TDD-0. This is expected since a high W value is applied and thus, the UE can download a large portion of the file using DL-heavy configuration, without providing ACKs for each transmitted sub-frame.

Figure 15 depicts the probability histogram of TDD configurations. We depict the statistical distribution of TDD configurations at the eNodeB, for SNR = 0 dB, W = 20 kbits and L_{ftp} = 800 kbits. In this case, we assume small window size, and as expected, eNB chooses TDD-0 and TDD-1 for most of the radio frames. In particular TDD-0 is being chosen 25% and

TDD-1 33%, whereas TDD-5 only 16%. Figure 16 depicts the probability histogram of TDD configurations, considering SNR = 0dB, W = 200 kbits and L_{ftp} = 800 kbits. In this case, for larger window size, DL-heavy TDD configurations are chosen for most of the radio frames by eNB. Therefore, the shape of the histogram is different and TDD-5 is being chosen 33%, TDD-4 24%, whereas TDD-0 3% and TDD-1 13%.

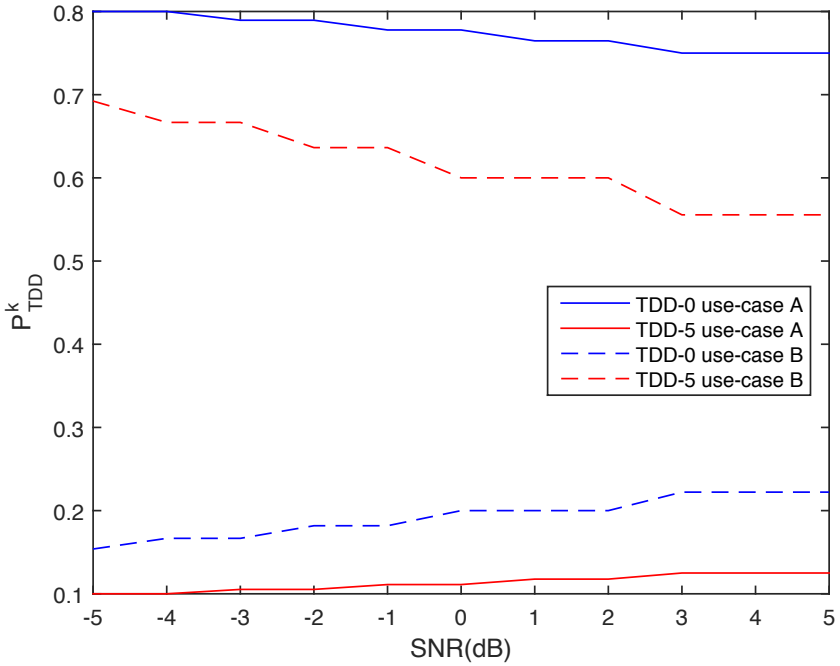

Figure 14. Probability of TDD configuration vs SNR [Use-case A, Use-case B] for TDD Configurations 0 and 5

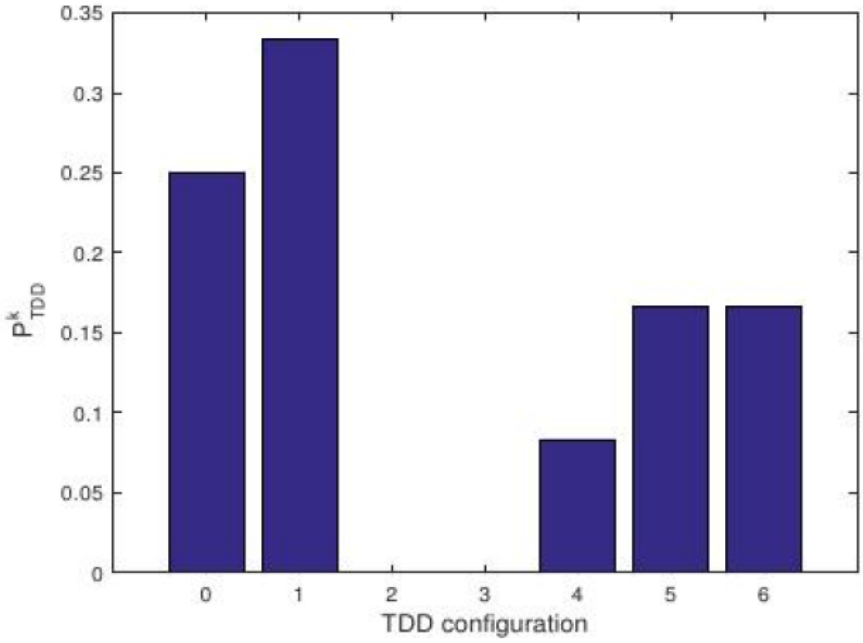

Figure 15. Probability vs TDD configurations for W = 20 kbits, L_{ftp} = 800 Kbits and SNR = 0 dB

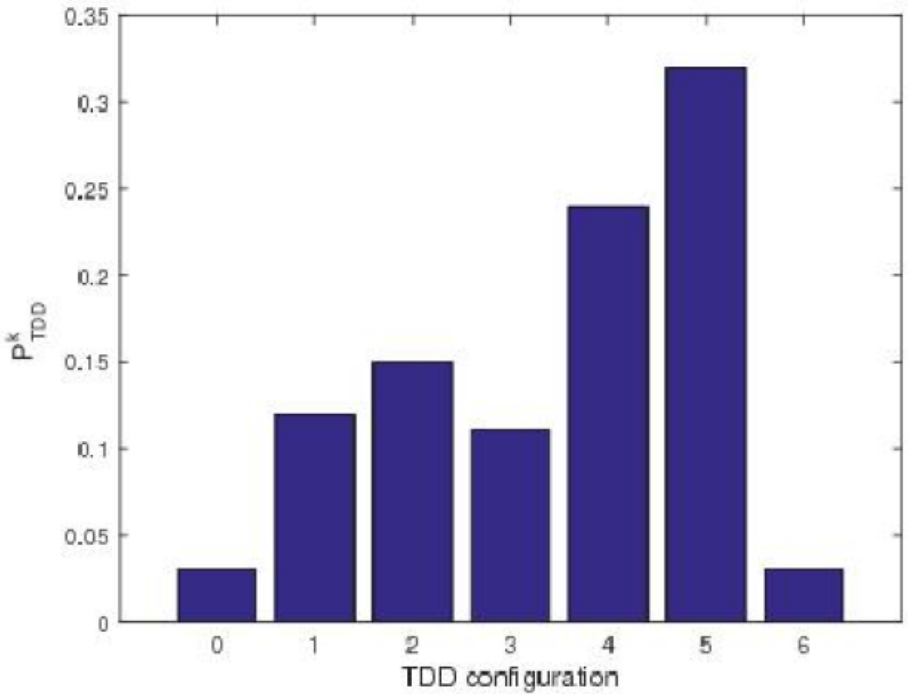

Figure 16. Probability vs TDD configurations for W = 200 Kbits, L_{ftp} = 800 Kbits and SNR = 0 dB

2.2.4 Conclusion

In this work, we provided a cross-layer framework for FDD-TDD CA . To this end, we first provide the corresponding CLD of the TDD mode transmission in order to formulate the achievable throughput under particular QoS constraints. Having obtained the analysis, we carry out simulations highlighting the tradeoffs towards making decisions of the most suitable TDD modes under certain channel conditions and requirements. Thus, a TDD frame adaptation framework for the 3GPP LTE-A system, which enables the dynamic TDD frame adaptation within the context of FDD-TDD CA. The TDD frame adaptation is configured using the DL and UL frames ratio derived from the utility function defined to this end. Simulation results were carried out, which reveal the probability distribution for the different TDD frame format configurations that was chosen by the eNodeB under certain channel conditions and QoS requirements.

2.3 Carrier-Aggregated Decoupled Downlink and Uplink 5G Systems

To address capacity issues in mobile communications systems, a set of technology enablers have become popular: (i) heterogeneous network (HetNet) designs, (ii) carrier aggregation (CA); and very recently (iii) downlink (DL) and uplink (UL) decoupling (DUDe). Proper cell and link selection during mobility and handovers is one of the most challenging tasks for emerging 5G systems if they are to leverage on these enablers. With the aim of significantly improving the UL communications, this section introduces and investigates the novel concept of CA-DUDe. In the light of inter-band CA, several association opportunities arise: first, allowing full flexibility, each UL carrier is connected to the cell that receives its highest power; second, both UL carriers are jointly decoupled at the same time. With the use of stochastic geometry this novel proposal is analyzed and compared against the classical DL received power association rule. Poisson point process and system level simulations under realistic

considerations demonstrating the benefits of the concept underpin a rigorous mathematical analysis.

DUDe is defined under the umbrella of dual connectivity, where one UE receives from, or transmits to, more than one cell. Besides, CA allows other system design options, for instance, inter-node radio resource aggregation is a potential solution to improve the cell edge throughput. This is particularly suitable for inter-band CA co-channel deployments, where the coverage region of both CCs are different. Given the scarcity of spectrum, full frequency reuse is typically aimed to maximize capacity. Hence, a HetNet deployed in such conditions must:

- Homogenize both the quality of experience (QoE) of all UEs, and the UL and DL data rates, allowing more flexible connections among cells.
- Control the generated interference not to impair the spectral efficiency.

To this end, here we propose the inclusion of DUDe in carrier-aggregating HetNets. An extension of the decoupled concept is studied, where each carrier can be associated independently based on the received power. As we thoroughly study here, when carriers from different bands are aggregated, and different radio propagation conditions are considered in both tiers and frequency, one UE may have two different serving cells in the UL. The main novelty presented in this work can be summarized as the recognition and study of all the possible combinations of association cases. In particular, three association rules are compared:

1. **PCD: Per Carrier DUDe.** This is a fully flexible association rule in which each UL carrier associates independently to the cell which receives the highest signal power. Note that to have different UL carriers connected to different cells, particular propagation conditions must be considered in both tiers, figure 1(a). This work constitutes the first study that considers different pathloss on each carrier and tier.
2. **BCD: Both Carriers DUDe.** A second case in which both carriers are decoupled together considering the association linked to the lowest frequency received power, shown in Figure X(b).
3. **DLRP: DL Received Power.** The classical association policy.

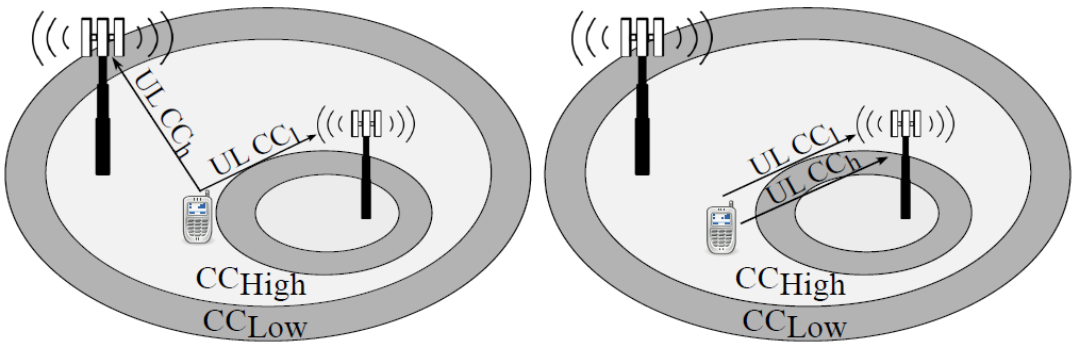

(a) Per-carrier UL/DL decoupling **(b) Both carriers UL/DL decoupling**

Figure 17. Decoupled associations studied, with the downlink not shown here since focus is on the uplink only.

2.3.1 System Model

Detailed information and derivation of our system model is available in [Lem2016]. In one sense, we define 4 cases and two sub-cases of one of those cases, reflecting the association of a device with the available Macro-cell (MCell) and Small-cell (SCell) for the given carriers. The cases defined are:

Case 1: All carriers connected to the MCell.

Case 2: DL connected to MCell and UL connected to SCell.

Case 2.1: The lowest frequency is associated to the SCell in the UL, and the highest frequency remains associated to the MCell for both links, UL and DL. This case is depicted in Figure X(a).

Case 2.2: All DL carriers are connected to the MCell and UL carriers are connected to the SCell, as shown in figure 1(b).

Case 3: DL connected to SCell and UL connected to MCell.

Case 4: All carriers associated to the SCell.

We then assess the probabilities of these happening as a range of input parameters, and derive overall results for a number of performance indicators as the results for each of these cases happening weighted by the probabilities of them happening.

2.3.2 Results

Numerical results

Table 3 summarizes configuration parameters. Here, P_m, P_s and P_d are respectively the transmission powers of the MCells, SCells, and devices, and λ_m and λ_d are the densities of the MCells and devices. **Table 4** expands further on all such notification used throughout this section and in [Lem2016].

Table 3. Configuration parameters for numerical results.

Parameter	Value	Parameter	Value
P_m, P_s	43 dBm, 20 dBm	P_d	23 dBm
λ_m	$1.47 * 10^{-5}$ MCells/Area	λ_d	0.037 UEs/Area
CC Bandwidth	20 MHz	Scenario layout	1650 m x 1650 m

Table 4. Mathematical notation.

Parameter	Value
Φ_v	PPP process
λ	Intensity
P_v	Transmit power
CC_i	Frequency CC
α_v	Path-loss exponent
x_v	Position of cell with respect to the origin
$\|x_v\|$, X_v	Distance of serving cell
S_v^{DL}	DL Received power
S_v^{UL}	UL Received power
C_{f_i}	Frequency dependent path-loss
β_v	Frequency dependent path-loss exponent
γ_v^{UL}	UL SINR
C_{x_v}	Capacity
σ^2	Noise power
I_{x_j}	Aggregate interference
R_j	Distance of interferer UE to its corresponding cell
$\|x_j\|$	Distance of interferer UE to target cell
P_0, γ	Open Loop Power Control

Figure 18(a) depicts the analytical and the simulated results for the association probability. In the figure, the line corresponds to the simulated result and the bullets are the probabilities obtained analytically. Results are very much aligned with the ones obtained in the literature for single carrier DUDe: as the density of the SCells increases the probability of decoupling one or both UL carriers is higher. However, note that per-carrier decoupling is very unlikely. This is because both frequency carriers are very close in band, so propagation losses are very similar. Figure 18(b) shows the case in which CCs are in very separated bands and then, it is remarkable the change in the association probabilities and in particular the per-carrier decoupling. The low frequency coverage grows, while the high frequency coverage shrinks, therefore the probability of each carrier having different optimal serving cells increases. This is an important observation given the disjoint pieces of spectrum that operators usually have in very different bands and the new for spectrum aggregation.

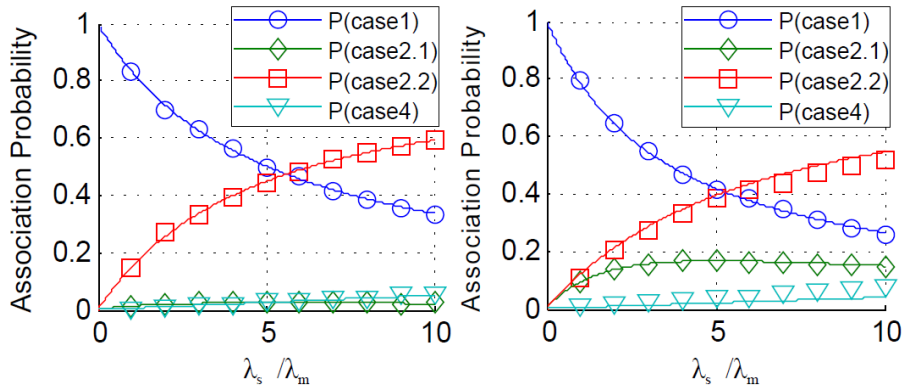

(a) 2 and 2.6 GHz carriers (b) 800MHz and 5 GHz carriers

Figure 18. Association probability with PCD, $\alpha = 3$, $\beta_m = 2$, $\beta_s = 2.55$.

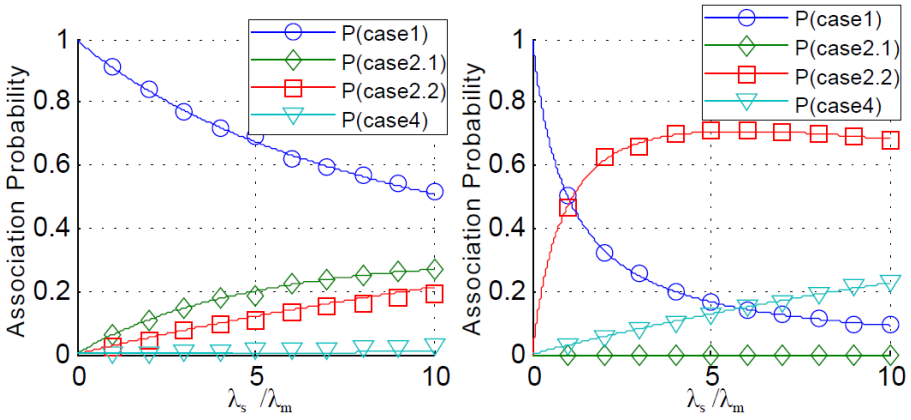

(a) $\beta_m = 2, \beta_s = 3$ (b) $\beta_m = \beta_s = 2$

Figure 19. Association probability with PCD, 800MHz and 5 GHz carriers, β_v impact $\alpha = 3$.

However, not only the frequency carrier affects the frequency dependent pathloss, it is also affected by β_v, the frequency dependent pathloss exponent, it is assumed that $\beta_m < \beta_s$. Figure 19 (a) shows the association when $\beta_s = 3$. When the propagation conditions in the SCell are deteriorated because of the increase in β_s, the probability of having only the lowest frequency decoupled increases (case 2.1), and it overpasses the probability of having both carriers decoupled. To have both UL carriers connected to the SCell, case 2.2, the events on the high frequency CC must be satisfied, according to the analysis in section II-B. Therefore, if the SCell provides a higher source of loss (owing to the rise of β_s) less UEs will decouple both carriers. Instead they will remain connected to the MCell, as it is the optimal option in terms of UL received power. On the other hand, if both cells provide the same frequency dependent pathloss because $\beta_m = \beta_s$, the probability of frequency dependent decoupling is nonexistent, as shown in Figure 19 (b) In this situation both frequency dependent pathloss components are equal generating the same coverage footprint, thus, when one CC is de-coupled the other is also. In this sense, there are no events that satisfy the probability of case 2.1.

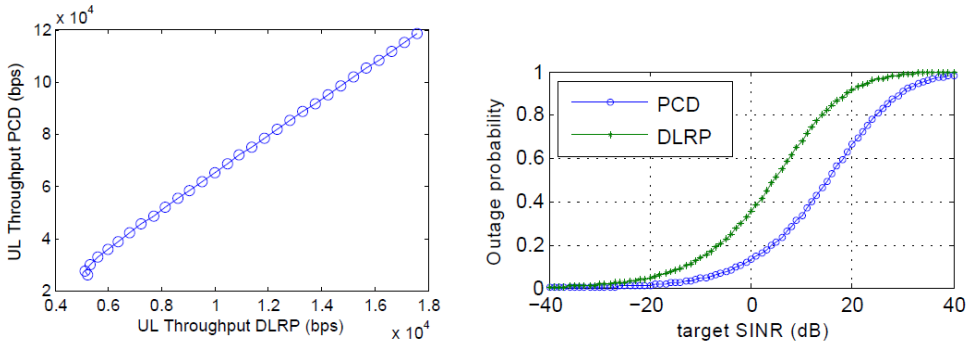

(a) Analytical UL Throughput (b) Analytical Outage

Figure 20. PCD vs DLRP, 800MHz and 2.6 GHz carriers, $\alpha = 4, \beta_m = 2, \beta_s = 2.55$.

Results for the suboptimal association rule with DLRP are compared with the PCD association case. Owing to the different propagation conditions, because β_m != β_s, the pathloss experienced in the high-frequency CC (CC_h) is lower to the MCell and the pathloss perceived in the low-frequency CC (CC_l) is lower to the SCell. In this regard, in CC_l, the suboptimal association following DLRP would be to the MCell. Based on the distance distribution to both cells for case 2.1, immediate gains can be inferred when decoupling, because the UE transmits to the cell which is the nearest. The suboptimal association provides a much poorer connection, essentially because the distance dependent path-loss is much lower towards the SCell than to the MCell. As a result the overall path-loss to the SCell is lower though the frequency dependent one is higher (because $\beta_s > \beta_m$).

Figure 20 (a) compares the UL achieved throughput with PCD association and the suboptimal DLRP association for a range of SCell densities. Each marker represented in the curve is the resulting throughput with each association rule, and goes from a less to a more dense network ($\lambda_s = \lambda_m$, $\lambda_s = 30\lambda_m$). UL throughput is calculated by multiplying the spectral efficiency derived in Section II-C2 of [Lem2016] by B/N_α, where B is the carrier bandwidth and N_α corresponds to the average number of associated users. Recall that the spectral efficiency and hence the achieved throughput are conditioned to the probability of case 2.1. There is an almost linear improvement when decoupling, as the SCell density grows. This is due to two main reasons: improvement in distance dependent path-loss and lower load N_α in the SCell. Significant gains in outage are also noted in Figure 20(b).

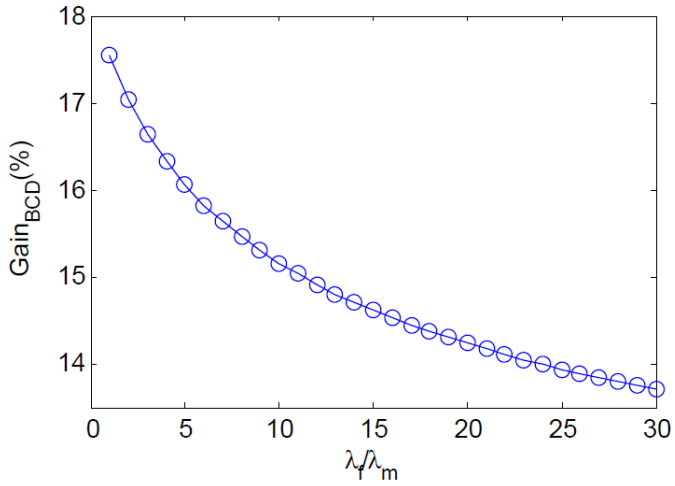

Figure 21. Gain in throughput, PCD vs BCD, 800MHz and 2.6 GHz carriers, $\alpha_p = 2, \beta_m = 2, \beta_s = 2.55$.

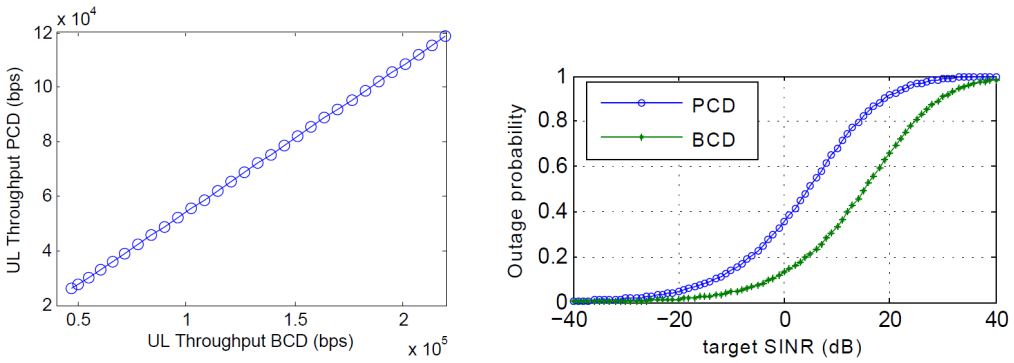

(a) Analytical UL Throughput (b) Analytical Outage. $\lambda_s/\lambda_m = 5$

Figure 22. PCD vs BCD, 800MHz and 2.6 GHz carriers, $\alpha_p = 4, \beta_m = 2, \beta_s = 2.55$.

Full flexibility is understood as the possibility of decoupling the UL carriers separately. The fully flexible PCD case is compared to the BCD one, in which both carriers are decoupled to the SCell based on the low frequency CC. Figure 21 shows the gain in UL throughput for an special case where only noise power is considered. Again, each marker represented in the curve corresponds to the gain obtained in throughput for one particular SCell density. Results in terms of UL throughput and outage are shown in Figure 22(a) and (b), respectively. Despite the relative benefits of PCD over BCD otherwise, when interference is considered, significant benefits of BCD over PCD can be seen. Since the interference depends on the distance distribution, when considering interferences is better to decouple both carriers together.

In general, these results demonstrate enhancement through SOLDER solutions of the throughput KPI defined in SOLDER D2.3 [D2.3], as well as others such as outage.

System-Level Simulations

System-level simulations of the performances of the spectrum aggregation decoupling schemes have also been undertaken. **Table 5** presents simulation scenario assumptions.

Table 5. Simulation scenario assumptions.

Parameter	Value	Parameter	Value
Bandwidth	2 x 80 PRBs	Carrier Frequency	800 MHz and 2.6 GHz
MCell ISD[1]	500 m	SCell minimum ISD	25 m
SCell-MCell minimum ISD	75 m	P_s, P_m	20 dBm, 43 dBm
SRS DLRP, SRS DUDe	8 PRBs, 16 PRBs	UEs served per TTI	10
Number of UEs connected	1000	UE Buffer size	1 Mb
Target BLER	10 %	$\alpha_s = \alpha_m$	3
β_s, β_m	2.55, 2	λ_s/λ_m	5

[1] ISD: Inter-site distance

Results in terms of association modes compare well and are as expected contrasting with the analytical results presented above. Further, **Table 6** shows that there is a significant preference for both-carrier and per-carrier association modes in CA scenarios. Figure 23, as one further (non-exhaustive) example of the results obtained under this work, shows the clear system-level throughput benefits of PCD and BCD. It is shown that the UE throughput on the uplink is almost doubled on average through the decoupling schemes shown. This meets an objective of improving throughput through the carrier aggregation scenarios as quoted in D2.3 [D2.3].

Table 6. Percentage of UEs transmitting in different association modes.

Strategy	CA Users
DLRP	48.7%
BCD	72.7%
PCD	72.4%

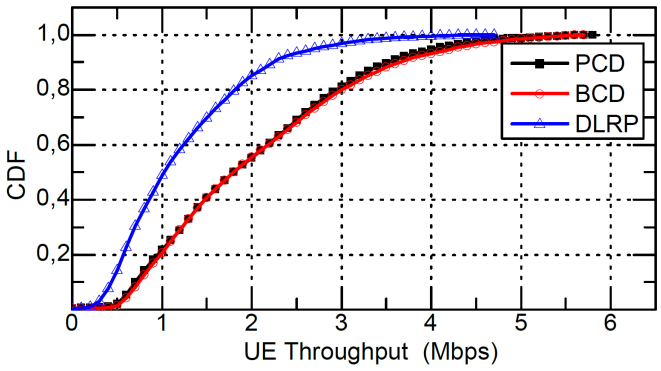

Figure 23. CDF of UE throughput distribution for PCD, BCD and DLRP association strategies.

2.3.3 Conclusion

HetNet scenarios imply significant differences in characteristics of the small-cells and macro-cells serving users, with the natures of those differences varying between the downlink and uplink. Therefore, it is very often more optimal to handle the downlink and uplink independently when choosing to associate with a macro-cell or small-cell, rather than both the downlink and uplink being served together either by the macro-cell or small-cell. This particularly applies in the context of aggregation, where the differences between frequency bands used for aggregation purposes lead to the need to handle the bands differently for aggregation purposes, e.g., it may be best for only one of the carriers to be served by the small-cell on the uplink, as opposed to moving them to the small-cell together.

This section provides the schemes for per-carrier and both-carrier decoupling in the light of this, and has investigated the benefits of the concept for a number of metrics and against the classical downlink received power association policy. Considerable gains in throughput and reductions in outage probability, among other measures, are shown. The results presented show that the solutions that can address aspirations regarding enhancements of KPIs such as throughput, given in D2.3 [D2.3].

The reader is encouraged to refer to Appendix 2.3 for a more detailed treatment of the solutions addressed in this section.

3. H-RAT aggregation

3.1 LTE+Wifi aggregation

3.1.1 Overview

As an alternative to the LTE-U scenario, operators and also the 3GPP is working on a tighter integration between LTE and WiFi without modifying the actual access technology. It is already possible to integrate WiFi into an LTE core network, but there is no seamless service handover between the two. In 3GPP Rel13 a study item on LTE-WLAN Radio Level Integration and Interworking Enhancement has been proposed that studies the possibility of aggregation of LTE and WiFi at the level of PDCP, while keeping the MAC and the PHY layer of WiFi "as is". In SOLDER we study the benefits of this scenario from a system level perspective using closed form expressions, thus avoiding averaging problems and complex system-level simulations. The methodology is based on two main analytical tools (stochastic geometry and queuing theory) as well as appropriate abstraction of different radio access technologies.

3.1.2 PHY and MAC layer modelling of LTE and WiFi

In order to proceed to a valuable performance analysis of LTE and WiFi Networks, we should first model both PHY and MAC layers of those. We have finalized this modelling procedure; can be found at Appendix 3.1.1. Our physical layer abstraction consists a mapping between user's SINR and their corresponding rate. On the other hand, we propose a proper queue models to represent the schedulers of each radio access technique (RAT), on the MAC layer.

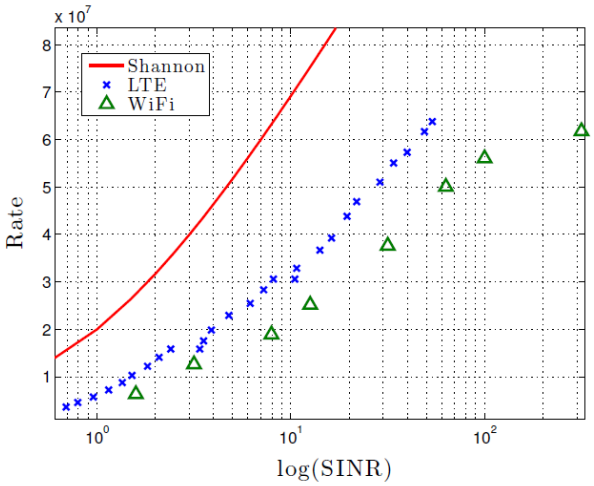

Figure 24 Comparison between MCS-base rates per RAT and Shannon's limit

Figure 24 presents the result of the above-mentioned PHY modelling procedure. We note here that it is common, when analyzing wireless networks, to use the Shannon's theorem to derive SINR-rate relationship, as actual RATs do not provide an elegant way to calculate the user's MCS and related rate. When a single network is analyzed, this assumption does not affect the validity of the qualitative results. However, in the case of HetNets, and especially HetNets operating with different RAT, this assumption does not hold, as the offered user rate does not scale the same with respect to SINR, for different RATs. For instance, the case of LTE and WiFi as presented in Figure 24. It is evident that LTE is, on average, 37% closer to

the Shannon rate compared to WiFi, for their common operating SINR range. Hence, if we were to model the SINR-rate relation for both LTE and WiFi according to the Shannon formula, we would significantly overestimate the performance of the WiFi tier.

Regarding to the MAC layer modelling, a simplified but still accurate approach of LTE scheduler is like a resource fair scheduler and can be modelled as M/G/1/PS (Processor Shearing) queue. The WiFi scheduler is operating close to throughput fait scheduler and can be modelled as a discriminatory PS queue. Unfortunately, discriminatory PS queue does not have closed form expression to calculate the average delay of the system. But as we see on Appendix 3.1.1 and Appendix 3.1.4 the common (egalitarian) PS as lower bound and the Avrachenkov's asymptotic approximation provide us very accurate results for the WiFi case for various values of flow/file sizes.

Figure 25 shows the theoretical delay of Resource Fair scheduler and Avrachenkov's approximation as well as the simulation results of Throughput Fair scheduler using WiFi's PHY characteristics and flow size equal with 1Mb (left) and 100Mb (right).

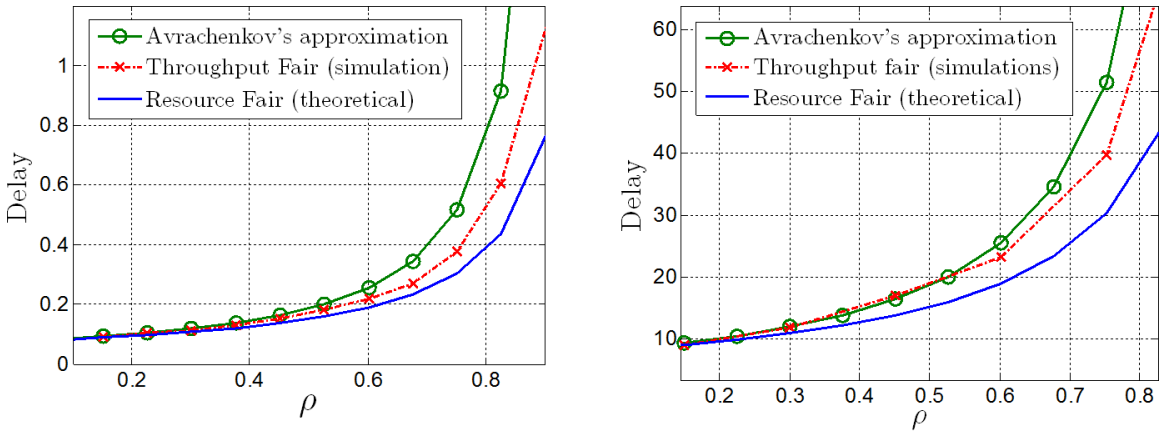

Figure 25 (left) comparison between Resources Fair, Avrachenkov's approximation and simulation data for (left) 1Mb and (right) 100Mb

3.1.3 Throughput analysis of two-tier HetNets

In Appendix 3.1.2, we use stochastic geometry in order to obtain the SINR statistics of random placed Base Stations (both eNodeBs and WiFi's AP) with different densities, transmit powers and Radio Access Technologies (RATs). Also, the users are assumed saturated (or with infinite demands / requirements). Combining the SINR statistics with the above-mentioned PHY layer modelling, we developed a flexible and accurate model in order to analyse the performance of heterogeneous cellular networks (HetNets). As performance metric we chose the average user rate and the congestion probability. Congestion probability is the probability that the providing user rate is less than a minimum threshold.

Novel elements of this work are i) the probabilistic approach to model network topologies and the number of associated users by stochastic geometry ii) the realistic modelling of different radio access techniques, in order to calculate the rate, instead of Shannon's law, which is problematic in the case of HetNets iii) we use our analytical framework to study the impact of popular user association policies like *Offload* (all users within range of a WiFi AP are associated to the WiFi network), *max-SINR*(a user is associated with the BS offering the best SINR, among any tier), and *max-RATE* (taking into consideration that different RAT achieving different rates for common SINR).

Figure 26 presents the performance of different association criterions. We see that the performance of *max-SINR* and *max-Rate* differs due to the heterogeneity of RATs (the

tier which provides the higher SINR is not mandatory the tier which provides the higher Rate).

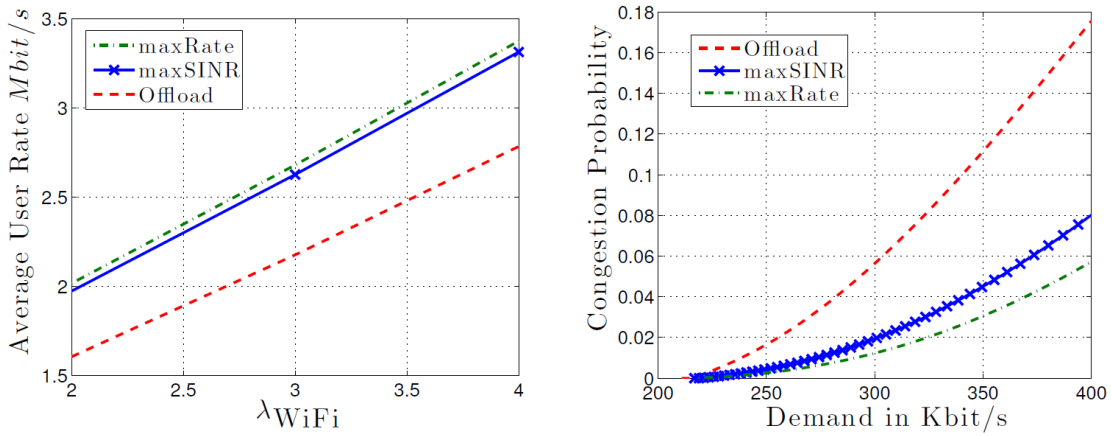

Figure 26 (left)Average user rate w.r.t. density of the secondary WiFi network, density of LTE BS is 1 and density of users 100, (right) Congestion Probability w.r.t. minimum demand

3.1.4 An Analytical Model for Flow-level Performance of Randomly Placed Cell Networks

In the next work (see Appendix 3.1.3), the scheduler of each RAT is modelled as a queuing system (section 3.1.2) in order to extend our analysis for non-saturated users and to provide an analytical model for flow-level performance of a random placed cellular network. Our performance metrics are the average network load, median user's delay and the congestion probability of the arbitrary BS.

As we already mentioned, to achieve this, we base our analysis on two main tools: (a) stochastic geometry, to understand the impact of topological randomness and intra- and inter-tier interaction in resulting coverage area, and (b) queueing theory, to model the competition between concurrent flows within the same BS, for each RAT.

The contributions of this work are i) We propose an analytical model that captures both physical and MAC layers performance, providing statistics for coverage maps and MCS distributions, as well as flow-level performance as perceived by the user (flow delay) and the network operator (average load, congestion probability); ii) We derive a semi-analytical model that computes the coverage probability of a random placed network, considering the fact that neighbouring BSs are not fully loaded (non-saturated) and thus create dynamic interference proportional to their load.

As we saw there is a huge gap at the performance results if assumed that the neighbouring BSs are interfering constantly (always ON) or if we assume that the interference of each BS is load based. Additionally, we implement a simulator to implement those scenarios in order to verify our theoretical estimations.

Figure 27 shows the performance of an LTE network, two first comments are i) both of theoretical results are quite accurate, ii) the gap between always ON and load-based interference could be extremely high. In Figure 27 (right) for flow density $\lambda_f = 0.015$ the always ON prediction is that the network is 70% loaded instead of 30% of the load-based. That means that the network could be much more robust w.r.t. data traffic than the studies that assume saturated BSs predict.

In Figure 27 (middle) for high density of BS always ON model predicts 50% utilized network, while load-based only 15%. The gap between always ON and load-based prediction increases w.r.t. density of the network. This happens because saturated analysis is able to capture only the gain coming from the fact that an ”arbitrary” BS on average serves fewer users at a denser network, but not the gain coming from the fact that surroundings BSs will be less loaded, and therefore will cause less interference. Thus, the gain to deploy a denser network is much higher than predicted by an analysis that does not take the load-depended interference into account.

Figure 27 (left), shows the median delay of the simulator as well as the theoretical predictions for saturated and load-based cases. Again the theoretical predictions are quite accurate, on the other hand, always ON interference differs orders of magnitude from the load based due to delay's sensitivity at average service rate.

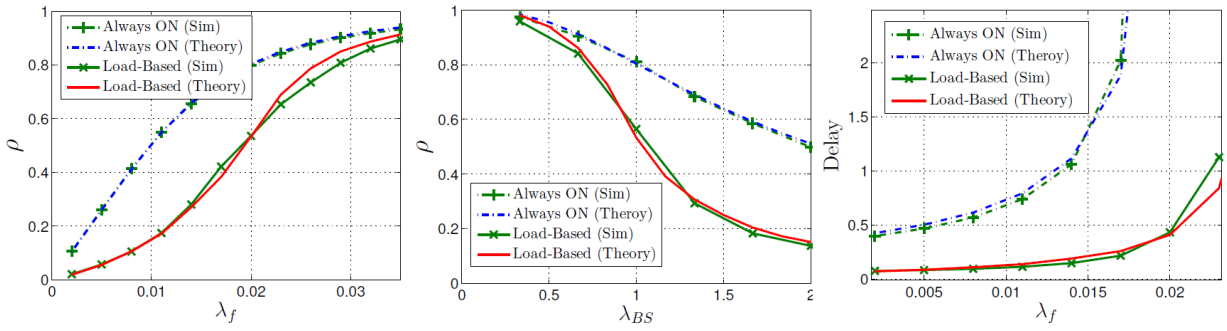

Figure 27 Performance / Validation plots for always-ON, load-based and simulation results

Figure 28 present the performance of both LTE and WiFi networks. First, focusing on the saturated case, perhaps is not clear why LTE network performs worst than WiFi, especially if we take into account that for same SINR, LTE operates with higher rate. The reason are the edge users, since LTE is much more robust to low SINR compared to WiF. Users with low SINR, are achieving a low bit rate in LTE, as opposed to WiFi where they would be regarded as "out of service", and therefore are not taken into consideration. We should mention that on the one hand both networks have the same number of connected users, but on the other hand LTE network's coverage area is wider than WiFi. For the always ON case, coverage area is 0.67 and 0.47 of the total area for LTE and WiFi networks respectively.

The values of coverage area, are drasticly dependend on load, for low values of load the coverage area is almost 1 for both RATs, while for a load around $\rho = 0.5$ coverage areas are 0.9 and 0.7 for LTE and WiFi respectively.

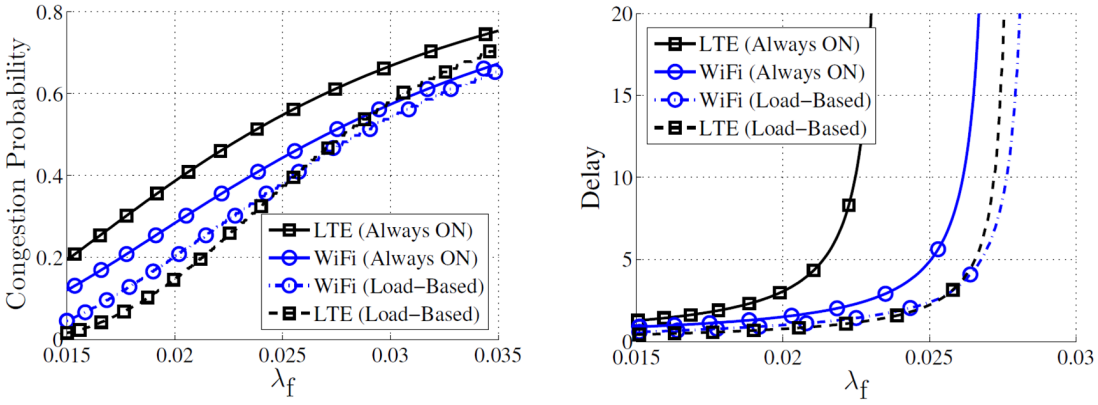

Figure 28 Flow level performance of LTE and WiFi networks

Another interesting remark is that for low or middle-load scenarios in contradiction to always ON case the LTE operates better than WiFi, this happened due to LTE's smaller granularity between the MCS. Those two reason leads the LTE to taking more advantage from SINR improvement. As the load increases the two networks approaching the always ON case which WiFi operates better.

3.1.5 An Analytical Model for Flow-level Performance in Heterogeneous Networks

In the next work (see Appendix 3.1.4) we generalised the aforementioned to K-tiers HetNets, in order to analyse the flow level performance (median delay, average network load and congestion probability) of different association criteria.

Thus, the main contribution of this work is that use our analytical framework to study the impact of popular user association policies like *Offload* (all users within range of a WiFi AP are associated to the WiFi network), *Max-SINR* (a user is associated with the BS offering the best SINR, among any tier), and *Min-Delay* (a user is associated with the BS which offering the best combination of throughput and load in order to minimize the average delay.

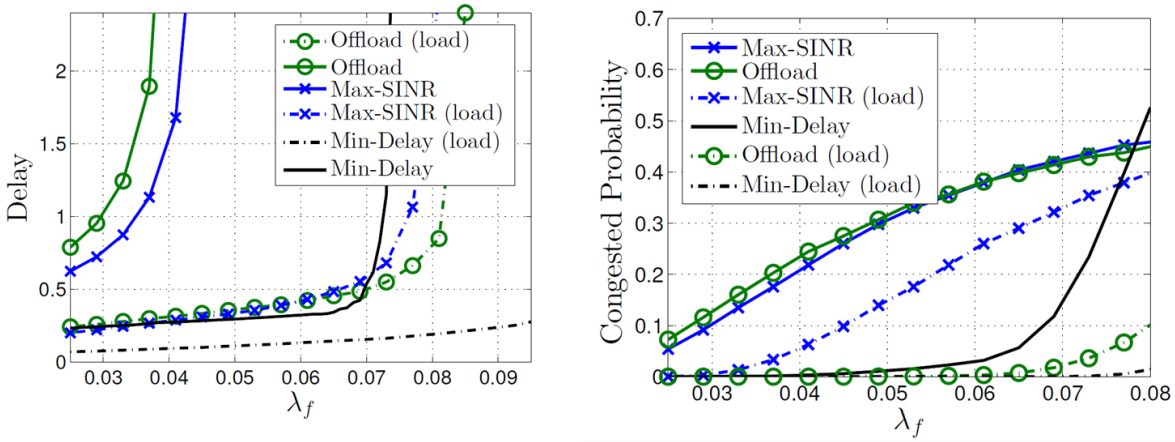

Figure 29 Flow-level performance of different association criteria

Figure 29 presents flow-level performance (delay and congestion probability) of different assosiation crteria. The scenario consists an LTE primary network of desity $\lambda_{LTE} = 1$, a WiFi secondary of density $\lambda_{WiFi} = 5$ and users with $\lambda_u = 100$. Focusing on *Offload* and *Max-SINR* criteria, at saturated case the congested probability of both cases is almost equal,

but respect to median delay, *Max-SINR* performs better. On the other hand, assuming load-based interference *Offload* is much more robust with respect to congestion probability and additionally performs better than *Max-SINR* and with respect to delay as well.

This inconsistency between saturated and load-based cases originates from fact that saturated analysis is able to capture only one part of denser network gain. On the one hand saturated case catching the point that the "arbitrary" BS on average serves less users at a denser network, but on the other hand fails to capture that the surroundings BSs will be less loaded as well, and therefore cause less interference. Due to the previews, saturated case underestimates association schemes that utilize more the denser network

Additionally, as expected, the *Min-Delay* association scheme that taking into account the load in order to minimize the delay is operates orders of magnitude batter than the other "dummies" criteria with respect to median delay.

3.1.6 Conclusion

We have presented an analytical framework for an accurate prediction of the flow-level performance of a large randomly placed network. This analysis considers both the case of always ON interfering neighboring BSs, as well as the case of load-depended interference. It turns out that the performance gap between the aforementioned cases could be rather high, affecting not only quantitative insights, but often qualitative conclusions as well, and thus should be carefully taken into account during network design. Additionally, we have considered multi-tier topologies, modeling some common associated criteria, and evaluating their impact on both user- and network-centric performance. This initial study was not meant to be conclusive, given the large range of parameters and degrees of freedom in such multi-tier scenarios, but rather to provide some initial representative insights, and demonstrate the utility of our proposed analytical framework.

Here we can point three general conclusions: i) The scheduling policy could strongly effect system's flow-level performance, even if the PHY characteristics are the same. ii) The two different interference approaches, always ON and load-based, change totally the performance of the system (single-tier or multi-tier), so we should be very careful about this assumption when model a system. iii) Comparing the different association schemes, the gain of the load related association policy is surprisingly high comparing to the more traditional criteria (Off-load Max-SINR).

3.2 Dynamic spectrum reallocation in multi-RAT networks

A promising way of providing more spectrum to LTE-A systems is by coordinating the exploitation of spectrum assigned to multiple legacy RATs and reallocate it to LTE-A systems where the need is greater. 3GPP has issued a study about the joint coordination of m-RAT systems [3GPP37.870], in order to describe the cases where coordination mechanisms can be applied between different RATs in order to efficiently exploit a spectrum band that is gradually abandoned by a legacy RAT, creating spectrum holes, and assign the surplus spectrum to the LTE-A. This additional spectrum to the LTE-A system can be utilized using CA for dynamic spectrum expansion.

Our proposed solution is the provision of two different functionalities in m-RAT CA systems in order to utilize the bandwidth of a frequency band more efficiently. The first option suggests that the legacy RAT reserves the amount of bandwidth needed to ensure a minimum performance guarantee for its users and the rest of the bandwidth is utilized by LTE-A. For the second option, both spectrum and resource allocation are handled jointly for both RATs

in a more efficient but also more complex manner. Both solutions are very important for dynamic SR in cases where the legacy RAT has decreasing bandwidth requirements due to the reduction of users, while LTE-A networks require more spectrum.

3.2.1 Overview of Spectrum Reallocation and Refarming

3GPP defines the Spectrum ReFarming (SRF) and Spectrum Reallocation (SR) in [3GPP37.870]. In particular, the SR is the term used to describe the procedure of reallocating spectrum that is initially assigned to some legacy RAT, to the spectrum demanding LTE-A technology. This procedure can be applied in several cases with respect to the frequency at which reallocation decisions are made depending on the traffic load of legacy RAT and LTE-A networks. The cases of SR considered are the followings:

- *Dynamic:* SR occurs every few seconds/minutes. It can guarantee maximum efficiency and utilization of spectrum resources for all co-deployed RATs.
- *Semi-static:* SR occurs every few hours/days. Several preconfigured plans can be defined to alter resource partitioning between RATs in a fixed way according to current traffic conditions and requirements.
- *Static:* SR occurs every few months/years. This is the case of the so called SRF, where a legacy RAT band is reallocated permanently to LTE for exclusive exploitation, where obviously SRF is a sub-category of SR. The solutions considered so far, only concern static and semi-static SR due to the fact that the required mechanisms to exchange data between RATs are simple. However, the gains of Dynamic SR (DSR), where spectrum and resource allocation decisions are made more frequently are expected to overcome the increased architectural complexity it entails.

The effect of SR is visualized in Figure 31. The Legacy RAT is assigned with sometimes too much spectrum, resulting in an underutilized part. This part becomes shared under the SR concept and can be assigned to either RAT (Legacy or LTE-A). Two considerations of SR are displayed. In the first case, Static Spectrum Reallocation (i.e. SRF), where the shared band is exclusively reallocated to LTE-A. In the case of DSR however the assignment of the shared band between the two RATs is made dynamically according to the traffic load of each RAT, aiming to satisfy both legacy and LTE-A users as efficiently as possible.

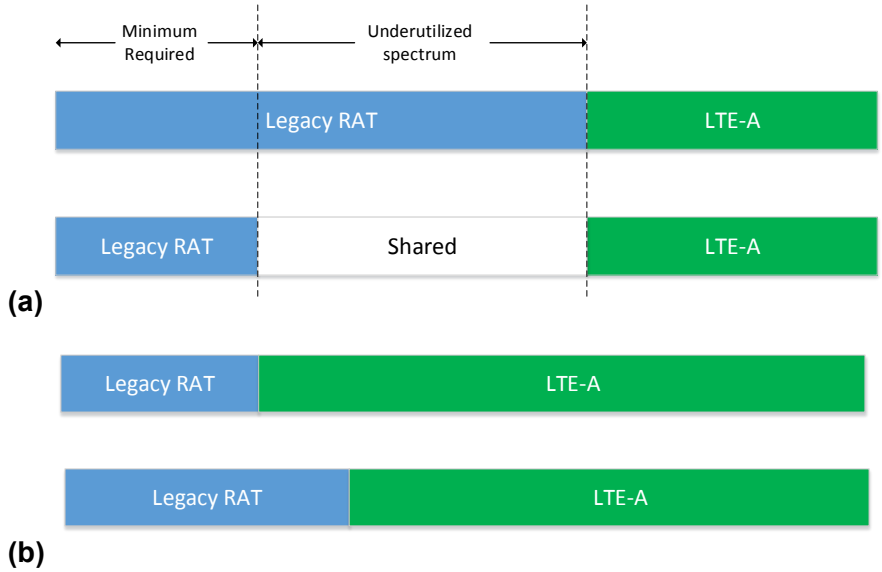

Figure 30 (a) Original Spectrum Allocation and Spectrum Reallocation concept. (b) Static Spectrum Reallocation (Spectrum Refarming) and Dynamic Spectrum Reallocation.

Further, the key idea about m-RAT joint coordination is to define under which conditions different RATs deployed in the same geographical area can communicate in order to perform some sort of spectrum assignment and resource allocation, by making as few modifications to the system architecture as possible. Special coordination functions should be implemented for this joint resource allocation at each RAT, or through a coordination point that collects information mainly about the load and the average data rate of the users of each RAT [NGMN]. About the available spectrum, the specified scenarios define that the legacy RAT has a minimum required bandwidth to satisfy a certain data rate need and the rest of it is pooled for the coordination mechanism to decide the allocation. There are two main considerations with different architectural impact on the system as well as potential performance gains for both RAT subscribers. The necessary coordination functions that need to be implemented are marked with gray color in Figure 31.

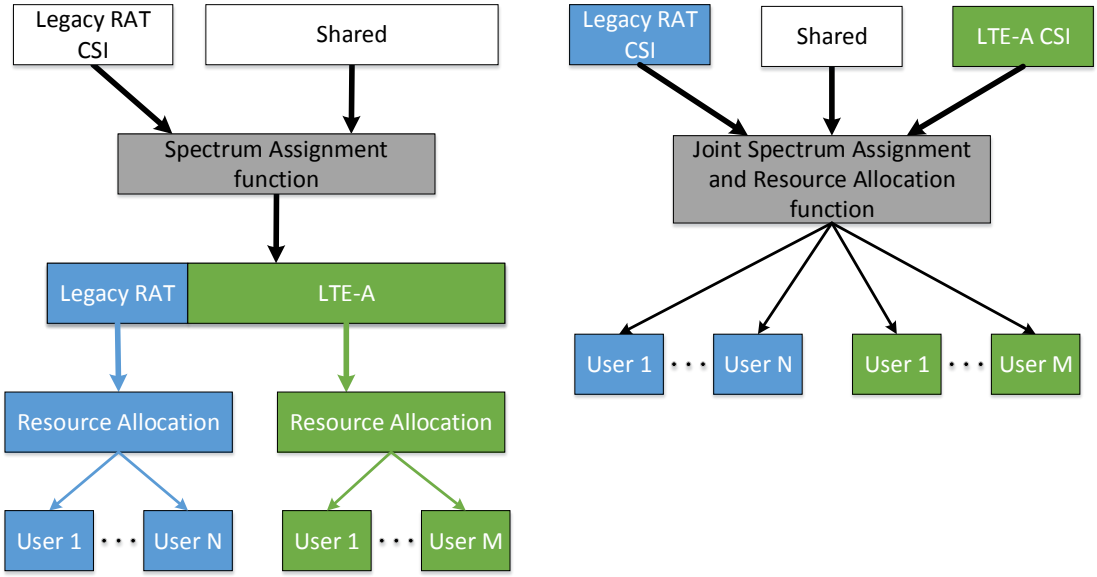

Figure 31: Functional diagrams of Spectrum Assignment (SPA) and Spectrum Assignment and Resource Allocation (SPARA) for the shared band.

3.2.2 m-RAT Spectrum Reallocation Solutions and Results

In this section, we describe how spectrum assignment (SPA) and joint spectrum assignment and resource allocation (SPARA) can be implemented in a specific m-RAT application scenario starting with the simulation setup and continuing with the design solutions including also the results. We assume a continuous bandwidth of 50 MHz like in Figure 31(b). As an example it is noted that such wide bands exist, e.g. bands 1, 3, 7 are even wider at 60, 75 and 70 MHz respectively. Suppose that originally the legacy RAT owned 30 MHz of bandwidth and LTE-A the next 20 MHz. Due to the users migration to LTE-A, the minimum required bandwidth for the legacy RAT has minimized to 10 MHz. The next 20 MHz of spectrum that were previously assigned to the legacy RAT, are now shared with LTE-A, and finally the remaining 20 MHz are still assigned to LTE-A only. The entire bandwidth can be split into a number of CCs that consist a set K. For the rest of the analysis, we define the legacy RAT as RAT-1 to be HSPA and LTE-A as RAT-2, as well as the sets N and M to be the sets of users of RAT-1 and RAT-2 respectively. The development of the simulation and HSPA/LTE processing chains was developed using Matlab. A summary of the simulation parameters used to acquire the results of the proposed solutions is presented in Table I

found in Sec.IV.A in the Appendix 3.2.

The Spectrum Assignment (SPA) and Joint Spectrum Assignment and Resource Allocation (SPARA) algorithms can be found in Sec.IV.B and Sec.IV.C in the the Appendix 3.2. We provide below the results with the corresponding description.

Figure 32 presents the average data rate experienced by the HSPA users. Observe, that when for a specific number of HSPA users we get an increase in bandwidth, as a result of the application of SPA function f1 , there is a corresponding increase to the data rate in Figure 33due to the application of CA. Note that the average data rate is above the threshold in cases where not the entire shared band is assigned to HSPA as a result of f1. If the shared band is assigned to HSPA due to HSPA system load, there is no guarantee about the average data rate performance and thus the average data rate drops below the required threshold, especially in the low SNR case.

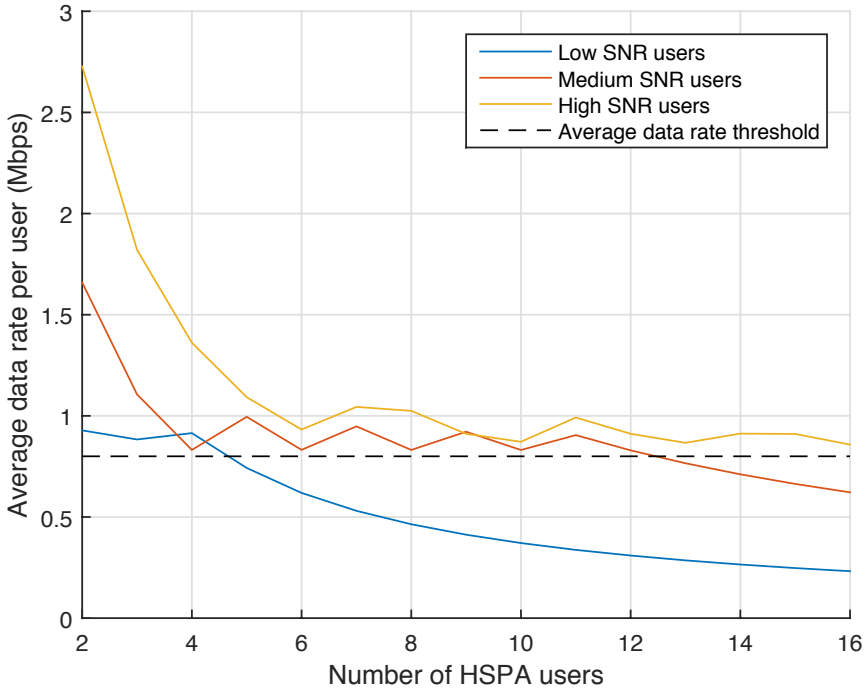

Figure 32: Average data rate over number of HSPA users for SPA implementation.

In the following simulation results, we aim to demonstrate the effect of SPA and joint SPARA on both HSPA and LTE-A RATs and compare the two methods in terms of throughput performance per RAT. In Figure 33, the HSPA user throughput in Mbps is plotted for a number of HSPA/LTE-A users that vary from 2 to 16 each. It is evident that joint SPARA outperforms SPA for every combination of HSPA/LTE-A users. Especially for a low number of HSPA/LTE-A users the benefit is significant due to the low average data rate threshold set by the SPA function. Moreover, we can notice that the joint SPARA functions provides a smoother degradation of performance as both RATs number of users increases. With SPA however, HSPA throughput is unaffected by the increase of LTE-A users and only decreases with the number of HSPA users. This is because SPA considers only HSPA load to allocate spectrum based on a target HSPA rate threshold and resource allocation is handled independently by each RAT.

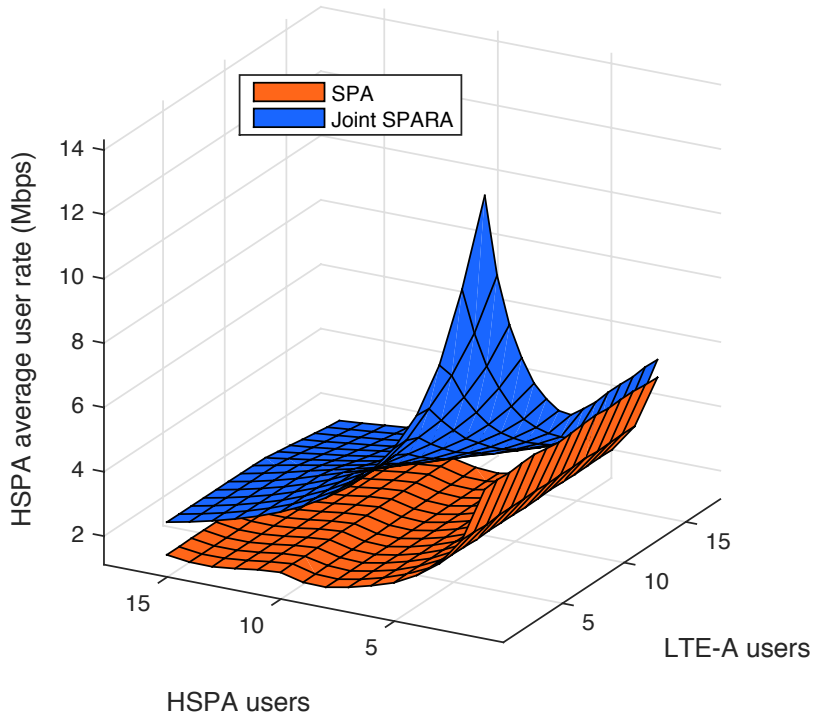

Figure 33: HSPA user throughput versus number of HSPA/LTE-A users.

Similar conclusions are made for LTE-A user throughput as shown in Figure 34. Notice the SPARA surface of Fig. 8 that is always above the respective SPA surface, meaning higher throughput for any number of HSPA/LTE-A users. Again here for a small number of HSPA/LTE-A users the performance is maximized (upper left corner of Fig. 8), while as both HSPA and LTE-A users increase in number, the maximization in throughput is lower. In contrast with Figure 34. it can be seen that the difference in performance between SPA and joint SPARA is not that high, especially for few HSPA/LTE-A user cases. This is due to the data rate threshold set by SPA again. This threshold determines the amount of spectrum that will be spared for LTE-A utilization. This directly affects not only HSPA performance but also LTE-A for the SPA function. Decreasing or increasing the threshold can result in SPA and joint SPARA surfaces in Figure 32 to diverge or converge and in Figure 33 to converge or diverge respectively. With that said, in cases where high average data rates are required by the HSPA network, a SPA solution might be a better choice in order to satisfy HSPA users but LTE-A users will experience as much performance improvement.

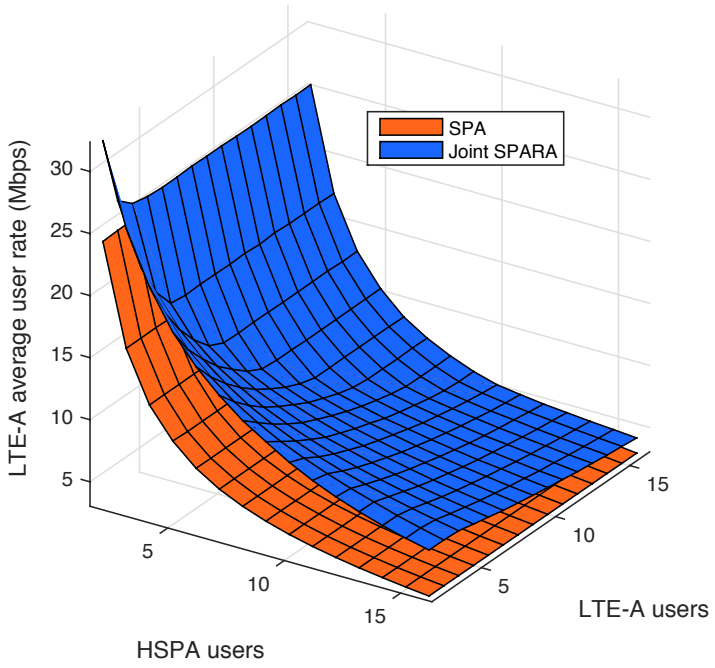

Figure 34: LTE-A user throughput versus number of HSPA/LTE-A users.

3.2.3 Conclusion

Our work on multi-RAT CA is related to the 3GPP concept of joint coordination in multi-RAT networks and the spectrum reallocation feature of Rel.13. Activating CA in such a context, a framework for agile spectrum assignment between a legacy RAT (HSPA), that continuously requires less spectrum to satisfy a decreasing number of subscribers, and LTE-A that needs more spectrum for its users is proposed. In particular, spectrum reallocation can be provided dynamically applying the concept of SPA and joint SPARA. In SPA, the CCs are assigned to HSPA RAT, so that a minimum data rate threshold is provided to HSPA users. The rest of the spectrum can be utilized by CA enabled LTEA users. In SPARA, both HSPA and LTE-A systems utilize the available CCs jointly and are able to provide enhanced performance to their associated users compared to the SPA solution.

3.3 Energy Efficient power allocation for CA systems

3.3.1 Modeling and Analysis

The problem of optimal power allocation design for Carrier Aggregation (CA) enabled systems exploiting multiple Parallel Frequency Bands (PFBs) is investigated, based on an Energy Efficiency (EE) maximization criterion. Both the cases of full Channel State Information at the Transmitter (CSIT) and quantized CSIT are studied and novel EE-optimal power allocation policies are derived. While the initially derived policies consider circuit power consumption to be a deterministic constant, they are then extended such as to account for the fact that, in practice, power consumption is related to the number of system Radio-Frequency (RF) chains actually employed for transmission, that is strongly connected to the number of employed PFBs and transmit antennas. The derived algorithms are used in order to investigate the relation between the system's EE and design parameters, e.g. the number

of PFBs, antennas, and feedback bits. A greedy optimization algorithm is introduced to jointly optimize the aforementioned parameters. By means of simulations is observed that strict constraints on the number of feedback bits limit the achievable EE gains of CA. Moreover, the RF chains power consumption is found to further limit the achievable EE. Finally, it is found that the solution reached by the proposed system optimization algorithm achieves performance almost identical to the optimal solution.

A MISO communications system is considered where communication is achieved using several PFBs by means of CA. That is, the user of interest employs a Frequency Band (FB) B_0 assigned to it for its transmission as well as, by means of CA, the FBs out of the set $\{B_1,...,B_M\}$ that are not employed by any other user of the system. Within a HetNet CA scheme, such a scenario can be encountered for example in the case of a two-tier network consisting of macrocells and small-cells used in order to assist communication. In such a case, band B_0 may correspond to the FB allocated to the user of interest by the macrocell, and FBs $\{B_1,...,B_M\}$ may correspond to the FBs allocated to the same user by nearby small-cells. On the other hand, in the case of a homogeneous network, such a scenario may exist in case that a user exploits, in a CR fashion, resources allocated to other users or cells of the network. More details about our system model can be found in the Appendix 3.3. The system model also provides the required analysis with full and partial (i.e. quantized) CSIT.

Next, we provide the analysis of the energy efficiency and optimal power allocation for systems with perfect CSIT and perfect RF chains. The problem of the optimal design of the power allocation policies $P_m(g,I), m=0,...,M$, provided that (p.t.) $I_m \neq 0, M \succ 1$ can be mathematically expressed as:

$$\max_{P_m(g,I),m=0,...,M,p.t.I_m\neq 0,m\geq 1} : E_{eff} \quad (3)$$

$$\text{subject to: } P_m(g,I) \geq 0, m=0,...,M, \ p.t. I_m \neq 0, m \geq 1.$$

where the optimization problem is concave and it can be solved applying fractional programming principles. Following the procedure that can be found in the Appendix 3.3, the following optimal power allocation is obtained for this case:

$$\begin{aligned} &P_m(g,I) = \frac{B_m}{\lambda - \mu_m(g,I)} - \frac{N_0 B_m}{g_m}, m=0,...,M, \\ &\mu_m(g,I)P_m(g,I)=0, P_m(g,I)\geq 0, \mu_m(g,I)\geq 0, \\ &C = \lambda \overline{P}, u(P_c+\overline{P})=1 \end{aligned} \quad (4)$$

where $\mu_m(g,I)$ is the Lagrange Multiplier corresponding to the constraint $P_m(g,I)$.

In the sequel, we provide the analysis of the energy efficiency and optimal power allocation for systems with quantized feedback and perfect RF chains. Let us consider the case where Tx, along with CDI and knowledge of ***I*** has quantized knowledge concerning the values of fading coefficients $\gamma_m, \mu = 0,...,\mathrm{M}$. In such a case, the information available at Tx is essentially the information that event ε_{m,i_m}, defined as $\varepsilon_{m,i_m}: Q_{m,i} \leq \gamma_m \leq Q_{m,i+1}, m=0,...,M$ has occurred for some $i \in \{0,...,N_\mu - 1\}$.

By defining the vector $e = [\varepsilon_{0,i_0},...,\varepsilon_{M,i_M}]$ and the set **ε** of all possible realizations for vector e, we are then interested in finding the optimal power policies $\hat{P}_m(e,I), I_m \neq 0$ such as to maximize the EE of the communications system. To this end, in the following subsection we first express the EE for the case of quantized CSIT in closed form.

Having defined the EE in case of Quantized CSIT as $\hat{E}_{eff}$ the problem to be solved is formulated as follows:

$$\max_{\hat{P}_m(g,I),m=0,...,M,p.t.I_m\neq 0,m\geq 1} : \hat{E}_{eff} \quad (5)$$

$$\text{subject to: } \hat{P}_m(e,I)\geq 0, m=0,...,M,\ \ p.t.I_m\neq 0, m\geq 1.$$

Using again fractional programming tools, the optimal power allocation is given as the root of the following equations:

$$\frac{\partial \hat{R}(\hat{P}_0(e,I),....,\hat{P}_m(e,I),e,I)}{\partial \hat{P}_m(e,I)} - \lambda \Pr(e) = 0 \quad (6)$$

where the Lagrange Multiplier λ is selected such that the $\hat{C} = \lambda(P_c + \hat{P})$ is satisfied.

In the sequel and in order to derive suboptimal low-complexity power allocation policies for the EE maximization problem, we propose to design a power allocation policy maximizing an approximation to the EE as described in Sec.V of Appendix 3.3 that we omit here for space limitation reasons.

We continue this work with the EE maximization accounting for systems with multiple RF chains. In particular, we investigate the effects of realistic power consumption models for systems accounting for multiple RF chains, as a consequence of the use of multiple transmit antennas at the transmitter, and multiple PFBs. Our analysis not only takes into account the power consumption characteristics of the RF chains but also the fact that in cases that no transmission takes place, the power consumption of the circuits is also affected, thus allowing for a more realistic system design.

First, the power consumption for multiple RF chains is obtained in Sec.VI.A of Appendix 3.3. In particular, Eq.(40) provides the total power consumption denoted as $\hat{P}_{tot}(M,K)$. The design of power allocation policies for systems with multiple RF chains in case of Quantized CSIT follows. The problem under consideration is formulated as follows:

$$\max_{\lambda} : \tilde{E}_{eff,real} = \frac{\tilde{C}(\lambda)}{\hat{P}_{tot}(\lambda)}, \quad (7)$$

$$\text{subject to: } \lambda \geq 0.$$

As it will become evident in the following analysis, optimization problem in Eq.(5) above can be easily solved, applying convex optimization techniques. Details about the solution can be found in Sec.IV.B of Appendix 3.3.

In this section, we present results concerning the achievable performance of the proposed power allocation policies. To facilitate the presentation of the results, we separately examine the cases of systems with perfect RF chains. The solution to this problem is given by performing an exhaustive search over all possible, feasible quadruples of the form $\{N_{b,\mu}, \mathrm{N}_{b,\delta}, \mathrm{K}, \mathrm{M}\}$ solving for each one of these quadruples problem, and selecting the quadruple that maximizes the EE . Such an approach requires solving $\mathrm{N}_b \times \mathrm{K}_{\max} \times (\mathrm{M}_{\max}+1)$ problems of the original form. To cope with the complexity of such an approach, we propose following a suboptimum, greedy approach, which leads to a local optimal for optimization problem.

Having provided the optimal power allocation policies for all special cases mentioned above

such as full and quantized feedback, multiple antennas and RF chains, we now focus on comparing the optimal achievable EE in the presence of quantized CSIT with the achievable EE in the presence of perfect CSIT for different cases concerning the number of transmit antennas. To enable this comparison, in Figure 35 we present the optimal achievable EE in case that the power policy of Theorem 3 (see Appendixc 3.3) is applied, as a function of the available number of quantization bits per FB, for a system employing two FBs, bands B0 and B1 , with the fading, channel availability and bandwidth parameters given in Table I of Appendix 3.3. Commenting on the results presented in Figure 35, we should note that as K increases, the achievable EE in the presence of both quantized and full CSIT increases. On the other hand, as K increases, the performance gap between the case of full and quantized CSIT becomes more evident, for the same number of feedback bits per FB. This is mainly due to the fact that for higher K , the number of feedback bits required for the fine quantization of CDI information increases. As a result, the presence of strict feedback constraints limits the performance gains that multiple transmit antennas can promise.

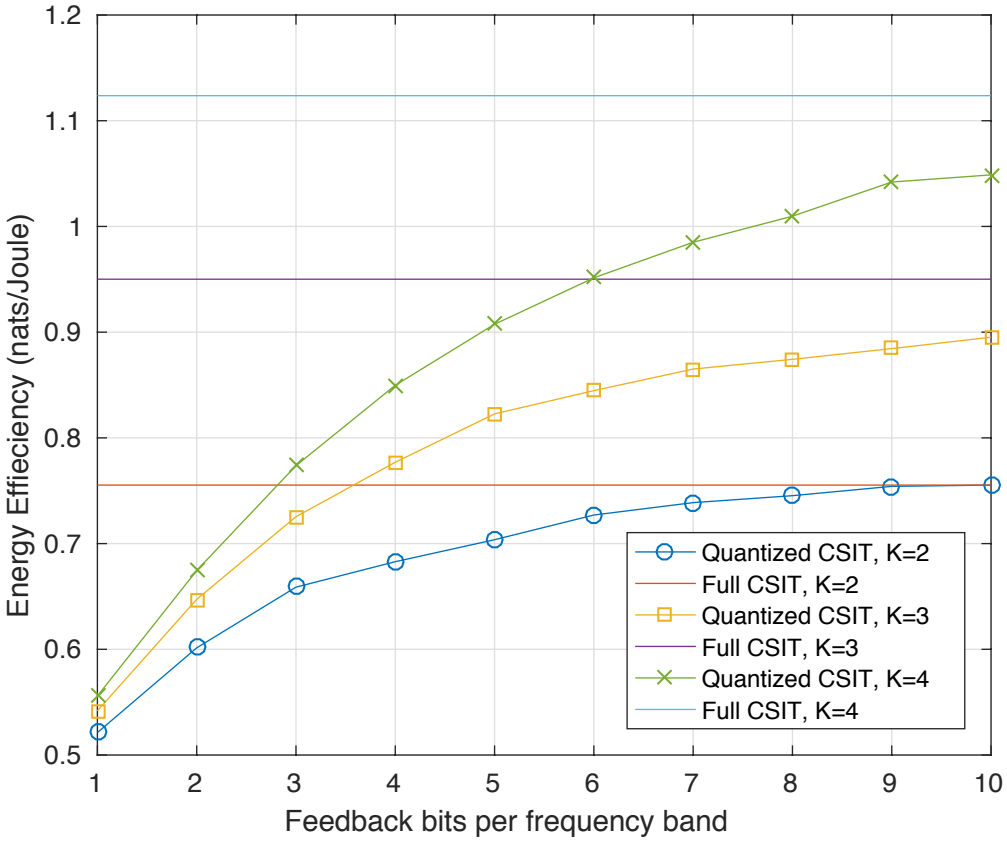

Figure 35: The achievable EE of the power policy of Theorem 3 as a function of the number of feedback bits per FB for different values of the number of transmit antennas.

Yet another parameter that needs to be investigated is the effect of the existence of multiple PFBs M, available by means of CA, in the achievable EE. To investigate this effect, in Figure 36, we present the achievable EE as a function of the number of available feedback bits per FB. The achievable EE for a specific number of available feedback bits N_b per carrier has been found by solving the following integer optimization. Moreover, for the simulations shown in Figure 36 we have set the numbers of transmit antennas to be equal to $K = 4$. The

parameters of the several PFBs were set to the values shown in Table I of Appendix 3.3. By inspecting the results shown in Figure 36, one can see that the benefits of multiple PFBs become more important as the number of feedback bits per FB N_b increases, proving the necessity for feedback, in order to fully harvest the benefits of CA. Having presented the performance study for the case of systems with perfect RF chains, we now change our focus, towards systems with power amplifiers and RF chains with non-ideal power consumption characteristics.

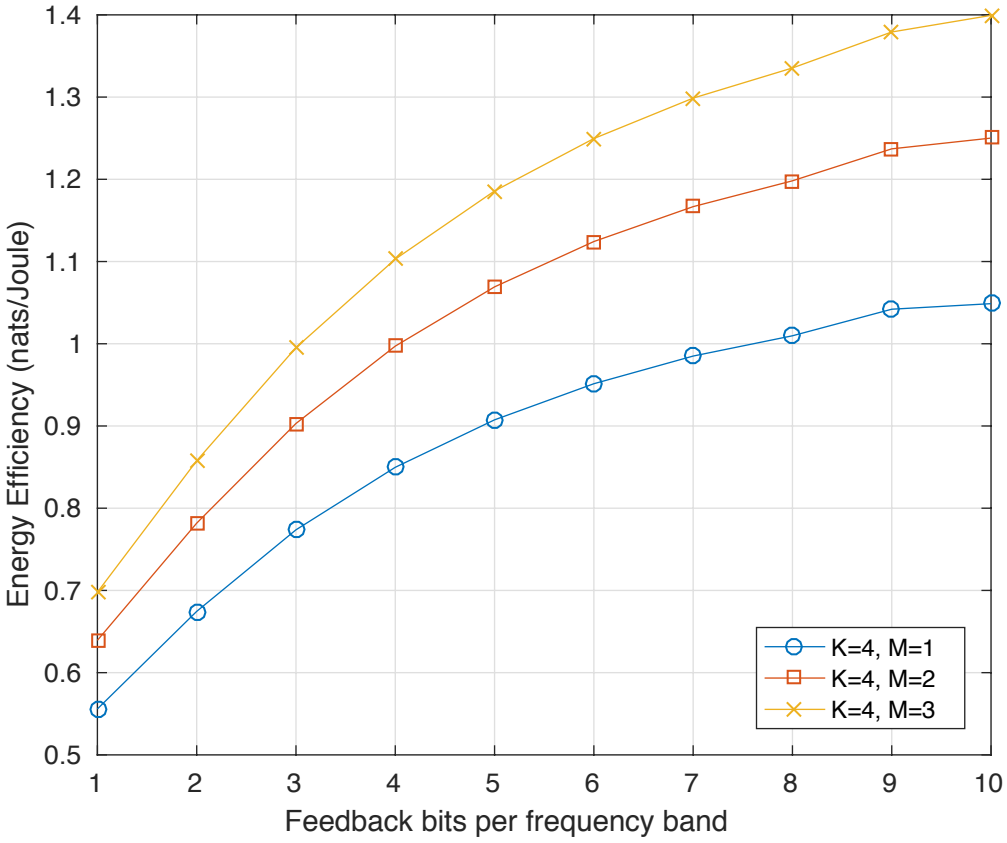

Figure 36: The achievable EE of the power policy of Theorem 3 and as a function of the number of feedback bits per FB for different values of the number of PFBs.

In Figure 37, we investigate the effects of the bandwidth of the several PFBs on the achievable EE. To this end,we illustrate the achievable EE, as a function of the $\rho = P_{RF} / P_{STA}$ for different values of M, for a system with $K = 4$ antennas, for two different cases concerning the bandwidth of PFBs $B_m, m = 1,...,M$. In more detail, in the first case, shown in Figure 37 (a) we have assumed that $B_m = 2Hz, m = 1,...,M$: : ;M , while in the second, shown in Figure 37 (b), we have assumed that $B_m 0.5Hz, m = 1,...,M$. The remaining system parameters were set to the values shown in Table I of Appendix 3.3. As it can be seen in Fig. 38 (b), the fact the PFBs $B_m, m > 1 1$ have smaller bandwidth results in reductions in the achievable EE, as M increases, thus eliminating the benefits of CA in terms of EE.

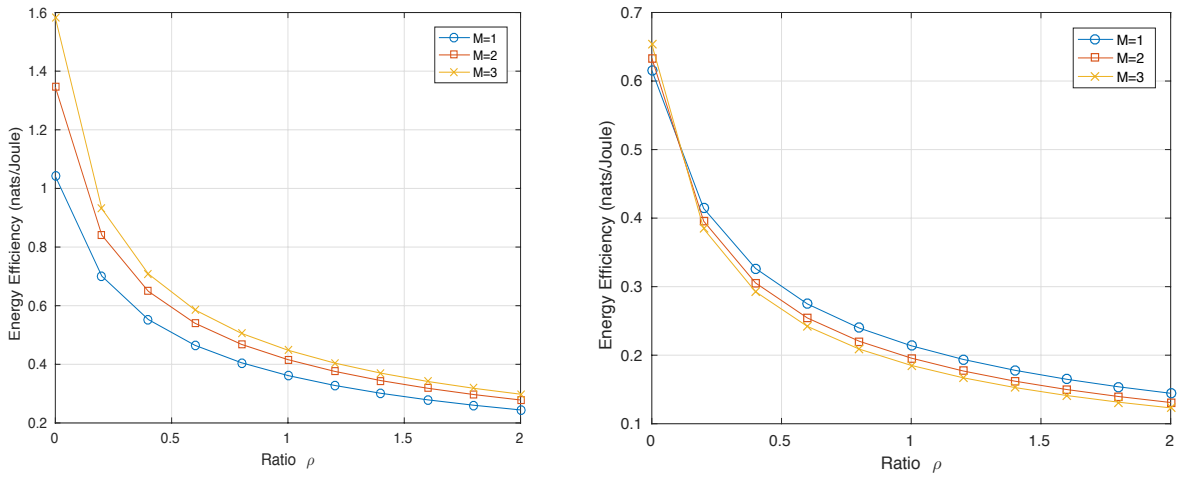

Figure 37: The EE of the power policy (Annex: Subsection VI-B) as a function of the ratio $\rho = P_{RF} / P_{sta}$ for different values for the number of CA enabled carriers M for (a) $B_m = 2Hz$, (b) $B_m = 0.5Hz$.

3.3.2 Conclusion

The problem of EE-optimal power allocation policy design in CA enabled systems was studied for both systems operating in the presence of full and quantized CSIT and perfect RF chains and related algorithms have been derived. Focusing on the more realistic case of quantized feedback acquisition at Tx, the developed algorithms were then extended in order to account for non-ideal power consumption characteristics of RF chains, and a novel greedy algorithm have been presented for addressing the problem of jointly optimizing the feedback allocation per FB, the number of transmit antennas, and the number of employed PFBs. By means of simulations, it was then shown that the achievable benefits of CA in the presence of quantized CSIT are limited, in the presence of strict feedback constrains, while they are also further limited, if not eliminated, when the power consumption of RF chains are taken into account. Moreover, the problem of joint optimally determining the number of transmit antennas, employed PFBs and optimal feedback allocation was investigated and a suboptimal algorithm has been proposed for this purpose, that has been shown to achieve performance similar to the performance of the optimal solution. Finally, it has been observed that scenarios where CA can enable substantial rate benefits lead towards selecting to increase the number of used PFBs, at the expense of reducing the number of transmit antennas, in order to avoid an excessive increase in the total power consumption. On the other hands, scenarios where the potential benefits of CA are limited, lead towards selecting to increase the number of employed antennas, at the expense of reducing the number of employed PFBs, in order again to avoid an excessive increase in the total power consumption.

3.4 Coding Middleware for Higher-Layer Aggregation of H-RATs

Although there are solutions that can achieve aggregation at lower layers such as presented in the previous sections, often it will not be possible to aggregate at lower layers. This is because in many cases the lower layers are defined by very different and incompatible radio interfaces, perhaps even operating at vastly different frequencies. Moreover, changing the radio interfaces to support aggregation will not be possible in some cases because such changes would violate the standards associated with those radio interfaces.

In order to address this, we propose a coding middleware that is able to aggregate such resources at a high layer. The middleware works by appropriately dimensioning fountain coding for the application type, such as the RaptorQ coding scheme detailed in [Lub2011], in order to cope with the heterogeneity of lower layers and combine the received data to reconstruct the transfer with minimal loss in efficiency through unnecessary duplicate reception of content.

The middleware consists of a sub-layer of fountain coding/decoding, respectively at the server and client, employed between the application layer and transport layer. Unique coded packets are transmitted whenever possible to maximise the amount of information received over the interfaces that is useful. The coding block size in this case is set depending on whether it is required for the information to be streamed, or received and processed in complete files. If the transfer is of complete files—such as for the transfer of a large upgrade download for example, or in the download of web pages—then it is generally best if all the information is coded in a single block, as each packet will therefore be useful to all receivers (presuming that no duplicate packets or freshly coded packets are always sent). If computational resources or the utilised coding scheme don't allow such a single block, then the information should be sent across a minimal number of multiple blocks. If the information had to be streamed, then the block size would be set based on: (i) the expected sum rate over the aggregated links for a receiver, and (ii) any acceptable buffering delay transmitting and receiving the first block.

Reliability of the links being aggregated is crucial in the configuration of this scheme. We consider three cases, where we assume that the reliable links are always unicast (i.e., reliable multicast/broadcast protocols are not supported—noting that there has been limited take-up of reliable multicast/broadcast protocols to date despite convincing such protocols having been around for some considerable time):

1. All links being aggregated are reliable, e.g., as in the case of conventional Wi-Fi and LTE flows being combined.
2. None of the links are reliable, e.g., all of the links are broadcasts.
3. One or more of the links is unreliable, e.g., as in the case of a packet broadcast being combined with a licensed LTE or Wi-Fi transmission.

3.4.1 Case 1: All links are reliable

The single requirement here is that all received packets are useful, hence, only coded packets that have not been received at a receiver are transmitted to that receiver—noting that the source will have information on which receivers have received which coded packets. There are no challenges in the implementation of this scheme either in the case where a single block for coding is assumed, or where multiple coded blocks are assumed. However, flows over different aggregated resources to a receiver will have different (and likely unpredictable) rates, hence, it will not be possible to accurately attribute which parts of a content transfer should go over which links. This justifies the use of the coding middleware discussed in this section to deal with the challenges of matching which subsets of the transfer to send over which of the aggregated resources to a receiver.

3.4.2 Case 2: None of the links are reliable

In this case, feedback is not possible to the server of the content, hence there is no knowledge upon which the server can base decisions on which content should be prioritized to maximise efficiency. However, the server must have some *a priori* knowledge of expected radio interface performance to given receiver sets (or coverage areas, with known loss characteristics to those areas) in terms of bit hence packet loss, which can be linked to a given loss rate distribution among receivers. The source will keep transmitting until certain reliabil-

ity or confidence limit on receiving of the content is achieved, based on this distribution, before moving on to another block, content set, or perhaps repeating the content set (in the case of a data carousel being applied).

The use of the previously mentioned fountain coding middleware is again needed to automatically correct the random losses; moreover, it will be preferable for the content to be provided as a single encoded block if possible—in which case it is far easier to make transmitted packets useful at more receivers. Division of the content into multiple blocks can occur if the content size is too large for the processing capability at the source/receivers or the given coding scheme, or if the content must be received in stages (e.g., for a video streaming based on progressive downloads on the block level).

3.4.3 Case 3: Some of the links are reliable

This case is divided into two sub-cases.

Unicast only to Receivers

In the case where unicast links are unreliable, the source must again have some *a priori* assumption on the required reliability of the content in order to transmit an appropriate surplus of coded packets and realise the required reliability at the receiver side. This can be adjusted by a knowledge of the number of packets that are successfully received if one of the aggregated links at each receiver is reliable unicast; even if only some of the aggregated links at some of the receivers are reliable unicast, the statistics on the received data for the unreliable unicast links can be used by the server to adjust the level of coding required to maintain a given confidence limit among all the receivers of the unreliable content.

Unicast combined with multicast/broadcast to receivers

This case is of particular interest to the SOLDER work given the definition of the “augmented broadcast” scenario as well as a PoC being based on that in WP4. Here, reliable unicast flows to receivers will be operating at different (and varying) rates, and the multicast/broadcast itself will also be operating at its own individual rate. Moreover, there is no guarantee that the packets sent over broadcast will be successful, as there is no feedback in this case to confirm their success or trigger retransmissions. In this context, packets that are transmitted over the broadcast will be useful to only a subset of the receivers, as some receivers will have received them already over the unicast interface. An alternative solution of defining multicast groups at short timescales to address receivers that require increased coded content for the block or content set will clearly not be possible due to the latency and signalling in forming multicast groups. If, however, a RaptorQ-coded packet were broadcast, with the packet being coded over a single block, then it would be possible for it to be useful to more receivers—especially if it were a fresh packet coded and sent *on the fly* such that it were unique among the entire receiver set. Such a solution greatly increases efficiency compared with repeating uncoded packets, which some receivers would have received already, e.g., due to having more reliable channels or better Wi-Fi connections.

D3.2 [D3.2] has provided some discussion on the ordering of packet transmissions and how to use feedback information to prioritise packets. Figure 38 expands on this for the case of a multi-block file transfer with a reliable unicast interface and broadcast interface being aggregated, noting that the single-block file transfer case is straightforward so is not considered here. In the case of the multi-block transfer, the broadcast should give preference to the block with most packets needed among the receivers, however, the nature of that preference depends very much on distribution of the unicast rates. For streaming video, preference should be given to blocks for which buffer under-runs are more likely among users.

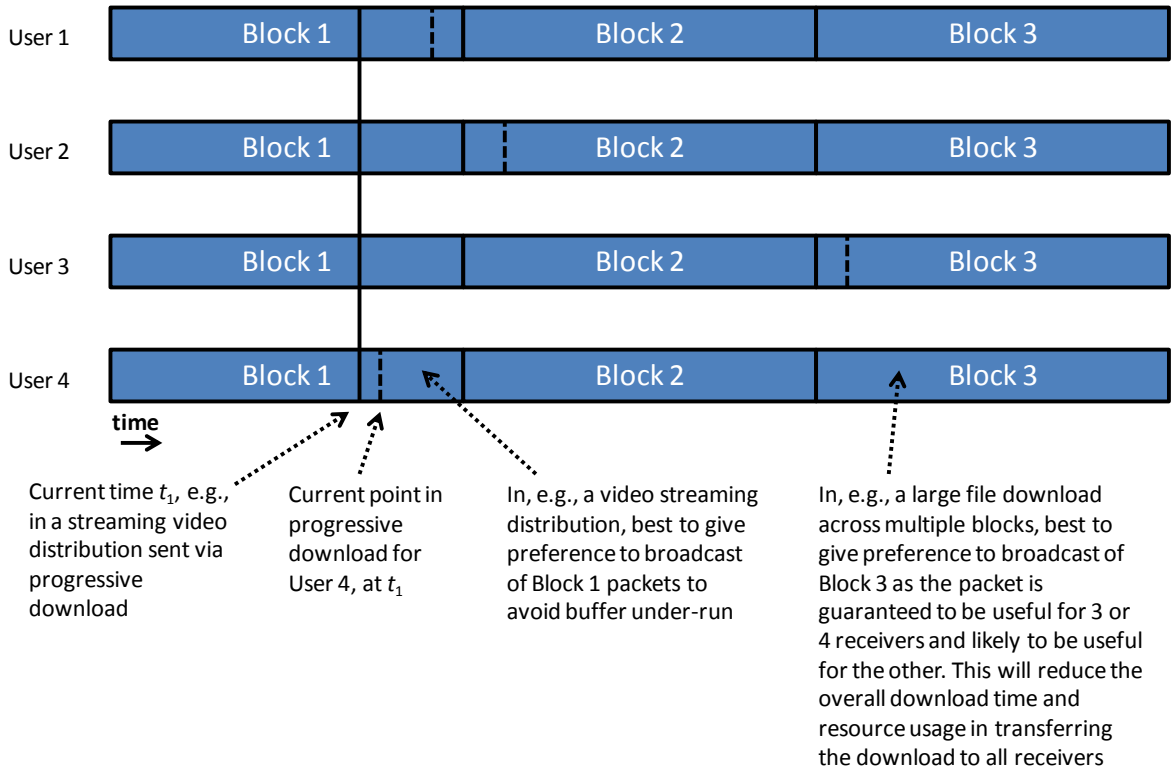

Figure 38: Differing prioritization of blocks for broadcast transmissions when aggregated with unicast.

A simulation platform has been written to test different modes of selection of which blocks to prioritise in the context of reliable unicast interfaces to receivers being aggregated with unreliable broadcast. These include, for the file download case:

1. No intelligent prioritisation, e.g., blind broadcasting of blocks in numerical order.
2. Intelligent block prioritisation based on the number of receivers that have not finished each block.
3. Intelligent block prioritisation based on the number of packets needed among receivers in each block.

Results show approximately a 25% improvement in the average file download time among receivers for option 3 compared with option 1, under the assumption of the average rate of the unicast to receivers and the broadcast rate being the same. Solution 2 shows a slight reduction in this improvement.

At the time of writing, simulations are being performed to obtain more detailed results on these questions, with the aim of publishing soon.

4. Aggregation and unlicensed spectrum

There are, on a regulatory level, a number of proposals and novel deployed solutions that open up additional unlicensed spectrum, which can be used for aggregation purposes to increase capacity and for other benefits. These solutions are largely based on spectrum databases. The opportunities of that additional spectrum and such proposals should be considered. We first give a quick mention of such opportunities in the context of spectrum database-driven solutions in section 4.1, also providing a quick update on one key solution, TVWS, as part of that.

Further, as already introduced in previous deliverables, e.g. [D3.2] and [D2.3], the use of LTE in unlicensed spectrum is becoming a hot topic in the standardisation. The standard addresses the 5GHz band, with its specificities in terms of regulation. In context of SOLDER, we proposed innovative solutions to handle the regulatory constraints applicable to the specific context of LAA. These proposals were submitted to the 3GPP standard mostly in H1 2016. They are reported in section 4.2.

4.1 Update on regulatory solutions involving spectrum databases

It is noted that, depending on the locality and regulatory administration, there are immense regulatory shifts or revolutionary proposals in the way that unlicensed spectrum (or “license-exempt” access) is handled in some bands. As has been covered in earlier Deliverables (e.g., D3.2 [D3.2], D2.3 [D2.3], among others), there are major steps in terms of using spectrum/geolocation databases to determine local spectrum availability for license-exempt use in the scope of TV White Spaces (TVWS) [Ofc2013]. Further, extensive work is ongoing at the time of writing to define a sensing-populated “database” approach towards spectrum sharing for “Citizens Broadband Radio Services” (CBRS) at 3.5 GHz in the US [FCC2015], the “database” in this case being a “Spectrum Access System (SAS)” and the sensing systems being “Environmental Sensing Capabilities (ESCs)”. This is being defined within the Wireless Innovation Forum Spectrum Sharing Committee [WInnF2016], with companies such as Google and Federated Wireless, among many others, playing key roles in the development of this system. Ofcom in the UK has also recently prepared a consultation with extensive coverage on the use of an intermediary acting to facilitate spectrum sharing in the range of 3.8-4.2 GHz (see [Ofc2016], pages 23-26). This could be seen as both an extension of the use of the certified database as a decision making intermediary, e.g., exactly along the lines of the TVWS work in the UK, and also a scheme somewhat mirroring the US 3.5 GHz three-tier system with the intermediary also being able to license out spectrum as a kind of second tier (see Figure 39). Hence, the development of such automated processes for unlicensed spectrum, as well as more dynamic (while still controlled) licensed spectrum access, can be seen as progressing the concept and structures of the geolocation databases developed within the scope of TVWS. Such database-based concepts to facilitate “automated” spectrum sharing and enhanced spectrum availability, which will likely be applicable to aggregation purposes (e.g., much in the sense of LTE-U/LAA accessing unlicensed spectrum already) can indeed been seen as subject to a long-term planning and a set regulatory direction.

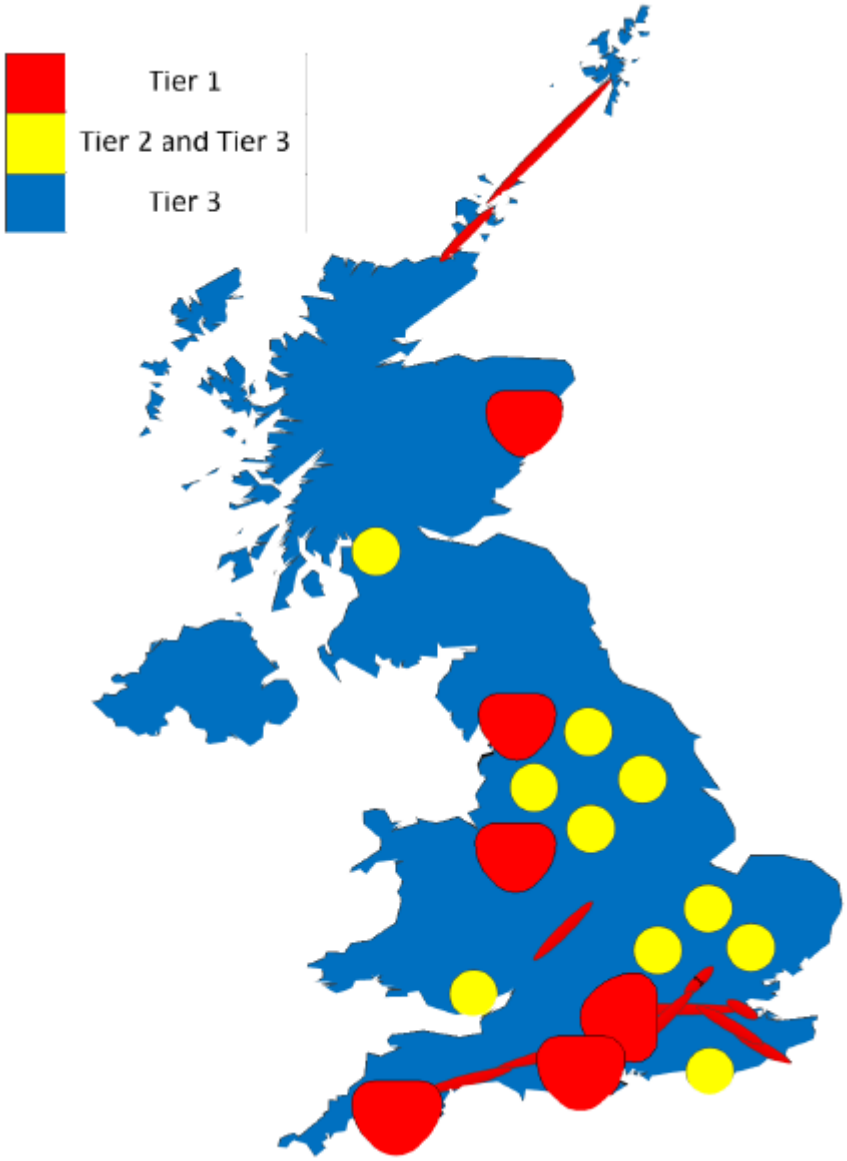

Figure 39: Illustration of the three-tier access approach in the UK (taken from [Ofc2016]).

To assist the understanding on how availability for such automated processes determining unlicensed spectrum vary, we provide an update on some latest important results regarding the availabilities as a result of TVWS processes in the UK. Importantly, Ofcom in the UK has changed to its allowed EIRP calculations in finalising its framework in the UK [Ofc2015], significantly affecting TVWS availability, and WRC 2015 has also, in November 2015, decided to make the upper end of the TV band (694-790 MHz) co-primary with mobile broadband in ITU Region 1, which encompasses the UK and wider EU. We highlight the differences in TVWS availability that these changes lead to. No other work in the literature has done this analysis, where it is noted that our insights present extremely important material for potential implementers/users of TVWS technologies in the UK, as well as in other countries of the EU through comparison, by virtue of ETSI EN 301 598 being a harmonised European standard [ETSI2014].

Using our implementation of a white space device (WSD) in the UK under the Ofcom TVWS Pilot [Hol2015a], we have sampled availability over a large area of England (~42,300 km^2—see Figure 40, Figure 41), at a resolution of 0.01 degrees equally in latitude and longitude. This equates to 54,400 locations being sampled across this area. Results are for a Class 3 WSD operating with specific operational parameters.

We assess the number of channels that are available under various criteria. We consider similar scenarios to [Hol2015a], [Hol2015b]: mobile broadband downlink (MBD) in TVWS, and indoor broadband provisioning or mobile broadband uplink (IBP/MBU) in TVWS. However, we also vary the parameters in order to consider, e.g., the benefits of reducing antenna height. Our main interest here is TVWS availability. Table 5 presents parameters used for our scenarios.

Table 7: Assumed parameters for investigated scenarios.

Scenario	Transmitter Height (m)	Required EIRP (dBm)
MBD	30	At least 30
IBP/MBU	1	At least 20

Results are presented in Table 8 and Figure 40—Figure 42. For the MBD scenario, there is a significant reduction in TVWS availability under the commercial database, with large areas of the investigated area of England having zero availability. The average number of available channels is reduced from 8.6 to 4.0. Results are more striking when narrowing down to the London area, which still has good availability for the most part, although reduced from 15.7 to around 4.7 channels being available on average. Uncertainty in the availability for both cases is also significantly increased.

The IBP/MBU scenario is far less affected, still with excellent availability for the commercial databases. Uncertainty in availability is also only marginally increased under the commercial databases.

Investigation of the effects of the WRC decision is done only for the London M25 area, as this area is dominated by the Crystal Palace TV transmitter operating on channels below 49, with relays and transmissions from other areas only minimally operating on channel 49 or above. Hence, the effects of re-planning the higher-frequency DTT transmitters due to mobile broadband taking 694-790 MHz can be largely neglected for the London M25 area. Results for both scenarios show a significant reduction in availability due to the WRC decision, although the IBP/MBU availability remains excellent with over 14 channels being available with a low variability.

Finally, we note that many of the observations in [Hol2015a], [Hol2015b] regarding the effects of spectrum mask classes still apply, with Class 1-3 achieving relatively similar availability, but classes 4 and 5 having significantly reduced availability. Moreover, we note that lowering the transmitter height for the MBD scenario can significantly increase availability; as an extreme example, lowering the antenna to 1m height above ground level leads to the average channel availability in the London M25 Future case (even while taking into account the WRC decision) increasing from 1.6 to 9.5, the CoV decreasing from 0.88 to 0.40, and the percentage of locations in which 1 and 3 channels can be used respectively increasing from 82.5% to 96.3%, and 21.0% to 94.0%. Ofcom uses different height ranges for DTT protection calculations, such that similarly exceptional results hold up to 3.2m height above ground lev-

el, and reductions in this availability occur if the height is raised above 3.2m, then above 7.4m, and then again above 12.4m. At 7.4m and 12.4m, the average number of channels available is 5.6 and 3.6 respectively, the CoV is 0.71 and 0.86 respectively, at least 1 channel is available in 78.7% and 78.2% of locations respectively, and 3 channels are available in 72.5% and 56.8% of locations respectively. Hence, even with such modest reductions in height, a lot of usable TVWS becomes available for the MBD scenario.

Table 8: Statistics on TVWS availability under past, present and future rules, for various scenarios and locations (Class 3).

Scenario	Database calculation	Location	Ave. no. chan.	Std. no. chan.	CoV no. chan.	% loc. >= 1 chan.	% loc. >= 3 chan.
MBD	Past	Wide area	8.6	7.2	0.83	98.0	81.6
		London M25	15.2	8.5	0.56	99.5	97.1
	Present	Wide area	4.0	4.9	1.21	74.1	43.1
		London M25	4.7	3.5	0.76	90.8	63.1
	Future (WRC)	London M25	1.6	1.4	0.88	82.5	21.0
IBP/ MBU	Past	Wide area	26.5	6.1	0.23	100.0	100.0
		London M25	25.5	3.6	0.14	100.0	99.9
	Present	Wide area	23.5	7.1	0.30	99.9	99.7
		London M25	24.8	4.7	0.19	100.0	99.9
	Future (WRC)	London M25	14.4	3.6	0.25	99.5	99.0

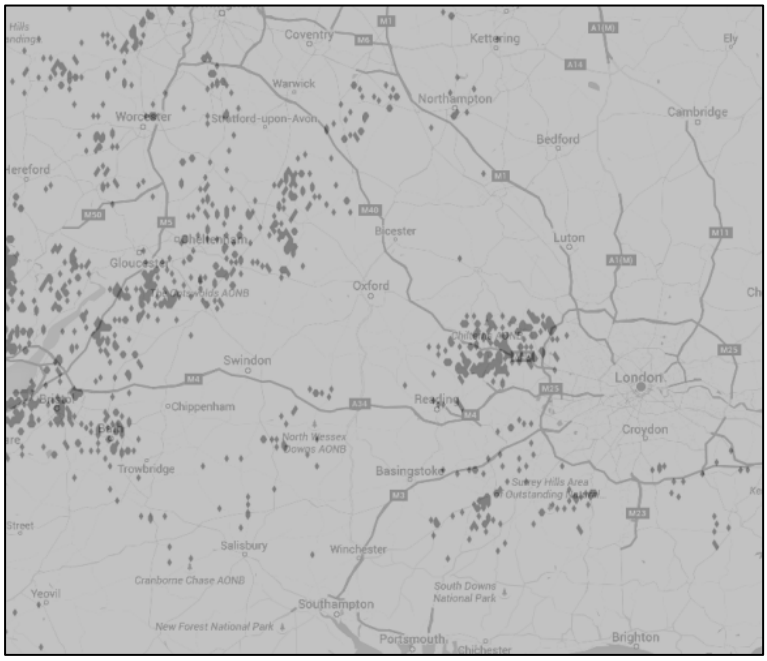

Figure 40: Locations for a large area of England in which at least one TV channel is available using the trial Ofcom TV white space databases for the MBD scenario. Dark

areas indicate no availability. Note, under the IBP/MBU scenario at least 1 channel is available in all locations.

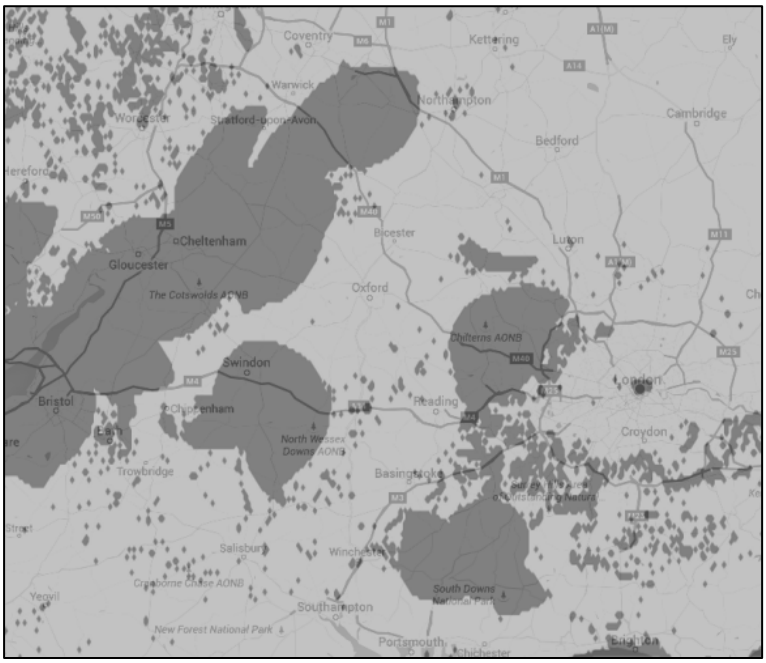

(a)

(b)

Figure 41: Locations for a large area of England in which at least one TV channel is available under commercially operated Ofcom TV white space databases. Dark areas indicate no availability. (a) MBD scenario, (b) IBP/MBU scenario.

(a)

(b)

Figure 42: Locations for only the London "M25" area in which at least one TV channel is available under commercially operated Ofcom TV white space databases for the MBD scenario. Dark areas indicate no availability. (a) Before implementation of the WRC 2015 decision, (b) after implementation of the WRC 2015 decision.

4.1.1 Conclusion

Novel regulatory proposals facilitating spectrum sharing are absolutely key to the realization of sufficient spectrum for aggregation to meet the requirements of future mobile and wireless communications systems such as capacity. Here we have presented an update on some such proposals involving spectrum databases, and particularly an update on the situation for

TVWS in the UK—a pioneer of the technology through instantiating a pilot and nuanced framework or TVWS, and more recently bringing the technology to commercialization.

4.2 Licensed Assisted Access (LAA)

Within Rel. 13, the 3GPP has investigated the use of LTE in unlicensed spectrum. The activity has started with a study item, completed in June 2015, and then moved into a work item. The initial work item was covering downlink only and was completed in Dec 2015. Then still in Dec 2015, another work item was approved in 3GPP to address Uplink aspects. The work item was entitled eLAA_LTE and original description of the objective is given in [RP-152272].

One of the objective of the WI is to define UL carrier aggregation scheme, compatible with regulatory constraints and providing satisfying efficiency, despite the unpredictable state of the unlicensed spectrum (mostly due to other users in the vicinity using the same band).

We address two different concerns; one related to regulatory constraints, the second one rather related to the efficiency of the resource allocation. Both issues are quite tied. The outcome of the work was captured in 3GPP Tdocs and submitted to 3GPP:

- February 2016 Malta, 15th – 19th February 2016
  - R1-160398, (updated into R1-161106): Considerations for LAA UL Carrier Allocation
  - R1-160399, Considerations for LAA UL Waveform Design
- April 2016 RAN1#84b Busan, Korea 11th - 15th April 2016
  - R1-162755, Considerations for eLAA UL Carrier Allocation
  - R1-162756 RB allocation for PUSCH

It should be noted that the contributions made in April are more or less resubmission of the previous ones, although updated to take into account the progress of the discussion held during the February meeting and on the 3GPP mailing list during Q1 2016.

4.2.1 UL carrier allocation

The regulation ensures a fair access to the unlicensed spectrum for all users. For that purpose, the regulation requests a listen-before-talk (LBT) mechanism at least in some regions (e.g., Japan and EU) before accessing the 5GHz spectrum. The LBT "*procedure is defined as a mechanism by which an equipment applies a clear channel assessment (CCA) check before using the channel. The CCA utilizes at least energy detection to determine the presence or absence of other signals on a channel in order to determine if a channel is occupied or clear, respectively.*" (extracted from [TR 36.889-d00]).

The CCA procedure usually detects the presence of energy in the channel before any transmission, and if the channel is detected as occupied, then the transmission cannot occur. As a result, this procedure could block an UE transmission even if a particular channel was allocated by the nodeB; Indeed, the nodeB could not necessarily predict the presence of another user in a given channel, despite all measurements that could be conducted in the past. This was actually the purpose of one outcome of [D3.2] related to the selection of the channel with the highest probability of being clear.

Because the nodeB cannot predict the exact availability of the carriers, our proposal is simply to allocate more carriers than required by the UE. As a result, this overbooking approach ensures that statistically the UE will get its required number of carrier and minimize the latency. However, too much overbooking would conduct to a waste of overall capacity as illustrated by the Figure 43.

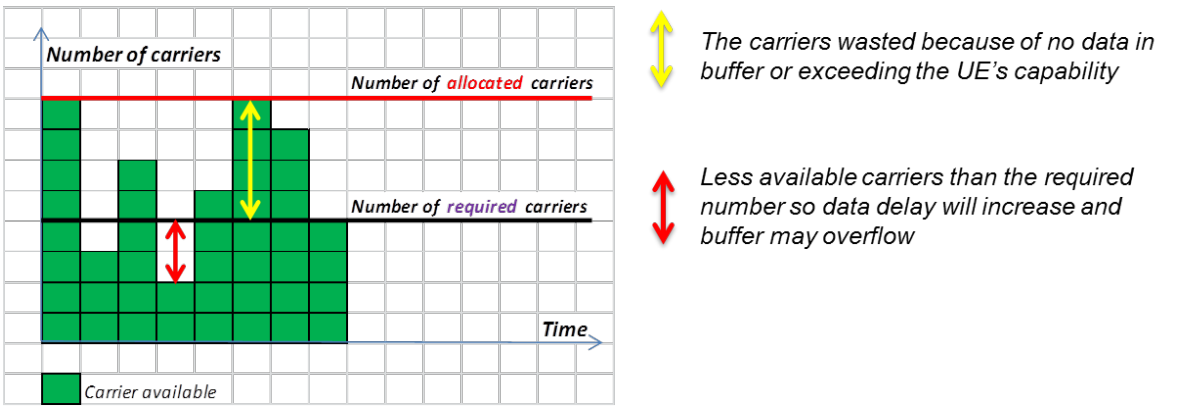

Figure 43. Proposed UL LAA carrier allocation

We therefore proposed to define two types of carrier: dedicated carriers for a given user, and shared carriers, that will be part of a pool of carriers for overbooking, with concurrent access from different users, as illustrated by the Figure 44. The concurrent access is naturally handled by the CCA mechanism.

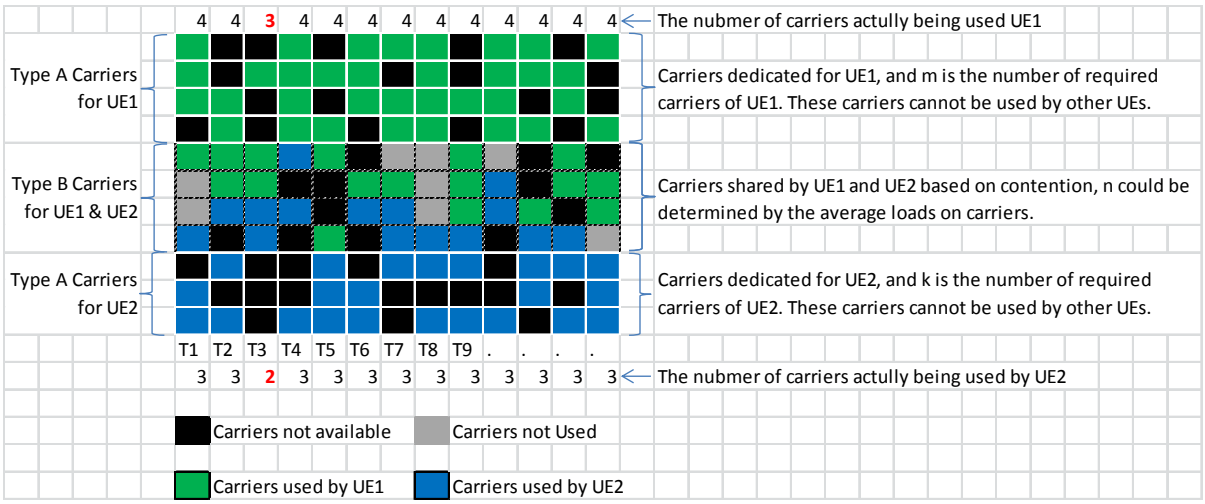

Figure 44. Improved UL LAA carrier allocation

We conducted simulation to validate the proposed approach, using 3 scenarios for allocation illustrated by Figure 45:

- **Dedicated Allocation:** two carriers are allocated to each UE and no carrier is shared between any two UEs (see (a)).
- **Shared Allocation:** each carrier is shared by two UEs, and the front UE has a higher priority than the rear UE which means the rear UE can only access the carrier when it is not needed by the front UE (see (c)). Note that for both UEs, LBT is always required as usual.
- **Mixed Allocation:** three carriers are allocated to three UEs with dedicated allocation and other three carriers care allocated to the same three UEs with shared allocation (see (b)).

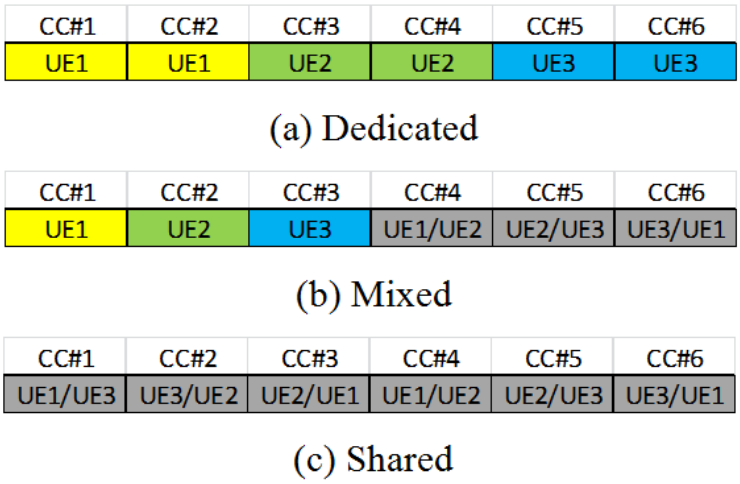

Figure 45. 3 scenarios for carrier allocation

The Figure 46 depicts the simulation results. It can be concluded that:

- For any allocation method, the latency increases when the load increases;
- The latency is reduced remarkably from dedicated allocation to mixed allocation and then shared allocation when the load is same;
- Shared allocation can work with a higher load than mixed allocation which in turn can work with a higher load than dedicated allocation. In the simulation, it is observed that dedicated allocation cannot work properly when the load is 0.5 or more and the UE buffer increases monotonically until being overflowed.

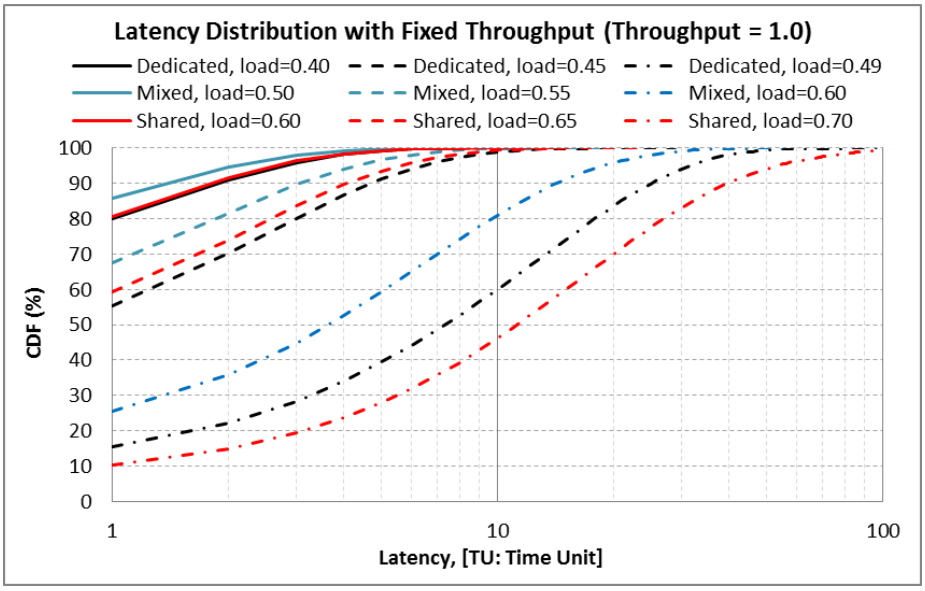

Figure 46. Simulation results

From the above simulation, potential gains of both latency (and reciprocally throughput) are quite promising by letting multiple UEs to access the same carriers based on contention.

Considering that in LAA, UE can only access the carriers scheduled by the eNB, it is very important to design a scheduling scheme to optimize the UL performance.

This carrier allocation proposal addresses the regulatory constraint of LBT driven by a fair access to the channel; however, it does not address another constraint related to the average transmission power, and the channel occupancy.

4.2.2 The 80% channel occupancy requirement

For the 5GHz unlicensed band, the access to the channel falls under the regulatory requirements expressed for instance in [ETSI301893] for European region.

Beyond the LBT already discussed, once a device uses the channel, it should use it plainly! The occupied channel bandwidth needs to be at least 80% of the declared nominal channel bandwidth. This requirement could be interpreted as a wish to use the channel efficiently and to prevent some users that could occupy it with small burst of transmitted data, lowering the global spectral efficiency.

This requirement could be understood in several ways, and therefore, we investigated a bit the ETSI standard. According to section 4.3.2 [ETSI301893] and the corresponding test method in section 5.3.3 [ETSI301893], the occupied channel bandwidth can be measured with the 99% bandwidth function of the spectrum analyzer. It is understood that an LAA device can pass the test with the system bandwidth occupied partially and discontinuously in frequency domain only if the two edges are separated far enough.

According the test method, for 20 MHz channel bandwidth, the frequency span is 40 MHz, the sweep time is > 1 s and the resolution filter bandwidth is 100 KHz so the charging time for the resolution filter is > 2.5 ms which is longer than two continuous LTE subframes.

This means one RB continuously transmitted with intra-subframe hopping or inter-subframe hopping can help the device to pass the channel occupation test only if the position in the first slot and the position in the second slot are separated by no less than 16 MHz. Or multiple RBs for one device can be mapped discontinuously in frequency domain and the first RB and the last RB need to be separated by no less than 16 MHz.

Similarly, According to the regulation requirement in section 4.4.2 [ETSI301893] and the corresponding test method in section 5.3.4 [ETSI301893] both the power spectrum density (PSD) per MHz and the total output power cannot exceed a set of specified power limits, for instance, 10 dBm per MHz and 23dBm for 20 MHz.

At last, this requirement should be understood for a single user, and cannot be fulfilled by several users (actually, one could imagine that the nodeB could allocate RB of several UE to meet the 80% requirement all together, but because of the CCA, it is not guaranteed that all UE could transmit at a given moment. In that case, the 80% rule would be not met).

Based on these requirements, allocation schemes in which RB are allocated in a spread way, (non contiguous manner) are proposed, which breaks the single carrier aspects of the UL waveform, and therefore increase the PAPR.

As a result, such allocation schemes, fulfilling the regulatory constraint of 80%, would theoretically require the definition of new waveform (beyond OFDM) in order to keep the out-of-band radiation at a reasonable value, as investigated in next section.

4.2.3 Conclusion

With these two studies, we propose improvement of the LAA mechanisms to improve UL efficiency. The first proposal relates to carrier allocation and intends to allocate more carrier than theoretically needed, in order to mitigate the impact of the LBT mechanism. The second

proposal deals with the regulatory constraint of filling 80% of the bandwidth when used that could limit smart scheduling of multiple user in a coordinated system.

5. 5G waveform aggregation

5.1 Overview

The physical layer selection of the future generation of civil radio system (beyond 2020) is an open topic. In SOLDER, we are considering FBMC PHY layer as a candidate for intra band CA because of its excellent spectral containment. In D3.1 [D3.1], we have identified the issues that arise when realistic transmitter front-end are taken into account, and more specifically a tremendous degradation of the transmitted spectrum. The linearization of the transmitter is a key enabling technique in order to sustain the good spectral containment of FBMC. Nevertheless, IQ modulator and demodulator imbalances, but also high PAPR, limit the benefit of the use a linearization technique. For that reasons, we have proposed fully digital algorithms in [D3.2] in order to calibrate the platform and to reduce the PAPR of FBMC signals to a reasonable value.

In this deliverable, we present the digital predistortion (DPD) that is proposed as a linearization technique for SOLDER. We first explain the DPD principle and the approach that is used for the parameters estimation. Then, we present the most relevant DPD techniques and we show how we have selected the chosen DPD technique and its parameterization. Finally, the performances are presented, and we highlight the benefit of the joint use of digital calibration and PAPR reduction.

Part of the work presented in this section will be presented at EuMW 2016 [Val2016a] and has been submitted at ISWCS 2016 [Val2016b]. A new Nyquist filter design (which is a natural derivation of our previous work on PAPR reduction [Tra2016a]) have been published at IEEE Communications Letters [Tra2016b]. The corresponding papers could be respectively found in Appendix 5.1a, 5.1b and 5.1c.

5.2 Generalities on linearization

The principle of the DPD is illustrated on the Figure 47. This technique consists in applying a distortion (basically a non-linearity) to the signal to be transmitted before the power amplifier (PA). The association of these two non-linear systems (DPD followed by the PA) gives a linear system. The DPD modifies the envelop and the phase of the signal to be transmitted in order to generate a signal that is the exact opposite of the PA gain and phase non-linear components.

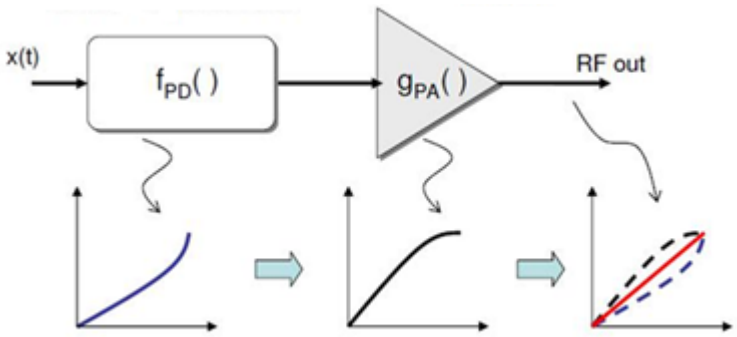

Figure 47: General principle of DPD

The DPD function shall have a $f_{PD}(.)$ function such as at the output of the PA we obtain the following relation:

$$g_{PA}\left(f_{PD}(x(t))\right) = G_{PD} \cdot x(t)$$

where $x(t)$ is the signal to be transmitted, $g_{PA}(.)$ is the power amplifier response, and G_{PD} is a scalar that refers to a gain factor.

Thus it is necessary to be able to create a distortion that is the exact inverse of the PA characteristic in order to anticipate the distortions before the transmission to the PA. The PA characteristic shall be known in order to determine the DPD function $f_{PD}(.)$. The DPD implementation requires to adaptively adjust the gain and phase compensations introduced by $f_{PD}(.)$. An adaptive module is necessary in order to minimize the difference between the signal to be transmitted and the signal at the PA output. This adaptive module modifies/updates properly $f_{PD}(.)$ according to an error criteria at the PA output that has to be minimized.

In practice, $f_{PD}(.)$ could be implemented by analog or digital components, on baseband or at an intermediate frequency. In SOLDER, we propose to use a digital predistortion generated at the baseband level because this approach provides very good performance and is extremely flexible and adaptive.

5.3 Direct and indirect learning

There exist two different DPD approaches [Paa2008]:

- "Direct learning" (Figure 48-a): the PA model is first computed ("Power amplifier estimation") based on the PA input/output signals. Then, the inverse PA model is estimated ("Adaptive inverse model" and "Predistortion computation") and applied ("Pre distorter") to the signal to be transmitted.
- "Indirect learning" (Figure 48-a): the PA output signal is directly post-distorted such as the error between the PA input and the post-distortion output is as low as possible. The block that is in charge of the post-distortion is called "Post distorter (A)". Once this block has been properly identified, the pre-distortion ("Pre distorter (Copy of A)") applies the same function realized by the post-distortion block.

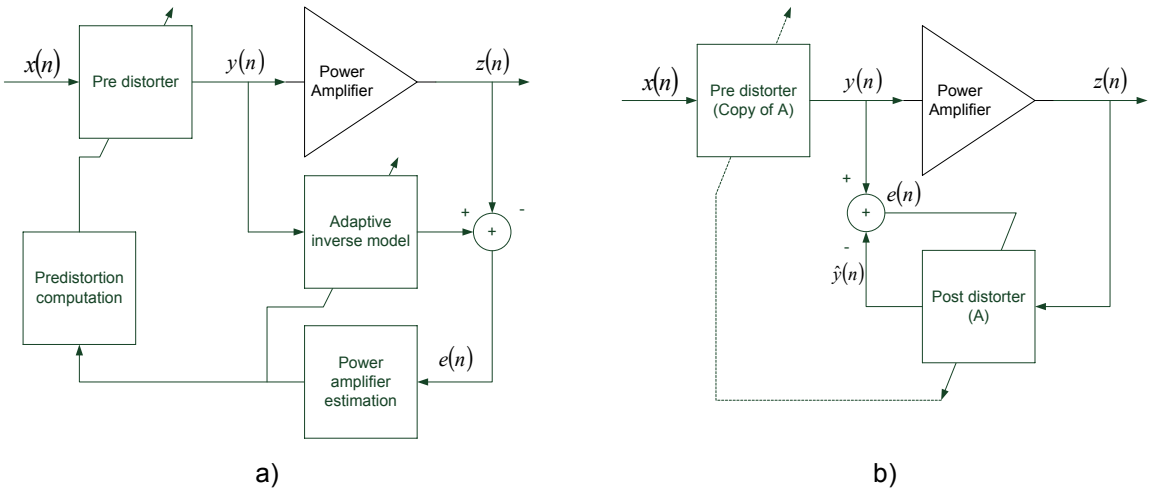

a) b)

Figure 48: a) Direct learning and b) Indirect learning DPD

The performances of the direct and indirect learning are very similar [Paa2008]. In SOLDER, we propose to consider the indirect learning approach because the implementation is less complex and it does not suffer from stability and convergence issues.

5.4 Digital Predistortion Techniques

We limit the presentation of DPD techniques to methods that are derivative of Volterra series because they have excellent performance capabilities to model memory non linearity. Among all existing techniques, we are considering the most promising:

- The memory polynomial (MP) [Din2004]
- The Dynamic Deviation Reduction-based Volterra (DDR) [Zhu2006]
- The generalized memory polynomial (GMP) [Mor2006]

All these techniques have in common the fact that their model linearly depends on the coefficients vector to be estimated. The coefficients computation can be solved thanks to least square (LS) criteria [Din2004].

5.4.1 Memory Polynomial

The MP DPD was the first technique taking into account PA memory effects [MP]. The MP basis corresponds to the diagonal of the full Volterra modeling and is extremely simplified with respect to Volterra series. The relation between the input $x(n)$ and the output $y(n)$ is as follows:

$$y(n) = \sum_{k=1}^{K} \sum_{m=0}^{M} \alpha_{k,m} x(n-m)|x(n-m)|^{k-1}$$

where K is the maximum polynomial order, M is the number of baseband samples used to compensate for the memory effects, and $\alpha_{k,m}$ are the $K(M+1)$ coefficients used for the DPD.

5.4.2 Dynamic Deviation Reduction

The DDR technique is more recent [Zhu2006], [Gua2011] and comes from the Volterra series applied to the discrete time and aims to limit their complexity but keeping good modeling capabilities. The DDR arises from the fact that the MP technique provides limiting modeling performance when complex memory effects have to be taken into account. The relation between the input $x(n)$ and the output $y(n)$ of a second-order DDR is as follows [Gua2011]:

$$
\begin{aligned}
y(n) \quad = \quad & \sum_{k=0}^{\frac{K-1}{2}} \sum_{m=0}^{M} g_{2k+1,1(i)} |x(n)|^{2k} x(n-m) \\
& + \sum_{k=1}^{\frac{K-1}{2}} \sum_{m=1}^{M} g_{2k+1,2(i)} |x(n)|^{2(k-1)} x(n)^2 x^*(n-m) \\
& + \sum_{k=1}^{\frac{K-1}{2}} \sum_{m=1}^{M} g_{2k+1,3(i)} |x(n)|^{2(k-1)} x(n) |x(n-m)|^2 \\
& + \sum_{k=1}^{\frac{K-1}{2}} \sum_{m=1}^{M} g_{2k+1,4(i)} |x(n)|^{2(k-1)} x^*(n)\, x(n-m)^2
\end{aligned}
$$

where $g_{2k+1,1(m)}$, $g_{2k+1,2(m)}$, $g_{2k+1,3(m1,m2)}$ and $g_{2k+1,4(m1,m2)}$ are the $\left(\frac{K-1}{2}+1\right)(M+1)+3M\frac{K-1}{2}$ coefficients used for the DPD.

5.4.3 Generalized Memory Polynomial

The GMP technique [Mor2006] is another simplification of Volterra series. The main difference with the DDR technique is that GMP has the capability to select only the most significant terms/kernels of the Volterra series. The relation between the input $x(n)$ and the output $y(n)$ of the GMP is as follows:

$$
\begin{aligned}
y(n) \quad = \quad & \sum_{k=0}^{K_a-1} \sum_{l=0}^{L_a-1} a_{k,m} x(n-l) |x(n-l)|^k \\
& + \sum_{k=1}^{K_b} \sum_{l=0}^{L_b-1} \sum_{m=1}^{M_b} b_{k,l,m} x(n-l) |x(n-l-m)|^k \\
& + \sum_{k=1}^{K_c} \sum_{l=0}^{L_c-1} \sum_{m=1}^{M_c} c_{k,l,m} x(n-l) |x(n-l+m)|^k
\end{aligned}
$$

where $a_{k,m}$, $b_{k,l,m}$ and $c_{k,l,m}$ are the $K_aL_a + K_bL_bM_b + K_cL_cM_c$ coefficients used for the DPD. K_aL_a are the number of coefficients for aligned signal and envelope (memory polynomial), $K_bL_bM_b$ are the number of coefficients for signal and lagging envelope, and $K_cL_cM_c$ are the number of coefficients for signal and leading envelope.

The GMP flexibility comes with the difficulty to properly set 8 parameters ($K_a, L_a, K_b, L_b, M_b, K_c, L_c, M_c$), instead of only 2 ($K$ and M) for MP and DDR techniques. The parameter setting is addressed in the next section.

5.5 DPD selection and parameters setting

In this section, we assess the performance of the MP, DDR and GMP DPD techniques in order to select the most efficient technique for a given complexity. The complexity is related to the number of coefficients required for the DPD. Indeed, the DPD estimation (using LS

estimation) requires a square matrix inversion which order is given by the number of coefficients [Mor2006].

Ideally, each DPD techniques shall be evaluated for different parameters setting analyzing the signal at the PA output with the application of the DPD. Unfortunately, this approach is not realistic since it requires a very large amount of experimentations. For that reason, we propose to assess the DPD performance using a very precise PA model that we have developed based on measurements of a UE PA provided by SKYWORKS for the 2.5 GHz band [Sky2016]. Figure 49 gives the AM/AM and AM/PM curves of the "SKY77706" PA and the PA model.

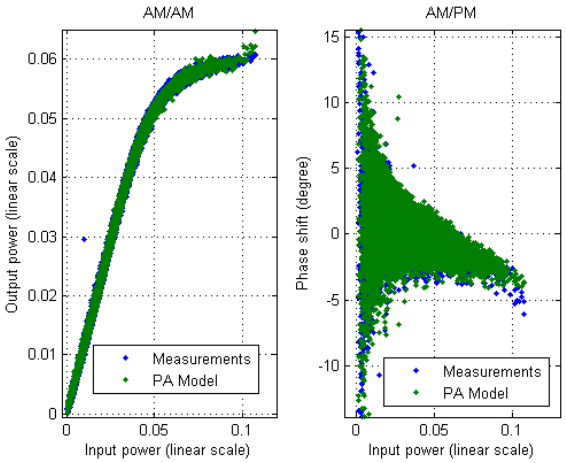

Figure 49: left) AM/AM and right) AM/PM comparisons between measurements and modeling of the SKYWORKS PA

We use the weighted error to signal power (WESP) ratio as the evaluation criteria [Wis2007]. WESP refers to the power of the frequency domain weighted error signal:

$$WESP(dB) = 10log\left[\frac{\sum_{i\in I}|Win(i)Err(i)|^2}{\sum_{i\in I}|Y(i)|^2}\right]$$

where I refers to the frequency bins, $Win(i)$ is the frequency domain window used as the weighting function, $Err(i)$ is the spectrum of the error signal ($y(n) - \hat{y}(n)$), and $Y(i)$ is the spectrum of the signal to be transmitted $y(n)$.

The main goal of the DPD is to improve the out-of-band emission at the output of the power amplifier and not necessarily to improve the in-band emission. Thus we propose to set the weighting function to 0 for the frequency indexes corresponding to the useful bandwidth, and to 0 everywhere else.

In SOLDER, we address the intra-band carrier aggregation (CA) at the PHY layer level for both contiguous and non-contiguous cases considering filter bank multicarrier (FBMC) [Sio2002] modulation. The corresponding examples of PHY layer configurations are presented in Table 9. Note that the parameters are set in order to be as much as possible in line with LTE parameters. Contiguous case signal refers to the transmission of a single (wide) band, whereas non-contiguous signal is composed of three different bands (both signals occupy the same useful bandwidth). Finally, the large initial peak-to-average power ratio (PAPR) is reduced to either 7.5 or 6.5 dB according to the methods proposed in [D3.2] and describes in [Val2015] and [Tra2016a].

Table 9: PHY layer parameters setting for contiguous and non-contiguous cases

Parameters	Case 1: contiguous case	Case 2: non-contiguous case
Sampling Frequency	16 x 3.84 MHz	16 x 3.84 MHz
FFT Size	4096	4096
Subcarrier spacing	15 kHz	15 kHz
Prototype filter length	K=4	K=4
Resource block (RB) size	12 subcarriers	12 subcarriers
Number of RB	Band #1: 37 RB	Band #1: 25 RB 5 MHz channelization Band #2: 6 RB 1.5 MHz channelization Band #3: 6 RB 1.5 MHz channelization
PAPR reduction algorithm	Filter Bank precoding [D3.2] [Val2015]	Peak Cancelation [D3.2] [Tra2016a]
Initial PAPR	11.5 dB	11.5 dB
PAPR after reduction	7.5 dB	6.5 dB

Figure 50 gives the WESP simulations according to i) the DPD technique, ii) the scenario (contiguous or non-contiguous), iii) the number of coefficients. We can observe that the results are quite similar for both scenarios: GMP method outperforms the performance of MP and DDR techniques. In SOLDER, we propose to limit the number of coefficients to 40 since this value provides a good trade-off between complexity and performance. In this case, it is interesting to note that the GMP parameter setting that gives the best WESP performance are identical for contiguous and non-contiguous cases, namely Ka=6 La=3 Kb=2 Lb=3 Mb=2 Kc=3 Lc=1 Mc=3.

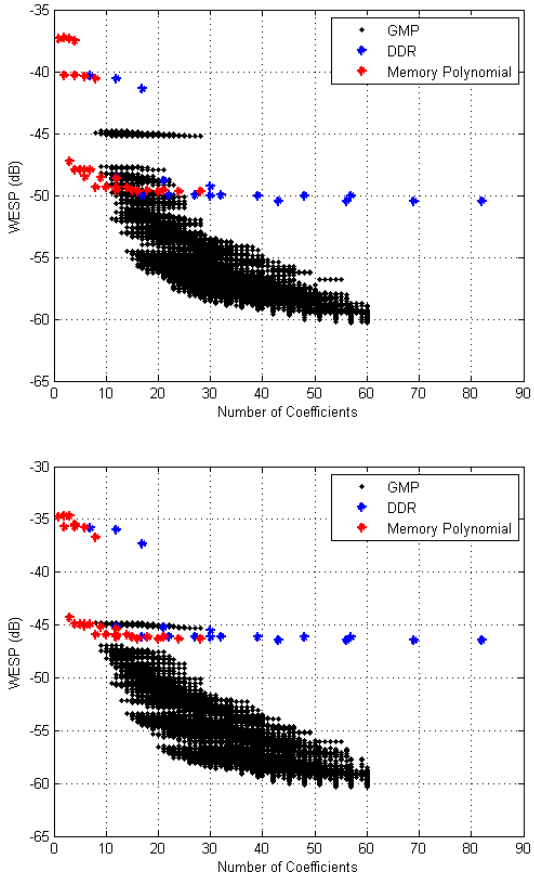

Figure 50: WESP for MP, DDR and GMP techniques according to the number of coefficients. Left) Contiguous case, Right) non-contiguous case

Figure 51 presents the spectrum at the PA output with and without the use of the GMP technique. We can observe that out-of-band rejection is reduced by about 30 dB and is well below -60 dBc. The deep spectrum notches that are created between bands thanks to the use of FBMC are drastically affected by the PA non linearity. The notch power ratio (NPR) is about -35 dB when the PA is not linearized, and in this case it is not acceptable to consider a PHY layer CA approach. When the DPD is activated, the NPR can be reduced to -70 dB enabling the use of FBMC as a CA technique.

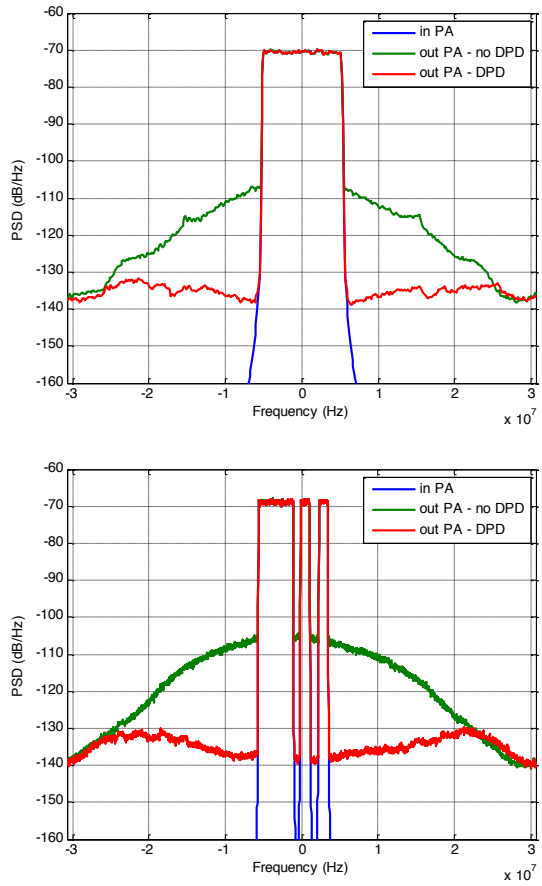

Figure 51: PSD of the signals to be transmitted (blue), at the PA output without DPD (green) and with DPD (red) for left) the contiguous case and right) the non contiguous case scenario

5.6 On the importance of IQ imbalance compensation

The ExpressMIMO2 platform uses direct-conversion (or Zero-IF) architecture for the frequency transpositions used for both transmission and feedback loop required for DPD learning. This architecture has the great advantage of lowering the number of components, decreasing the power consumption and having a small form factor. Nevertheless, Zero-IF is subjected to many drawbacks namely IQ imbalance and DC leakage. These imperfections are particularly harmful when a linearization technique has to be developed and can completely cancel out its capability. In deliverable D3.2 [D3.2], we have proposed a calibration technique to digitally compensate for these imperfections. In this section, we analyze the impact of IQ imbalance on DPD performance, and more specifically on the spectrum at the output of the PA. We are considering in our simulations realistic imperfection values given in Table 10.

Table 10: Simulated gain and phase IQ imbalances

IQ modulator imperfections (Tx)		IQ demodulator imperfection (Rx)	
Gain Imbalance	Phase Imbalance	Gain Imbalance	Phase Imbalance
+0.17 dB	+3°	+0.47 dB	-3.3°

Figure 52 presents the PSD results at the PA output according to the fact that Tx and Rx IQ imbalances are digitally compensated or not. On the one hand, Rx IQ imbalance introduces an out-of-band degradation of about 10 to 15 dB with respect to the ideal case, and a degradation of the NPR of about 20 dB. On the other hand, Tx imbalance generates a plateau in the DSP which level is 30 dB below the useful signal. As explained in deliverable D3.2 [D3.2], this plateau is due to the mirror image useful signal produced by the transmitter IQ imbalance

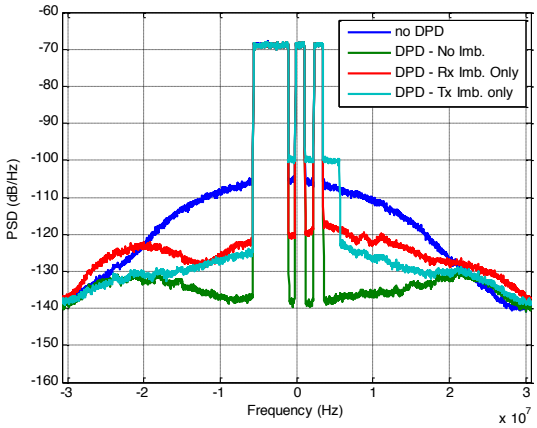

Figure 52: Impact of IQ imbalance on the PSD of the output signal: (green) both IQ modulator and demodulator are digitally compensated, (red) IQ modulator only and (cyan) IQ demodulator only

5.7 On the importance of PAPR reduction

In this section, we analyze the impact of the PAPR of the signal to be transmitted on the spectrum at the output of the PA, but also on the mean transmitted power. We are considering four cases corresponding to the activation/de-activation of DPD and/or PAPR reduction.

The PSD results for these cases are presented in Figure 53. We can observe that the PAPR reduction without DPD only slightly improves the out-of-band radiation. When the DPD is activated, the linearity performance without PAPR reduction is very good and is only few dB above the performance obtained with a reduced PAPR.

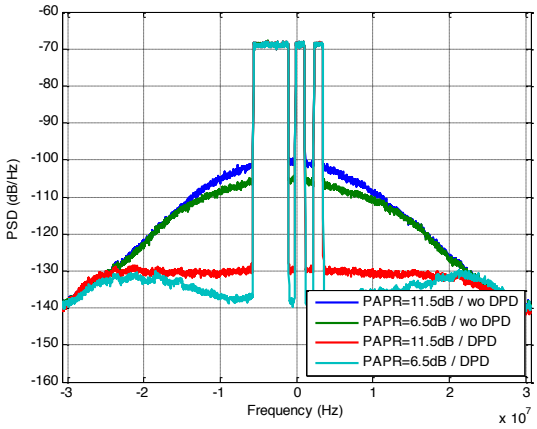

Figure 53: Impact of DPD and PAPR reduction on the transmitted spectrum

Figure 54 shows the AM-AM curves according to the PAPR of the signal to be transmitted. DPD technique tends to linearize the power amplifier up to the maximum instantaneous power. When the PAPR is reduced to 6.5 dB, the slopes of the AM-AM curve with and without DPD are almost identical meaning that the mean output power is almost not modified by the use of DPD. But when the PAPR is not reduced, the maximum instantaneous power at the output of the PA is located in the compression zone and very close to the saturation level. In this case, we can observe that the slope of the AM-AM curve after the linearization process (in red in Figure 54) is drastically attenuated, and the corresponding mean output power is reduced by the same amount.

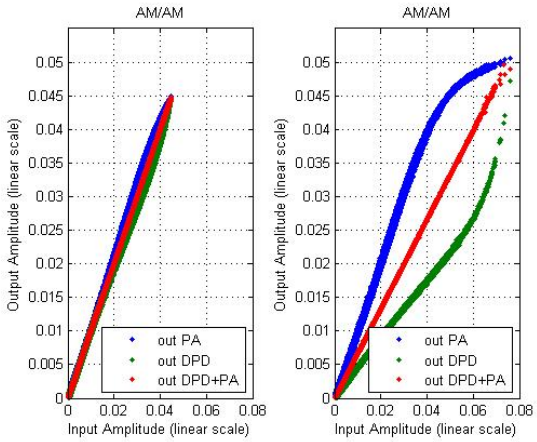

Figure 54: Impact of DPD and PAPR reduction on the AM-AM curves. Left) PAPR is reduced to 6.5 dB, right) PAPR is not reduced and is equal to 11.5 dB

Table 11 gives a recapitulation of the impact of the DPD and PAPR reduction on the mean output power and on the transmitted signal linearity.

Table 11: Impact of DPD and PAPR reduction on the mean output power and on the transmitted signal linearity

DPD	Not activated		Activated	
PAPR reduction	Off 11.5 dB	On 6.5 dB	Off 11.5 dB	On 6.5 dB
Estimated mean Output Power	22.94 dBm	23 dBm	19.45 dBm	22.6 dBm
Linearity	Very Poor	Poor	Good	Excellent

5.8 Conclusion

Among all existing techniques, the GMP approach has been selected in SOLDER for the linearization of the transmitter. It has been shown that the excellent GMP performance comes with the difficulty to properly set its parameters. Thus, we have proposed an approach based on the WESP criteria which limits the amount of coefficients without scarifying the spectral containment performance. The out-of-band radiation can be reduced by 25/30 dB and can be limited to -60 dBc. Finally, we have highlighted the benefit of the calibration process (IQ imbalance compensations), and we have shown that the PAPR reduction tech-

nique shall be used with DPD in order to improve the out-of-band radiation, but also to keep the mean transmitted power to a reasonable value.

6. Conclusion

This deliverable presented the latest results of WP3, Several aspects of carrier aggregation were investigated and we proposed techniques that already had some impacts through various dissemination channels:

- In the 3GPP standardisation for techniques related to LAA
- In the scientific community with publications
- In products (the RRM scheduler is going to be part of ISW offering)

Moreover, some of the techniques investigated in WP3 (from D3.2 mostly and D3.3) were transferred into WP4 for prototyping and further evaluation. As presented in [D4.2], the Table 12 presents the techniques under prototyping (covering all WP3 activities, not only those reported in this report).

Table 12:List of WP3 techniques that are transferred to WP4 for prototyping

Algorithm	PoC name
Rateless RaptorQ code	PoC 1a
Listen before talk (LBT)	PoC 1b
Discontinuous transmission (DTX)	
Transmit power control (TPC)	
Carrier Selection (CS)	
RF impairments compensation	PoC2
PAPR reduction for contiguous and non-contiguous Filter Bank MultiCarrier (FBMC) signals	
Digital PreDistortion (DPD) for contiguous and non-contiguous FBMC signals	
MAC-scheduler API	PoC3a
Advanced scheduler for carrier aggregation	
Low complexity PMI/RI calculation	PoC3b
Low-feedback rate channel assignment/allocation	

CA is more and more becoming a key enabler for future communications systems, used in many scenarios as we tried to illustrate throughout the investigation made in WP3. Our results provided enablers for such uses, and helped us to convince of the interest of CA.

Appendix

The following appendices are provided as separate pdf files together with this document.

- A2.2 “A Cross-layer-aware FDD TDD Carrier Aggregation Framework for LTE-A Networks”.
- A2.3 “Capacity & Performance of a Carrier-Aggregated Decoupled Downlink and Uplink 5G Systems”.
- A3.1.1 “PHY and MAC layer Modeling of LTE and WiFi RATs”.
- A3.1.2 “Stochastic Analysis of Two-Tier HetNets Employing LTE and WiFi”.
- A3.1.3 “An Analytical Model for Flow-level Performance of Large, Randomly Placed Small Cell Networks”.
- A3.1.4 “An Analytical Model for Flow-level Performance in Heterogeneous Wireless Networks”.
- A3.2 "Multi-RAT Spectrum Reallocation including Carrier Aggregation for 5G Networks".
- A3.3 "Energy Efficient Optimal Power Allocation for Carrier Aggregation: Circuit Power Aware System design with Quantized CSIT".
- A5.1a “A Family of Square-Root Nyquist Filter With Low Group Delay and High Stopband Attenuation”.
- A5.1b “Robustness of Filter Bank Multicarrier Signals To Power Amplifier Nonlinearities”.
- A5.1c “Spectral performances of PAPR reduced FBMC signals”.

List of Acronyms

Acronym	Meaning
3GPP	3rd Generation Partnership Project
AFB	Analysis Filter Bank
AWGN	Additive White Gaussian Noise
BER	Bit Error Rate
CA	Carrier Aggregation
CC	Component Carrier
CCDF	Complementary Cumulative Density Function
CLD	Cross-layer design
COT	Channel Occupancy Time
CQI	Channel Quality Indication
CS	Carrier Selection
CSI	Channel State Information
DDR	Dynamic Deviation Reduction
DPD	Digital PreDistortion
DFT	Discrete Fourier Transform
DTX	Discontinuous Transmission
ER	Equiripple
EVM	Error Vector Magnitude
FB	Filter Bank
FBMC	Filter Bank MultiCarrier
GMP	Generalized Memory Polynomial
HM	Hungarian Method
IBP/MBU	Indoor broadband provisioning or mobile broadband uplink
IDFT	Discret Fourier Transform
IF	Intermediate Frequency
LAA	Licensed Assisted Access
LBT	Listen Before Talk
LMS	Least Mean Square
LNA	Low Noise Amplifier
LS	Least Square
LTE	Long Term Evolution
MLNP	Mixed Integer Non Linear Programming
MIB	Master Information Block
MP	Memory Polynomial
OFDM	Orthogonal Frequency Division Multiplexing
OQAM	Offset Quadrature Amplitude Modulation
PA	Power Amplifier

PAPR	Peak to Average Power Ratio
PCell	Primary Cell
PMI	Precoding Matrix Indicator
PSD	Power Spectral Density
QAM	Quadrature Amplitude Modulation
RB	Resource Block
RC	Raised Cosine
RI	Rank Indicator
RL	Reinforcement Learning
RRC	Root Raised Cosine
SCell	Secondary Cell
SC-FDMA	Single Carrier Frequency Division Multiple Access
SFB	Synthesis Filter Bank
SI	Study Item
SM	Stable Matching
SRF	Spectrum ReFarming
TPC	Transmit Power Control
TVWS	TV White Space
WESP	Weighted Error to Signal Power
WI	Work Item

References

[3GPP37.870]	3GPP, TR 37.870 TSG RAN, “Study on multiple radio access technology (multi-rat) joint coordination (release 13),” Rel.13 v13.0.0, June 2015
[Arv2016]	Arvanitakis, George; Kaltenberger, Florian, “Stochastic analysis of two-tier HetNets employing LTE and wifi,” EUCNC 2016, 25th European Conference on Networks and Communications, June 27-30, 2016, Athens, Greece
[D2.3]	SOLDER Deliverable 2.3, “System-Level Requirements for Scenarios and Use Cases,” April 2015
[D3.2]	SOLDER D3.2, Innovative solution for Carrier aggregation in h-RATs, LTE-A and beyond, October 2015
[Din2004]	L. Ding, G. T. Zhou, D. R. Morgan, Z. Ma, J. S. Kenney, J. Kim, and C. R. Giardina, "A robust digital baseband predistorter constructed using memory polynomials," IEEE Transactions. on Communications, vol. 52, pp. 159-165, January 2004.
[Dual2016]	3GPP TR 36.932, Rel. 13. Scenarios and requirements for small cell enhancements for e-utra and e-utran, Jan. 2016.
[ETSI2014]	ETSI EN 301 398, “White Space Devices (WSD); Wireless Access Systems operating in the 470 MHz to 790 MHz frequency band; Harmonized EN covering the essential requirements of article 3.2 of the R&TTE Directive,” v1.1.1, Apr. 2014.
[ETSI301893]	ETSI EN301 893 V1.7.2, “Broadband Radio Access Networks (BRAN); 5 GHz high performance RLAN; Harmonized EN covering the essential requirements of article 3.2 of the R&TTE Directive”
[FCC2015]	FCC Rulemaking 12-354, “3.5 GHz Band / Citizens Broadband Radio Service,” April 2015, https://www.fcc.gov/rulemaking/12-354
[Gua2011]	L. Guan, A. Zhu, “Simplified dynamic deviation reduction-based Volterra model for Doherty power amplifiers”, Workshop on Integrated Nonlinear Microwave and Millimetre-Wave Circuits (INMMIC), pp 1-4, April. 2011.
[Hol2015a]	O. Holland, et al., “To White Space or Not To White Space: That is the Trial Within the Ofcom TV White Spaces Pilot,” IEEE DySPAN 2015, Stockholm, Sweden, Sept.-Oct. 2015.
[Hol2015b]	O. Holland, “TV white space in London, UK: availability and maximum achievable capacity,” Electronics Letters, Vol. 15, No. 12, Jun. 2015.
[Lem2016]	Maria A. Lema, Mario Garcia-Lozano, Silvia Ruiz, Mischa Dohler, O. Holland (authors TBC) “Capacity & Performance of a Carrier-Aggregated Decoupled Downlink and Uplink 5G Systems”, To be published, 2016.
[Lub2011]	M. Luby, A. Shokrollahi, M. Watson, T. Stockhammer, L. Minder, “RaptorQ Forward Error Correction Scheme for Object Delivery,” IETF RFC 6330.
[Mor2006]	D. R. Morgan, Z. Ma, Jaehyeong Kim, M. G. Zierdt, and J. Pastalan. “A generalized memory polynomial model for digital predistortion of RF power amplifiers”, IEEE Transactions on Signal Processing, Vol. 54, pp. 3852-3860, October 2006.
[NGMN]	Next Generation Mobile Networks, RAN Evolution Project, “Multi-rat joint radio operation (mrjro),” Rel.13 v 1.1, March 2015
[Ofc2013]	Ofcom, “Ofcom invites industry to pilot ‘white space’ devices,” press release, http://media.ofcom.org.uk/news/2013/industry-to-pilot-white-space-

	devices, accessed May 2016.
[Ofc2015]	Ofcom, “Implementing TV White Spaces,” statement, Feb. 2015.
[Ofc2016]	Ofcom, “3.8 GHz to 4.2 GHz band: Opportunities for Innovation,” consultation, April 2016. Accessible at http://stakeholders.ofcom.org.uk/consultations/opportunities-for-spectrum-sharing-innovation, accessed May 2016.
[Paa2008]	H. Paaso and A. Mämmelä, “Comparison of Direct Learning and Indirect Learning Predistortion Architectures”, IEEE International Symposium on Wireless Communication Systems, vol. 3, pp. 309-313, October. 2008.
[RP-152272]	RP-152272 - New Work Item on enhanced LAA for LTE
[Sio2002]	P. Siohan, C. Siclet, and N. Lacaille, “Analysis and design of OFDM/OQAM systems based on filterbank theory,” IEEE Trans. Signal Process., vol. 50, no. 5, pp. 1170–1183, May 2002.
[Sky2016]	SKYWORK 77106 Power Amplifier [Online] http://www.skyworksinc.com/Product/701/SKY77706
[TDD-FDD]	3GPP TR 36.847, ”LTE Time Division Duplex (TDD) – Frequency Division Duplex (FDD) joint operation including Carrier Aggregation (CA)”, ver. 12.0, Rel. 12.
[TR 36.889-d00]	3GPP TR 36.889 V13.0.0 (2015-06), Study on Licensed-Assisted Access to Unlicensed Spectrum; (Release 13)
[Tra2016a]	S. Traverso, “A New Family of Filters for PAPR Reduction of Carrier Aggregated Signals,” IEEE WCNC 2016, Doha, Qatar.
[Tra2016b]	S. Traverso, “A Family of Square-Root Nyquist Filter with Low Group Delay and High Stopband Attenuation,” IEEE Communications Letters 2016.
[Val2015]	A. Valette, S. Traverso, I. Fijalkow, M. Ariaudo and A. Cipriano, "Parameters Selection for Filter Bank Precoded Filter Bank Multicarrier Systems," 2015 IEEE Globecom Workshops (GC Wkshps), San Diego, CA, 2015, pp. 1-6.
[Val2016a]	A. Valette, S. Traverso, M. Ariaudo and I. Fijalkow, "Robustness of FBMC to Power Amplification Nonlinearities," 2016 IEEE European Microwave Week, London, 2016.
[Val2016b]	A. Valette, S. Traverso, M. Ariaudo and I. Fijalkow, "Spectral performances of PAPR reduced FBMC signals," submitted to 2016 IEEE ISWCS, Poznan, Poland.
[WInnF2016]	Wireless Innovation Forum Spectrum Sharing Committee, http://www.wirelessinnovation.org/ssc, accessed June 2016.
[Wis2007]	D. Wisell, M. Isaksson, and N. Keskitalo, ”A General Evaluation Criteria for Behavioral PA Models,” in 69th ARFTG Conf. Dig., Honolulu, HI, USA, 2007, pp. 251-255.
[Zhu2006]	A. Zhu, José C. Pedro, Thomas J. Brazil, “Dynamic Deviation Reduction-Based Volterra Behavioral Modeling of RF Power Amplifiers”, IEEE Transactions. on Microwave Theory and Techniques, Vol. 54, pp. 4323-4332, December. 2006.